

METALS HOSTS IN PENNSYLVANIAN HUSHPUCKNEY AND STARK BLACK  
SHALES FROM SELECTED AREAS IN KANSAS CITY

A DISSERTATION IN  
GEOSCIENCES AND CHEMISTRY

Presented to the Faculty of the University  
of Missouri-Kansas City in partial of fulfillment of  
the requirements for the degree

Doctor of Philosophy

By

Safaa Abdulfattah Abdulrazzaq Al-Janabi

BS Baghdad University, 1983

MS Baghdad University, 1986

Kansas City, Missouri

2017

© 2017

SAFAA A. A. AL-JANABI

ALL RIGHTS RESERVED

METALS HOSTS IN PENNSYLVANIAN HUSHPUCKNEY AND STARK BLACK  
SHALES FROM SELECTED AREAS IN KANSAS CITY

Safaa A. A. Al-Janabi, Candidate for the Doctoral of Philosophy Degree

University of Missouri-Kansas City, 2017

ABSTRACT

The Hushpuckney Shale of the Swope Formation and the Stark Shale of the Dennis Formation, two black shales in the Pennsylvanian Kansas City group, contain elevated concentrations of transition and based metal elements, notably zinc, lead, vanadium, and others. Both shales consist of an organic-rich black shale lower part and gray shale, organic-poor upper part.

The main rock-forming minerals in the shales include silicates (quartz and clay minerals), carbonates (calcite and dolomite), and phosphate (francolite). Various sulfide/selenide minerals (pyrite, sphalerite, chalcopyrite, clausthalite) account for most of the transition and base metal enrichment, though some appears to be hosted in organic material and on clays. Traces of barite, rutile, and mica were also detected. While the rock-forming minerals are detrital or diagenetic, most of the sulfides/selenide appear to be hydrothermal in origin.

Ni/Co and V/ (V+Ni) ratios indicate the sedimentary environment of Hushpuckney deposition was marginally oxic (in the upper part) to anoxic and euxinic (in the lower part). The same ratios applied to the black shale portion of the Stark indicate deposition in anoxic to euxinic conditions. The presence of hydrothermal sulfides suggest later introduction of

hydrothermal fluids and mineralization, probably during the Ouachita uplift to the south during the early Permian.

Elemental variation with depth, and interelemental correlations were determined using scanning XRF for a variety of major, minor, and trace elements, including Si, Al, Fe, Mg, Ca, K, and P (major elements), minor Ba, S, Co, Cu, Ni, and Sr, and trace V, Zn, Pb, Sc, La, Ti, Se, Rb and Sb elements. Interelement correlations generally agree with observations made using scanning electron microscopy/energy dispersive spectroscopy and X ray diffraction analyses, and can be explained by the mineralogy.

The organic material and clays appear to host vanadium whereas the other metals are present as sulfides (sphalerite, chalcopyrite, and pyrite) or selenide (clausthalite). The hydrothermal minerals appear to be associated with the francolite, suggesting that chemical reactions with the francolite played a role in sulfide deposition. Vanadium is also concentrated in some of the hydrothermal sulfides, suggesting remobilization and deposition of V during sulfide formation.

Metal enrichment in these two black shales thus appears to be due to a combination of adsorption or inclusion of elements such as V from seawater during sedimentation or diagenesis, and a later hydrothermal addition of zinc, lead, copper, and selenium.

The faculty listed below, appointed by the Dean of the School of Graduate Studies, have examined a dissertation titled “Metals hosts in the Pennsylvanian Hushpuckney and Stark Black Shales from Selected Areas in Kansas City”, presented by Safaa Abdulfattah Abdulrazzaq Al-Janabi, candidate for the Doctor of Philosophy degree, and hereby certify that in their opinion it is worthy of acceptance.

Supervisory Committee

James B. Murowchick, Ph.D., Committee Chair and Research Advisor

Department of Geosciences

Syed E. Hasan, Ph.D.

Department of Geosciences

Jejung Lee, Ph.D.

Department of Geosciences

Zhonghua Peng, Ph.D.

Department of Chemistry

Nathan Oyler, Ph.D.

Department of Chemistry

## TABLE OF CONTENTS

ABSTRACT .....	iii
LIST OF ILLUSTRATIONS .....	ix
LIST OF TABLES .....	xii
LIST OF PLATES .....	xiii
ACKNOWLEDGEMENTS .....	xvi
1. INTRODUCTION .....	1
Preface .....	1
Purpose of Study .....	1
Review .....	2
Swope Formation .....	3
Dennis Formation .....	5
Core Sample (Hushpuckney & Stark) Characterization .....	5
Previous Work .....	9
2. METHODOLOGY .....	12
3. MINERALOGY .....	20
Clay Minerals .....	20

Illite .....	20
Kaolinite .....	21
Clinochlore.....	21
Carbonate Minerals .....	22
Quartz .....	22
Phosphate Minerals .....	31
Pyrite.....	31
Sphalerite .....	32
Clausthalite .....	32
Other minerals.....	33
4. GEOCHEMISTRY .....	66
Element Maps and XRF Data .....	66
Elemental Correlations .....	75
Linear Correlation Discussion .....	89
5. DEPOSITIONAL ENVIRONMENT .....	94
Paleoenvironment .....	94
Paleoredox Discussion .....	96

Sphalerite and Clausthalite .....	98
Phosphates .....	100
Discussion .....	103
6. CONCLUSIONS .....	117
REFERENCE LIST .....	120
VITA .....	131



## ILLUSTRATIONS

Figure	Page
1.1	Stratigraphic column showing the two black shales studied in this investigation.....4
1.2	The Hushpuckney black shale and the lowest part for the Bethany Falls limestone..7
1.3	Core log illustrating the unweathered portion of Stark black shale .....8
2.1	Troost Avenue Bridge (BR) location, Kansas City, MO .....16
2.2	Greenwood (GW) quarry location- south of Greenwood, MO.....16
2.3	Stark black shale overlying the Bethany Falls limestone at the Bannister Road and Blue River Road section (BBS). Kansas City, MO.....17
2.4	87 <sup>th</sup> and Blue River Road section (87 <sup>th</sup> H).....18
2.5	63 <sup>rd</sup> street section location along the ramp to southbound Interstate 435 (63 <sup>rd</sup> H). Kansas City, MO.....18
2.6	Polished mounts of Stark (A-C) and Hushpuckney (D-F) black shale samples.....19
3.1	XRD powder pattern for Hushpuckney black shale total sample .....23
3.2	XRD powder pattern for Stark black shale total sample.....24
3.3	XRD pattern of clay oriented samples for Hushpuckney black shale unit .....25
3.4	XRD powder pattern of clay oriented samples for Stark black shale unit .....29
3.5	XRD powder pattern for the phosphate in Stark black shale unit .....34

3.6	Clausthalite EDS spectrum and composition in Stark black shale, Greenwood quarry.....	35
3.7	Fluorapatite EDS spectrum and composition .....	36
3.8	Sphalerite EDS spectrum and composition from Stark black shale, Greenwood quarry.....	37
3.9	Chalcopyrite EDS spectrum in Stark black shale, Greenwood quarry .....	38
4.1	Vertical distribution of major elements in the Hushpuckney black shale .....	69
4.2	Vertical distribution of minor and trace elements in the Hushpuckney black shale..	70
4.3	Vertical distribution of major elements in the Stark black shale.....	71
4.4	Vertical distribution of minor and trace elements in the Stark black shale.....	72
4.5	Linear correlation between P and other elements in Hushpuckney (H) and Stark (S) black shale.....	77
4.6	Linear correlation between Al and other elements in Hushpuckney (H) and Stark (S) black shales .....	81
4.7	Linear correlation between some elements as it indicates to each relationship in Hushpuckney and Stark black shale units.....	86
5.1	SEM photomicrograph of phosphate nodule (Ph) in shale (Sh).....	105
5.2	SEM photomicrograph of phosphate nodules (Ph) disseminated in shale (Sh) and organic matter (OM).....	106

5.3	EDS images for Hushpuckney. Sphalerite disseminated between the phosphate pellets and grains.....	107
5.4	EDS images for Hushpuckney. Sphalerite in phosphate grains.....	108
5.5	EDS images for Hushpuckney. Elemental maps of calcium and phosphorus explain the rounded shape for phosphate grains containing sphalerite and pyrite in Hushpuckney (BR8).....	109
5.6	SEM photomicrograph of phosphate nodule in Hushpuckney black shale unit.....	110
5.7	EDS images for Stark shale. Elemental maps for Ca, P, Al and Si showing isolated phosphate grains in shale.....	111
5.8	EDS images for Hushpuckney shale. Upper image, backscattered electron image. Lower image, composite elemental map with BSE image.....	112
5.9	Theoretical pe – pH – Eh diagram shows stability fields for strengite and apatite..	114

## TABLES

Table	Page
4.1 Major element compositions of Hushpuckney and Stark units.....	73
4.2 Minor and trace element compositions of Hushpuckney and Stark units.....	73
4.3 Comparison of average abundances of elements in different shales with the Hushpuckney and Stark black shale units.....	74
4.4 Correlation coefficients for major, minor and trace elements versus phosphorus.....	91
4.5 Correlation coefficients for major, minor and trace elements versus Aluminum.....	92
4.6 Correlation among selected elements .....	93
5.1 Redox proxies values and their ranges for oxic, dysoxic, anoxic and euxinic environments.....	97
5.2 Maximum, minimum and average values ratios for the two studied black shales.....	97

PLATES

Plate	Page
1 EDS maps for Stark shale showing distribution of secondary calcite (purple), “P and Ca” in phosphate clot, Zn and S in sphalerite. Sphalerite is filling the space between phosphate grains. Stark shale GW- SP10, Greenwood quarry, Greenwood, MO.....	39
2 EDS maps for Hushpuckney shale showing dolomite rhombs scattered in shale.....	40
3 EDS maps for Hushpuckney shale showing distribution of clausthalite, sphalerite, framboidal pyrite, phosphate, dolomite, clays and rutile.....	41
4 EDS maps for Stark shale showing dissemination of clausthalite in phosphate Stark shale.....	43
5 EDS maps for Hushpuckney shale showing distribution of clausthalite, sphalerite, framboidal pyrite, phosphate, clays, quartz, dolomite, organic matter, and Rutile.....	44
6 EDS maps for Hushpuckney shale showing distribution of sphalerite, phosphate and clays.....	46
7 EDS maps for Hushpuckney shale showing distribution of sphalerite, framboidal pyrite and pyrite, phosphate, clays, dolomite, and quartz.....	48
8 EDS maps for Hushpuckney shale showing distribution of sphalerite, framboidal pyrite, phosphate, clays, dolomite, and quartz.....	49
9 EDS maps for Hushpuckney shale showing distribution apatite (as conodont), framboidal pyrite, dolomite, clays and rutile.....	50

10	EDS maps for Hushpuckney shale showing distribution apatite (as conodont), framboidal pyrite, dolomite and clays .....	51
11	EDS maps for Stark shale showing distribution of euhedral pyrite and phosphate in Stark shale sample.....	52
12	EDS maps for Stark shale showing distribution of sphalerite, pyrite and phosphate.....	53
13	EDS maps for Stark shale showing distribution of sphalerite, pyrite and phosphate.....	54
14	EDS maps for Stark shale showing distribution of framboidal pyrite, pyrite and phosphate.....	55
15	SEM photomicrograph for Stark shale showing different sizes of framboids.....	56
16	SEM images for Hushpuckney and Stark shale detrital clay particles from Hushpuckney shale sample.....	57
17	EDS maps for Stark shale showing shape features for sphalerite embedded in phosphate Stark shale sample.....	58
18	EDS maps for Hushpuckney shale showing distribution of sphalerite and phosphate....	59
19	EDS maps for Hushpuckney shale showing distribution of sphalerite , framboidal pyrite, phosphate, clays and organic matter.....	60
20	EDS maps for Stark shale sphalerite and pyrite disseminated in phosphate.....	61
21	EDS maps for Stark shale showing distribution of sphalerite and phosphate.....	62

22	EDS maps for Stark shale showing distribution of sphalerite, phosphate and secondary calcite.....	63
23	SEM images for barite in Hushpuckney shale.....	64
24	SEM photomicrograph for Hushpuckney shale showing detrital mica and framboidal pyrite.....	65

## ACKNOWLEDGEMENTS

First and above all, I would like to express my great thanks to my Almighty Allah, for helping me to accomplish this work.

I wish to express my sincere gratitude and appreciation to my academic supervisor, Dr. James Murowchick, Ph.D., Chair of the Research Advisory Committee, for his many years of instruction, guidance, inspiration, continued encouragement and support toward completion of this work.

I thank the committee members for their essential assistance with my geologic studies, readings, and editings of my dissertation: Dr. Syed E. Hasan, Dr. Jejung Lee, Dr. Zhonghua Peng and Dr. Nathan Oyler.

I would like to offer my thanks to the Ministry of Higher Education and Scientific Research, Baghdad, Iraq, for granting a full scholarship to complete my doctoral degree in Economic Geology.

My great thanks to my friends Dr. Ali Gyara and Dr. Mazen Tamar-Agha, Faculty of Geoscience Department - Baghdad University, for their help in reviewing the research.

My thanks and appreciation to John Szturo - Geologist HNTB Company for providing the rock core samples, and Bill Beggs who helped me to get fresh black shale samples from the Greenwood Quarry.

Appreciation is expressed to Dr. Khaldoun Al-Bassam (senior geologist - GEOSURVE, IRAQ) for his help to provide me references and discussion.

I wish to express my gratitude to my friends Dr. Khaldoun Ahmad and Ahmad Saeed for their help and support in my research.



I would also thank my wife, my two daughters and my son who supported me during my study, they encouraged me all the time.

I am especially grateful to my sisters and their families and my relatives for their prayers, support, and encouragement.

I thank all my friends in Iraq and USA for their support.

Finally, I would thank everyone who helped me and I apologize if I failed to recall anyone who offered me help or support.

**I dedicate this work to**

**The spirit of my parent**

**My wife**

**My children**

**My sisters and their families**

**All my friends**

# CHAPTER 1

## INTRODUCTION

### **Preface**

Black shale is a detrital sedimentary rock found in many parts of the world. The sediments that formed black shale were deposited in immobile aquatic environments with high organic productivity and oxygen deficiency at the bottom, creating sediments rich in organic matter and sulphides. Black shale is also known to contain high amounts of metals and other trace elements. Many of these black shales have economic importance in different countries for the contents of metals and organic materials.

### **Purpose of Study**

Previous black shale researchers have often found a high concentration for metals in black shales, but the Host phases were not always identified. The objective of this research is to study the mineralogic and petrographic characteristics of the two black shale units in Kansas City area: the Hushpuckney shale member of the Swope Formation and the Stark shale member of the Dennis Formation in the Pennsylvanian Kansas City group, and to identify the host phases for a variety of elements in these two black shale units. This investigation also seeks to find an explanation for zinc enrichment in the Hushpuckney and Stark black shales, but not the adjacent gray shale and limestone, which have low zinc concentrations. Although these black shales host no commercial deposits, understanding the processes of enrichment of minor elements in black shale may lead to discoveries of economic concentrations of minor elements, such as in the Kupferschiefer deposits in Europe. The metal contents of the shales may lead to environmental pollution.

## **Review**

The Kupferschiefer of the Permian age in central Europe is a spectacular example of metal-enriched black shale, containing Cu and Pb that can be mined (Tourtelot, 1979). Another example is the Cambrian nickel–molybdenum ores in south China. These Ni-Mo ores occur in a 1600- km- long belt within the Cambrian metalliferous black shales of the Niutitang and Qiongzhusi formations (Lott et al., 1999). The rare transition metals most characteristic of shales with high organic carbon content are vanadium, nickel, cobalt, copper, and molybdenum (Krauskopf, 1956), which are economically important metals. Shales could act as sources of pollution if any undesired elements they contain are mobilized by surface or groundwaters. If the shales could act as pollutant sinks adsorbing undesired elements with which they come into contact, and serve as hydraulic barriers, the shales are then useful for environmental protection (Vine and Tourtelot, 1970).

Sediments forming shales are usually deposited with varying amounts of organic matter. Gray shales contain about 1% organic carbon and black shales contain about 3% organic carbon (Vine and Tourtelot, 1970). Black shales can be source rocks for hydrocarbons because of the amount of initial organic matter in them (Blatt et al., 1980). Most of the known marine oil source beds are in shales that were originally deposited during transgression and under anaerobic conditions (DeMaison and Moore, 1980). Knowing the geochemistry of transgressive and regressive shales should help narrow the possible exploration areas in the search for hydrocarbons and for transition metals of economic value.

In many localities around Kansas City, there are several layers of exposed black shale of the Pennsylvanian age, including, the Hushpuckney shale of the Swope Formation and the Stark shale of the Dennis Formation. These two formations belong to the Bronson subgroup,

which in turn belongs to the Kansas City group of the Pennsylvanian age (Howe & Koenig, 1961). Many researchers have noticed that these two black shales have high zinc concentration as sphalerite (Vine & Tourtelot, 1970 and Coveney, 1979).

Pennsylvanian rocks cover much of the Missouri. The Pennsylvanian strata split into five series which are from older to younger: the Morrowan, Atokan, Desmoinesian, Missourian, and Virgilian. The Missourian series is divided into four groups, the Pleasanton, Kansas City, Lansing, and Pedee. These groups outcrop in the Kansas City area and extend across western and northern Missouri. The Kansas City group includes three subgroups: Bronson (the oldest), Linn, and Zarah (the youngest). The Bronson subgroup contains, in ascending order, the Hertha, Ladore, Swope, Galesburg, and Dennis formations (Figure 1.1) (Howe & Koenig, 1961). This study will concentrate on the black shale units of the Hushpuckney and Stark in Swope and Dennis formations, respectively.

### **Swope Formation**

The Swope Formation comprises, in ascending order, of the Middle Creek limestone, Hushpuckney black shale, and Bethany Falls limestone members. The Swope Formation overlies the Ladore Formation and underlies the Galesburg Formation, and crops out across northwestern Missouri forming a prominent eastward-facing escarpment (Parizek & Gentile, 1965). The Middle Creek member contains one to two thin beds of dark gray limestone, and the average thickness is less than one foot. The Hushpuckney member consists of dark gray to black fissile shale in its lower and middle parts and becomes gray shale in its upper part. The upper member is the Bethany Falls Limestone, and it is the most extensively quarried

Pennsylvanian limestone in western Missouri (Howe & Koenig, 1961). It consists of massive gray limestone roughly 25 feet thick, and the uppermost part is oolitic and weathered.

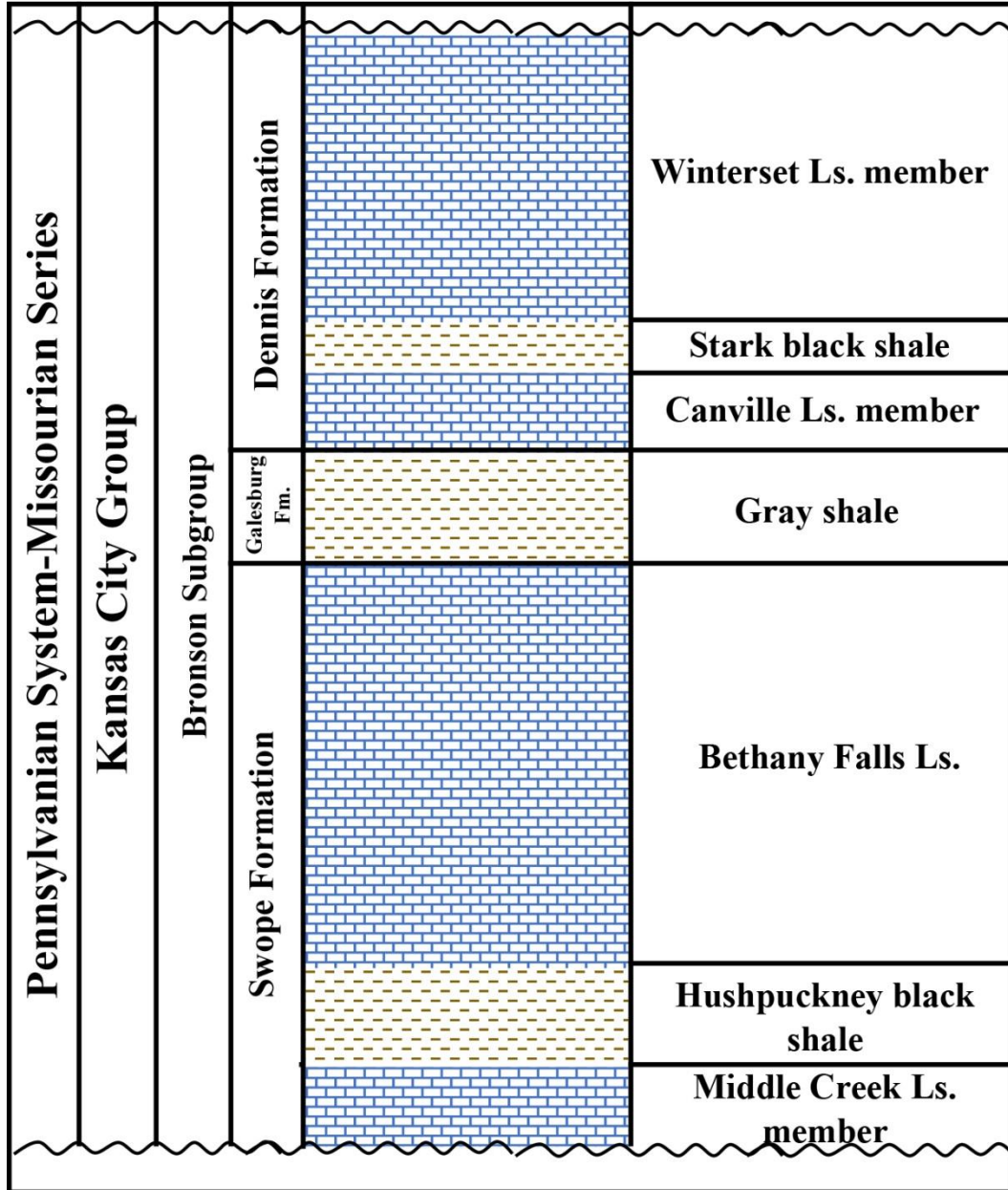


Figure 1.1. Stratigraphic column showing the two black shales (Hushpuckney and Stark) studied in this investigation (after Howe & Koenig, 1961). Not to scale.

## **Dennis Formation**

The Stark black shale is a middle member in the Dennis Formation, which also contains two limestone members. The Canville limestone is the lower member, and is a dark gray thin limestone which occurs in only a few counties in western Missouri (Howe & Koenig, 1961). The Stark member is a dark gray to black fissile shale that grades upward into medium gray shale. The Winterset member is the upper part of the Dennis Formation, and it is a thinly to thickly bedded limestone with many thin shale beds (Howe & Koenig, 1961).

## **Core Samples (Hushpuckney and Stark) Characterization**

The lithologic description for the studied core samples (Hushpuckney and Stark black shales units) as follow:

1- The stratigraphic interval preserved in the core samples that were studied is about 105 cm long, and includes the Hushpuckney black shale and the lowest part for the Bethany Falls limestone. Starting from the bottom for the Hushpuckney, the core material is dark gray to black shale with organic matter and phosphate. The phosphates occur as thin laminations varying in thickness from 1-3 mm and sometimes occur as lenticular nodules smaller than 9 mm in maximum dimension. Their color generally is light gray to brownish gray Figure 1-2. These phosphate laminations or nodules commonly extend laterally but not continuously in the black shale. Continuing upwards, the shale color gradually changes from dark gray to light gray. The gray shale seems more friable and fissile, and becomes more calcareous in the upper part. Also, it was noted that the upper most part of the gray shale is bioturbated. The core then becomes fossiliferous limestone above the shale.

2- The total thickness for unweathered Stark black shale is about 48 cm. The color of the Stark in the core is dark gray to black and it contains phosphate laminations or nodules scattered in the shale. Some of the phosphate nodules are larger than 3cm in diameter parallel to bedding Figure 1-3.

The exposed outcrops for both units the Hushpuckney and Stark are thinly laminated and weathered. The fissility increases with weathering along the bedding plane.



Age	Fn.	Unit	Depth (cm)	Core	Lithology	Description
Pennsylvanian System-Missourian Series	Swope Formation	Bethany Falls	1737			Recrystallized fossiliferous limestone
			1740			
			1743			
			1745			
			1748			
			1751			
			1754			
			1757			
			1760			
			1762			
		1765				
		1768			Calcareous gray shale with bioturbation activity	
		1771				
		1774				
		1776				
		1779				
		1782				
		1785				
		1788				
		1790				
		1793				
		1796				
		1799				
		1802				
		1805				
		1807				
		1810				
		1813				
		1816				
		1819			Dark gray to black shale containing organic matter & brownish gray phosphate lenticular lamination or nodules	
1821						
1824						
1827						
1830						
1833						
1836						
1838						
1841						
1844						
1847						
1850						
1852						
1855						
1858						
1861						
1864						
		Hushpuckney				

Figure 1.2. Core log of Hushpuckney black shale and the lowest part of the Bethany Falls limestone (BR8).



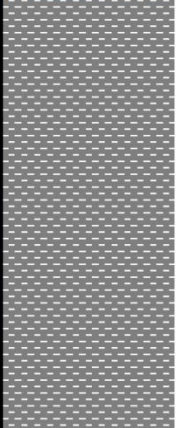
Age	Fn.	Unit	Depth (cm)	Core	Lithology	Description
Pennsylvanian System-Missourian Series	Dennis Formation	Stark black shale				Dark gray to black shale containing organic matter and brownish gray lenticular phosphate lamination or nodules.
						Dark gray to black shale containing organic matter

Figure 1. 3. Core log illustrating the unweathered portion of Stark black shale (BR8)

## **Previous work**

Many layers of black shale are exposed in the stratigraphic column of the United States. These layers have varied thicknesses, and sometimes they are interstratified with carbonate rocks. Researchers commonly have found that these black shales have a high concentration of metals making them interesting subjects for research on the origins of those metals.

Vine and Tourtelot (1970) studied black shale from different environments in the United States and Canada. In their work, they tried to classify these deposits (using geochemical parameters) as metal-rich deposits containing on minor elements occurring in concentrations well above normal background. Coveney, (1979) investigated metal concentration in four upper Pennsylvanian black shales (the Hushpuckney, Stark, Muncie Creek, and Eudora) known for their unusually high concentration of sphalerite in each unit. Zinc was detected in various black shales with an average of 2,500 ppm from the Hushpuckney, 1,570 ppm in the Stark, 2,100 ppm in the Muncie Creek, and 700 ppm in the Eudora. Cubitt and Merriam (1979) found that the Pennsylvanian cyclothem core shales, which are black shales, are enriched in molybdenum, lead, chromium, copper, nickel, vanadium, and zinc due to the low redox potential of the original sediments.

Black shales have also been implicated in substrate expansion damage to structures. Rudy (1982) studied the effects of expansion of the shale on many structures in southern and southeastern parts of Kansas City, Missouri. He suggested that the chief causes for shale expansion and building damages are stresses from tectonic forces, crystallization of sulfate minerals, and expansion of clay minerals which occur separately or in combination with each other.

Multiple authors have related geochemical characteristics of the black shales to depositional environments. Martin (1982) studied the Hushpuckney and Mecca Quarry shales at twenty locations in Missouri, Iowa, Illinois, and Indiana. Full sections of the Mecca Quarry shale and the lower portion of the Hushpuckney shale were sampled. Trace element contents were determined by quantitative X-ray fluorescence spectrography. Wenger and Baker (1986) described organic geochemistry of Pennsylvanian cyclothem in Kansas and Oklahoma; they found that vanadium and nickel increased with increasing anaerobic conditions. Organic carbon showed rapid increase stratigraphically suggesting a connection with initial rapid marine transgression resulting in increased productivity and organic preservation in flooded coastal swamps. They attributed the slow decline of organic carbon to deeper submergence of the coastal swamps such that productivity declined slowly. Schultz (1989) distinguished between aerobic, restricted, and inhospitable conditions by using the extent of pyritization in Kansas black shales. According to variations in trace element values the Hushpuckney shale was deposited in deeper waters than the Mecca Quarry shale.

Coveney and co-workers recognized Heebner-type and Mecca-type Pennsylvanian black shales on the basis of sedimentation rates, type of organic matter, area of deposition, and elemental composition (Coveney and Martin, 1983; Coveney et al., 1987, 1989; and Coveney & Glascock, 1989). Heebner-type shale formed offshore in deep waters under slow sedimentation and contains low concentrations of molybdenum, vanadium, and uranium. Its organic matter is mainly marine origin. Phosphate, calcite, and dolomite are abundant and the content of coal is low. Mecca-type shale formed nearshore in shallow waters under rapid sedimentation and contains high concentrations of molybdenum, vanadium, and uranium. Its

organic matter is mostly of terrestrial origin. The phosphate, calcite, dolomite, and kaolinite contents are high.

The upper Pennsylvanian Muncie Creek Shale Member of the Iola Formation was studied by Hamilton (1989) in the vicinity of Kansas City, Missouri, to determine whether or not elements are leached from shale by weathering to a degree significant enough to constitute an environmental hazard. Ziegler (1989) used Soxhlet extraction to leach middle Pennsylvanian sedimentary rocks, including black shales, to determine the sources of metals in ground and surface waters at coal mines near Montrose, Missouri. Bailey (1995) studied the Stark Shale Member of the Dennis Formation in a selected area in Kansas and Missouri to determine if the Stark shale could yield Zn, Cd, Cr, and Pb to ground water at levels exceeding current federal drinking water regulations. The purpose of studying the Hushpuckney and the Stark shale members in Kansas City area by Forseh (1997) was to determine the potential of this metal-rich black shale to yield metals to surface water.

Alego and Maynard (2004) studied three core shales from the Kansas City group eastern Kansas: (1) the Hushpuckney Shale member of the Swope Formation, (2) the Stark Shale member of the Dennis Formation, and (3) the Muncie Creek Shale member of the Iola Formation. They investigated these shales because they are composed of a lower laminated black shale submember and an upper bioturbated gray shale submember, this stratigraphy represents a range of redox conditions from dysoxic to strongly anoxic, possibly, euxinic. They suggested in their work the use of a multiproxy procedure for redox-facies analysis is more reliable than single-proxy indicators based on trace elements.

## CHAPTER 2

### Methodology

This study incorporates both field and laboratory work. The field work included collecting core rock samples from the construction company HNTB. These drill core samples were collected for the Troost Avenue Bridge project over Brush Creek (BR) in Kansas City, Missouri during July 2006 Figure 2.1. Randomly-selected samples of fresh shale were collected from the Greenwood quarry (GW) located south-east of Lee's Summit, Missouri Figure 2.2. There are many exposures of Hushpuckney and Stark black shale units in Kansas City, but they are usually weathered and eroded, making them unsuitable for analysis. Relatively fresh samples were collected from the following locations: Bannister Road and Blue River Road section (BBS), Kansas City, MO Figure 2.3; 87<sup>th</sup> Street and Blue River Road section (87<sup>th</sup> H), Kansas City, MO Figure 2.4; and 63<sup>rd</sup> Street section near Interstate 435 (63<sup>rd</sup> H), Kansas City, MO Figure 2.5.

The main tools used to study these samples are scanning electron microscopy/energy dispersive spectroscopy (SEM/EDS), powder X-ray diffraction identification (XRD), and X-ray fluorescence analysis (XRF) techniques. Scanning electron microscopy is the most useful tool in this study because the shale is very fine-grained and it is difficult to observe and describe using optical microscopy techniques. The high magnification and resolution capability of SEM is ideally suited to study the very fine grained rock features, including texture, composition, diagenetic features, and porosity down to the nanometer scale (Trewin, 1988). The mechanics of modern scanning electron microscope systems provide various imaging and detection techniques that can be used to study important aspects of the composition of shale samples at very high resolution (Camp et. al., 2013). These tools,

including EDS, provide qualitative and quantitative microanalysis through the multipoint spectrum of the elements contained in the sample, quantitative data about the sample composition, image acquisition, and element mapping.

The SEM/EDS used to identify the mineral phases in black shale and the distribution of metals through these phases is a Tescan Vega 3 LMU variable pressure scanning electron microscope with a Bruker Quantax 6 10 SDD EDS system at the UMKC Department of Geosciences. The backscattered electron detector (BSE) provided an image with compositional contrast, while the secondary electron detector (SE) shows the surface features, utilizing topographic contrast. Polished mounts for SEM/EDS examination were prepared by cutting, mounting, grinding and polishing the samples. Then, these samples were coated with carbon by using the Cressington 108 Carbon/A carbon coater to prevent any charging on the sample surface. Some of the weathered samples were tested as individual pieces by using double-sided tape mounting on a stub.

A total of 77 samples were analyzed by SEM/EDS. The samples were prepared as polished sections cut perpendicular to the bedding as shown in Figure 2.6. For the Hushpuckney unit and the lowest part of Bethany Falls limestone, 31 samples were prepared from well drill core BR8, Troost Avenue Bridge project and 9 samples from the 87<sup>th</sup> Street and 63<sup>rd</sup> Street Hushpuckney sections. For the Stark unit, 32 samples were prepared from the Green-wood quarry, well BR8, and BBS sections. 5 samples of phosphate were prepared in sections cut parallel to the bedding surface to check horizontal or lateral changes.

Powder X-ray diffraction (XRD) was used to identify the bulk mineralogy of pulverized material from whole samples, and oriented mounts were prepared for clay minerals analyses (Hutchison, 1974). XRD was conducted using a Rigaku MiniFlex

automated diffractometer with Ni-filtered Cu-K $\alpha$  radiation at 30kV, 15mA. The samples were scanned at 1° 2 $\theta$ /minute from 4 to 65°. The diffractograms were processed using Jade 8 software (Materials Data, Inc., Livermore. CA).

Thirteen samples selected as channel samples were prepared for mineral identification by XRD. Nine samples were chosen from the Hushpuckney Member and overlying Bethany Falls limestone and four samples were selected from the Stark member. All shale samples were ground to smaller than 100 micrometers in size and prepared for X-ray diffraction analysis. Clay minerals were separated from carbonate in the samples by treating the samples first with 30% H<sub>2</sub>O<sub>2</sub> to remove the organic matter, then with 0.5 M acetic acid, according to the method of (Ostrom, 1961). Three oriented clay mounts were prepared for X-ray diffraction (XRD) study by smearing the clay onto petrographic slides (Carver, 1971; Hutchison, 1974; and Gibbs, 1974). One sample mount was then air dried, the second was treated with ethylene glycol, and the third was heated to 550°C for 2 hours (Carroll, 1970; Thorez, 1976; and Hardy & Tucker, 1988), collecting a diffractogram after each treatment.

XRF scanning technology for geochemical analysis (to determine major, minor and trace elements concentrations) was used for the black shale. ITRAX core scanning XRF (Cox Analytical Systems) at the University of Minnesota-Duluth was used. The samples were scanned at 0.2 mm resolution using 15 seconds dwell time. The selected core samples comprise 13 intervals, selected according to changes in lithology, having different lengths. The samples were split lengthwise into two halves, and one half was taken to the lab at the University of Minnesota – Duluth for testing. Thirteen samples of various lengths were provided for analysis. The total length of the Hushpuckney core is about 105 cm, which



includes the Hushpuckney black shale and the lowest part of the Bethany Falls limestone (9 intervals). The total thickness of unweathered Stark black shale is about 48 cm (4 intervals).

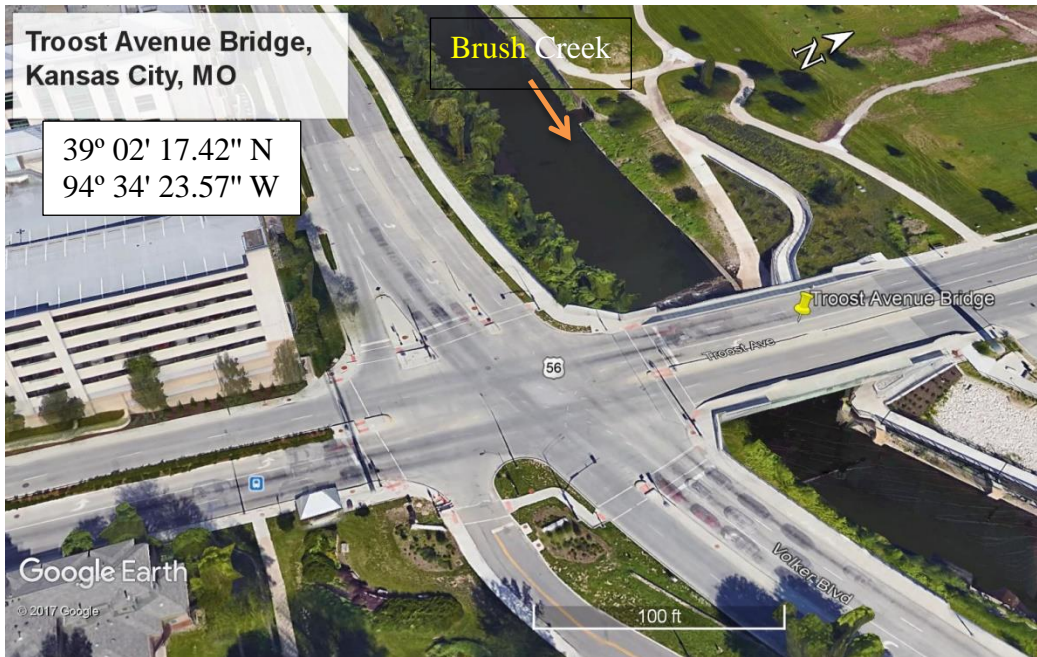


Figure 2.1 Troost Avenue Bridge (BR) location, Kansas City, MO



Figure 2.2 Greenwood (GW) quarry location- south of Greenwood, MO



Figure 2.3 Stark black shale (orange arrow) underlying the Winterset limestone at the Bannister Road and Blue River Road section (BBS). Kansas City, MO.



Figure 2.4. 87<sup>th</sup> and Blue River Road section (87<sup>th</sup> H) pointed with the red arrow.

Kansas City, MO



Figure 2.5. 63<sup>rd</sup> street section location along the ramp to southbound Interstate 435 (63<sup>rd</sup> H) circled with red line. Kansas City, MO.

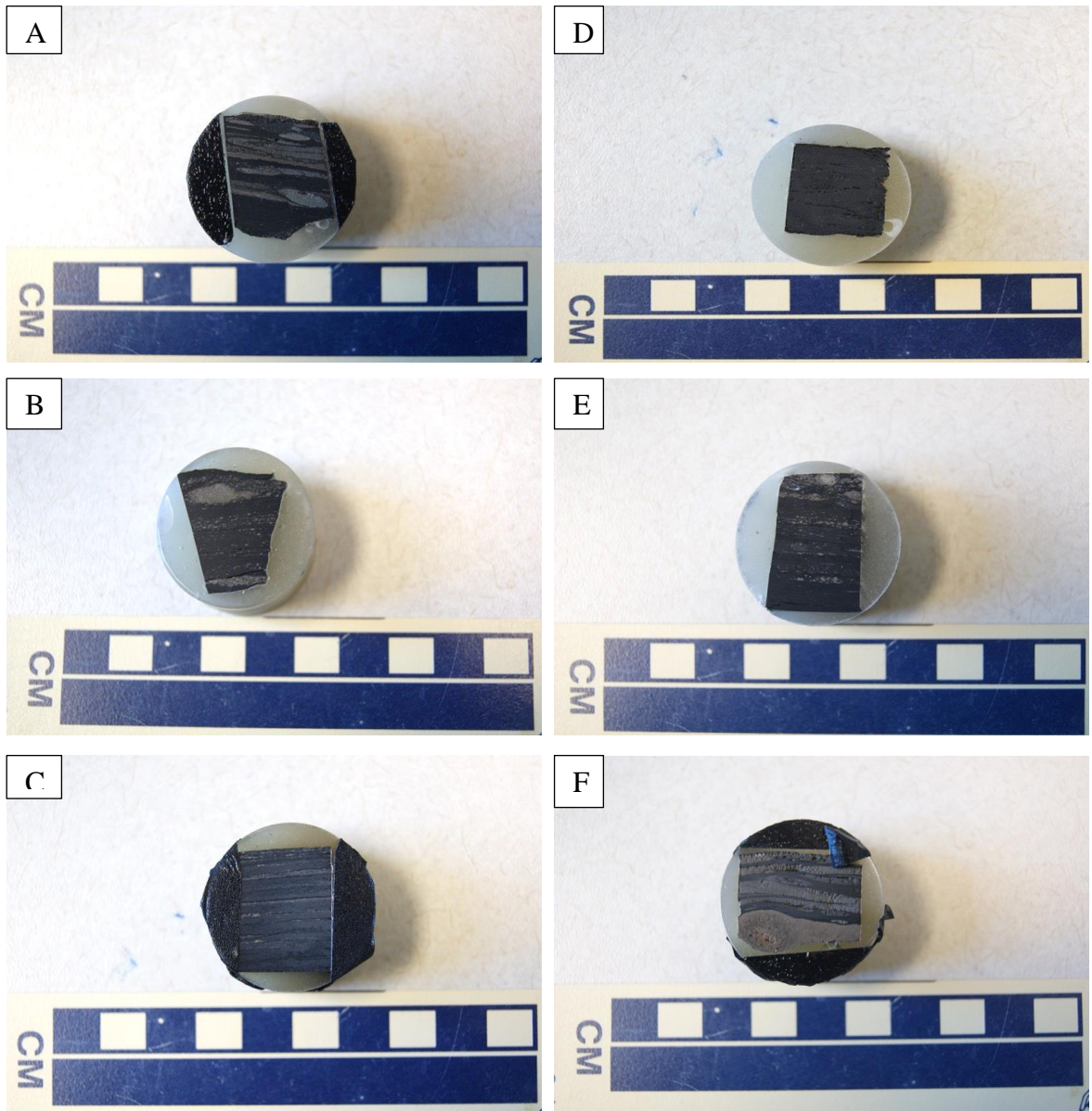


Figure 2.6. Polished mounts of Stark (A-C) and Hushpuckney (D-F) black shale samples.

## CHAPTER 3

### MINERALOGY

The mineralogical study of the Hushpuckney and Stark black shales showed that the two units contain the following minerals: clays (mainly illite, kaolinite  $\text{Al}_2\text{Si}_2\text{O}_5(\text{OH})_4$ , and Clinocllore), quartz ( $\text{SiO}_2$ ), carbonates (calcite -  $\text{CaCO}_3$ , and dolomite -  $\text{CaMg}(\text{CO}_3)_2$ ), fluorapatite ( $\text{Ca}_5(\text{PO}_4)_3\text{F}$ , “francolite”), pyrite ( $\text{FeS}_2$ ), sphalerite ( $\text{ZnS}$ ) and clausthalite ( $\text{PbSe}$ ). These minerals were detected by XRD and/or SEM. In addition, EDS revealed the presence of low-abundance minerals not detected by XRD, including chalcopyrite ( $\text{CuFeS}_2$ ), barite ( $\text{BaSO}_4$ ), rutile ( $\text{TiO}_2$ ) and mica.

#### **Clay Minerals**

Clay minerals in shales can provide information on the nature of the source rocks as well as the distance from these source materials (Weaver, 1958). They can also indicate changes in sedimentary environments when they have variable distribution in the stratigraphic column (Keller, 1963). The following clay minerals were identified in the black shales by the basal reflections (001) d-spacings (Grim, 1968; Carroll, 1970; Thorez, 1976; and Brindley and Brown, 1984): illite, kaolinite, and chlorite as shown in Figures 3-3 and 3-4 and Plates 3, 5, 6, 7, 8, 9, 10, 14 and 19. Those clay minerals were interpreted to be detrital in origin due to lack of well-formed crystals (Plate 16).

#### **Illite**

Illite is the most abundant clay mineral in shales and carbonates (Weaver, 1959 & 1967). The potassium ion ( $\text{K}^+$ ) fits very tightly into the interlayer exchangeable sites, making

illite very stable configuration. Also, it was noted by (Weaver, 1958 and 1960) that marine black shales are usually dominated by illite or illite-smectite mixed layer clays, while continental black shale are kaolinitic. In general, illite is stable in an alkaline, metal-rich environment such as the ocean (Keller, 1970 and Weaver & Pollard, 1975). Ness (2000) suggested that montmorillonite and kaolinite may be considered sources for illite formation by diagenetic alteration with increasing depth burial. Figures 3.3 and 3.4 show illite is relatively more abundant than the other clay minerals.

### **Kaolinite**

Kaolinite is considered to be a secondary mineral derived from the weathering of alumino-silicate minerals. Illite is more stable in marine sediments and kaolinite is more stable in freshwater sediments (Weaver, 1967). Illite forms where chelating processes in wet and warm (tropical) areas and evaporation rates favor removal of many ions as soluble salts. In contrast, kaolinite forms where alumina and silica are enriched and alkali cations are removed. Kaolinite can also be formed by extreme weathering and washing of granite and ferromagnesian rocks (Millot, 1970; Potter et al, 1980. Figures 3.3 and 3.4 show that the abundance of kaolinite is lower than that of illite in the shales.

### **Clinochlore**

Clinochlore is a member of the chlorite group. Chlorite is a very common accessory clay mineral. It is estimated to occur in 75-90 % of all sedimentary rocks with the bulk being of detrital origin (Weaver and Pollard, 1975). The formation of chlorite could be a major control in the early diagenesis of marine sediments. Drever (1971) suggested that Fe-chlorite could be a source of iron for anaerobic processes yielding pyrite and Mg-chlorite

(clinochlore), with a concomitant lowering of pH and possible carbonate dissolution. Figures 3.3 and 3.4 show the small clinochlore (001) peak along with the more intense illite and kaolinite (001) peaks.

### **Carbonate Minerals**

Calcite and dolomite are the main carbonate minerals in both black shale units Figures 3.1 and 3.2. Calcite shows different forms depending on whether it is primary or secondary as shown in Plates 1, 21 and 22. Dolomite exists as rhombohedra scattered in the black shale and in the overlying Bethany Falls limestone Plates 2, 7, 8, 9 and 14.

### **Quartz**

Quartz is distributed in the black and gray shales of both the Hushpuckney and Stark Members (Figures 3.1 and 3.2). Its grains are very small in size and it is associated with clay particles. Figures 3.3 and 3.4 and Plates 7 and 20 show its distribution through the element map.



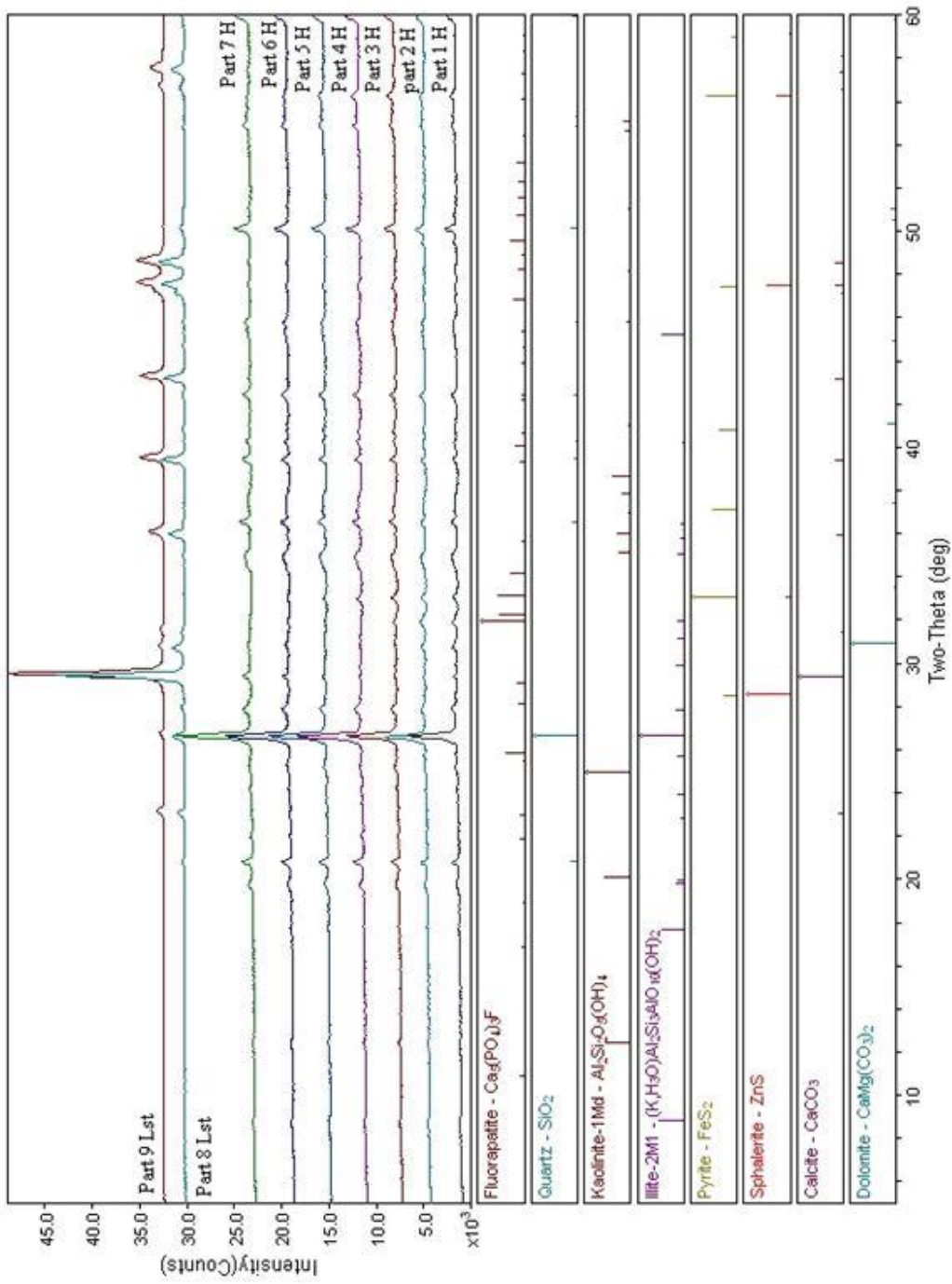


Figure 3.1. XRD powder pattern shows minerals for total sample of Hushpuckney black shale unit and Bethany Falls limestone (BR8).

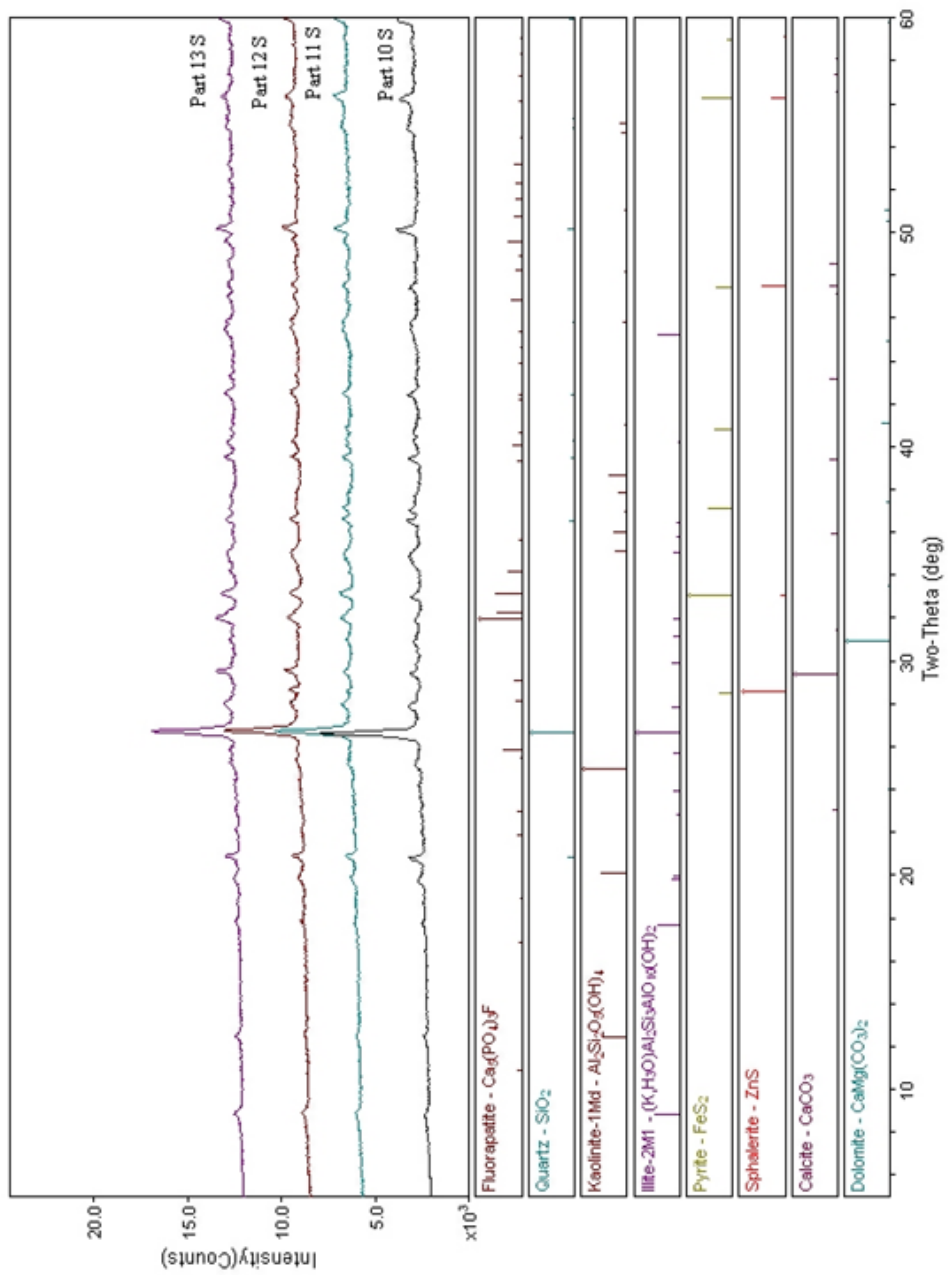


Figure 3.2. XRD powder pattern shows minerals for total sample of Stark black shale unit (BR8).

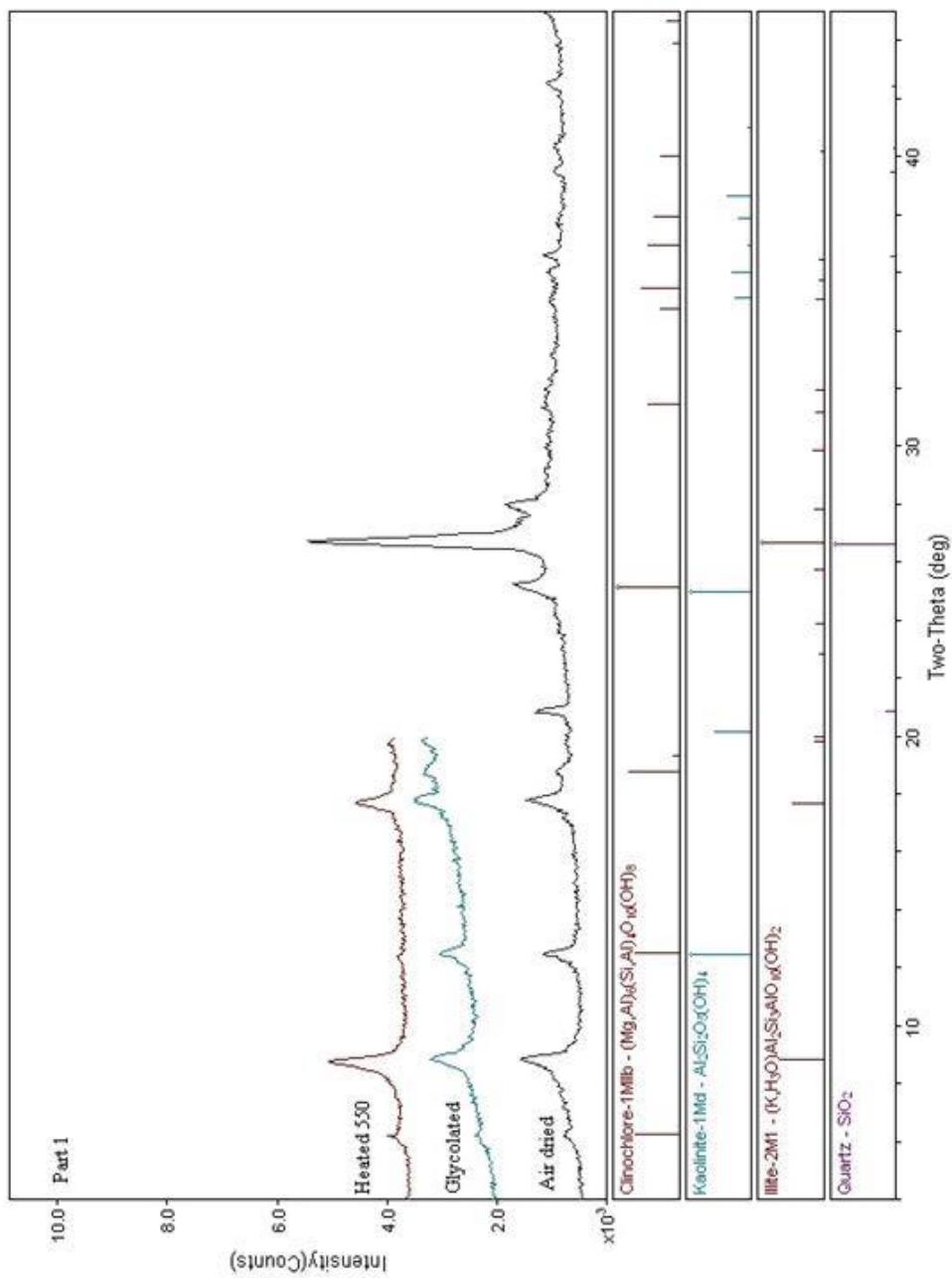


Figure 3.3. XRD pattern of clay oriented samples (Air dried, glycolated and heated to 550°) for Hushpuckney black shale unit

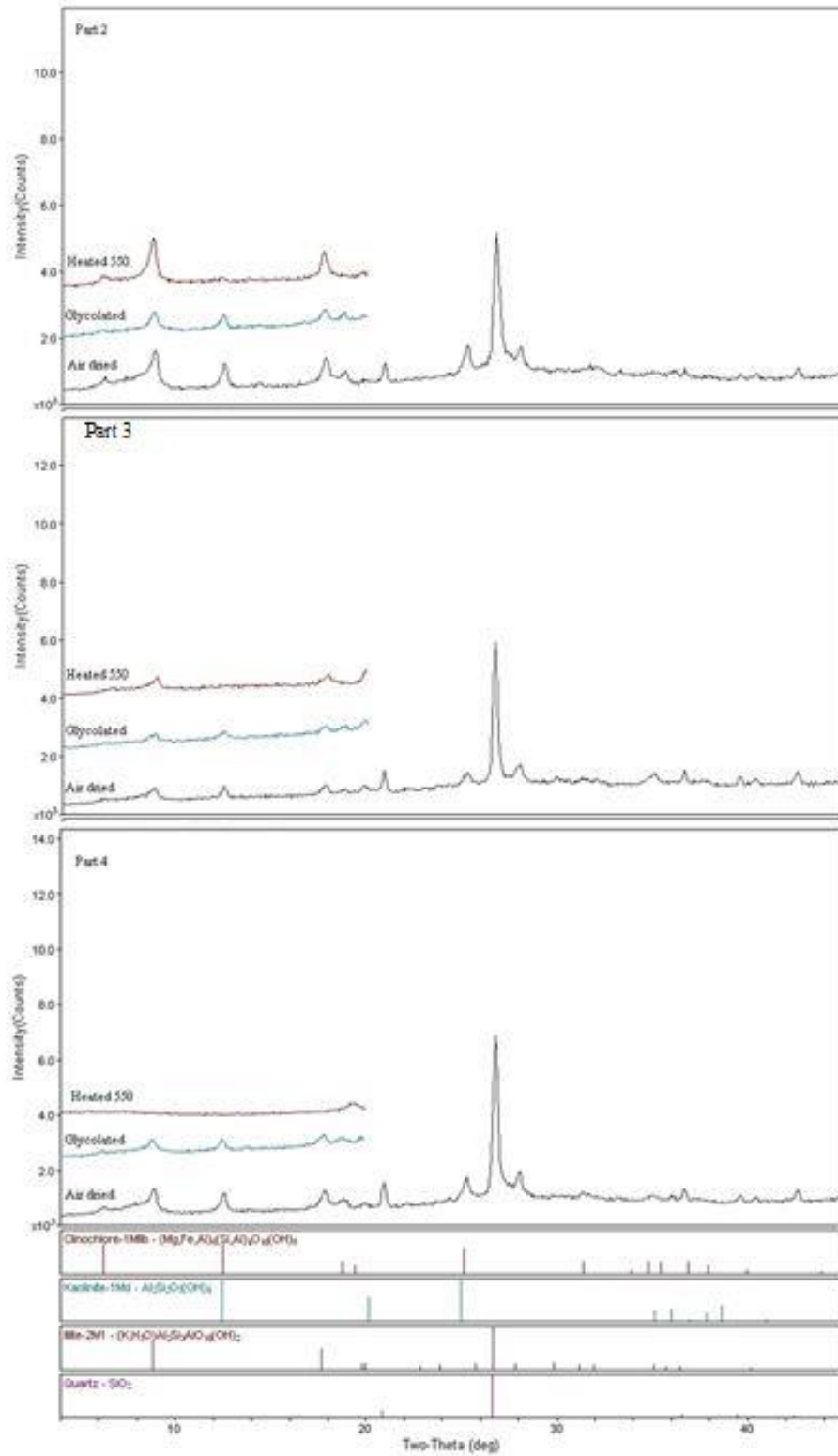


Figure 3.3 continued

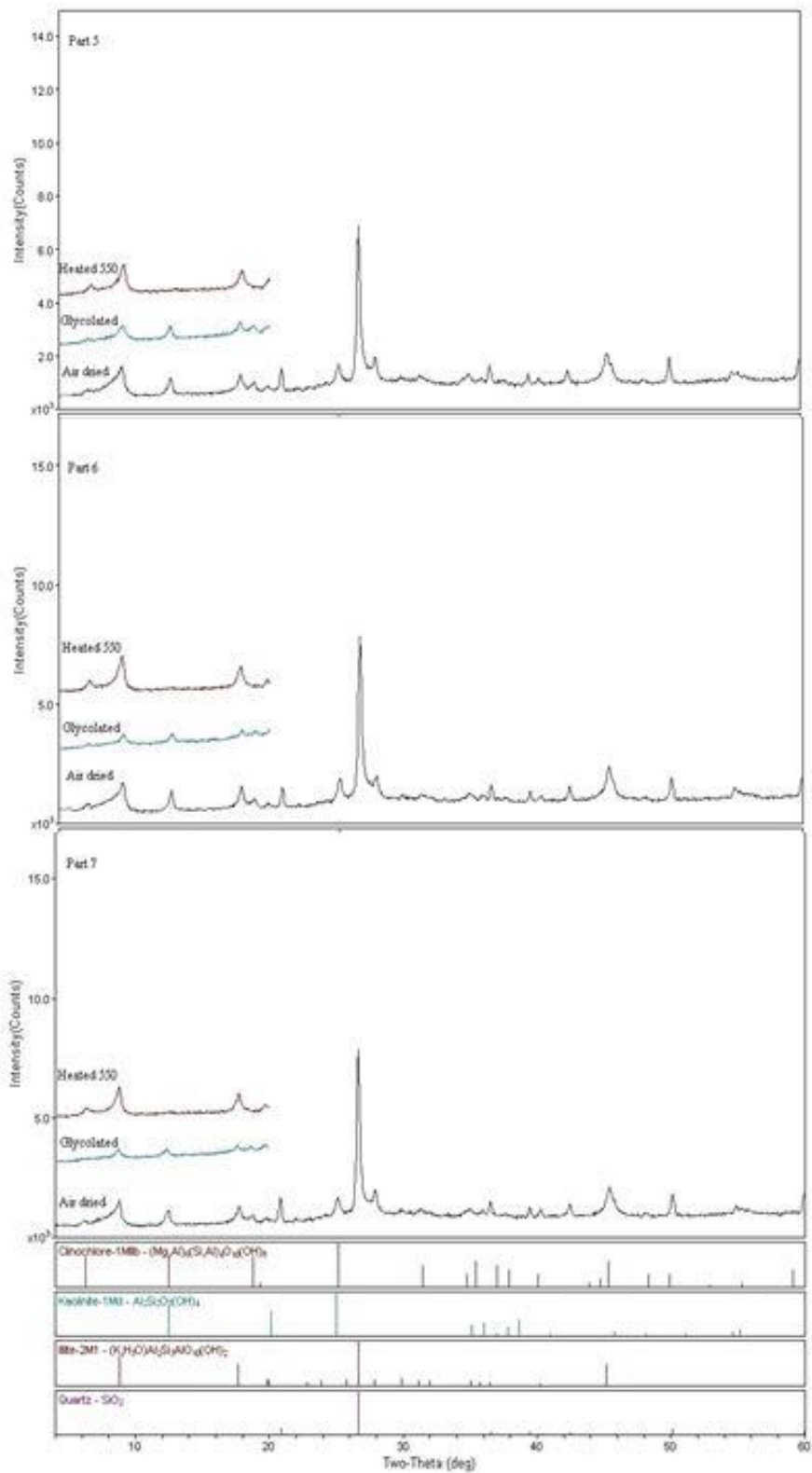


Figure 3.3 continued

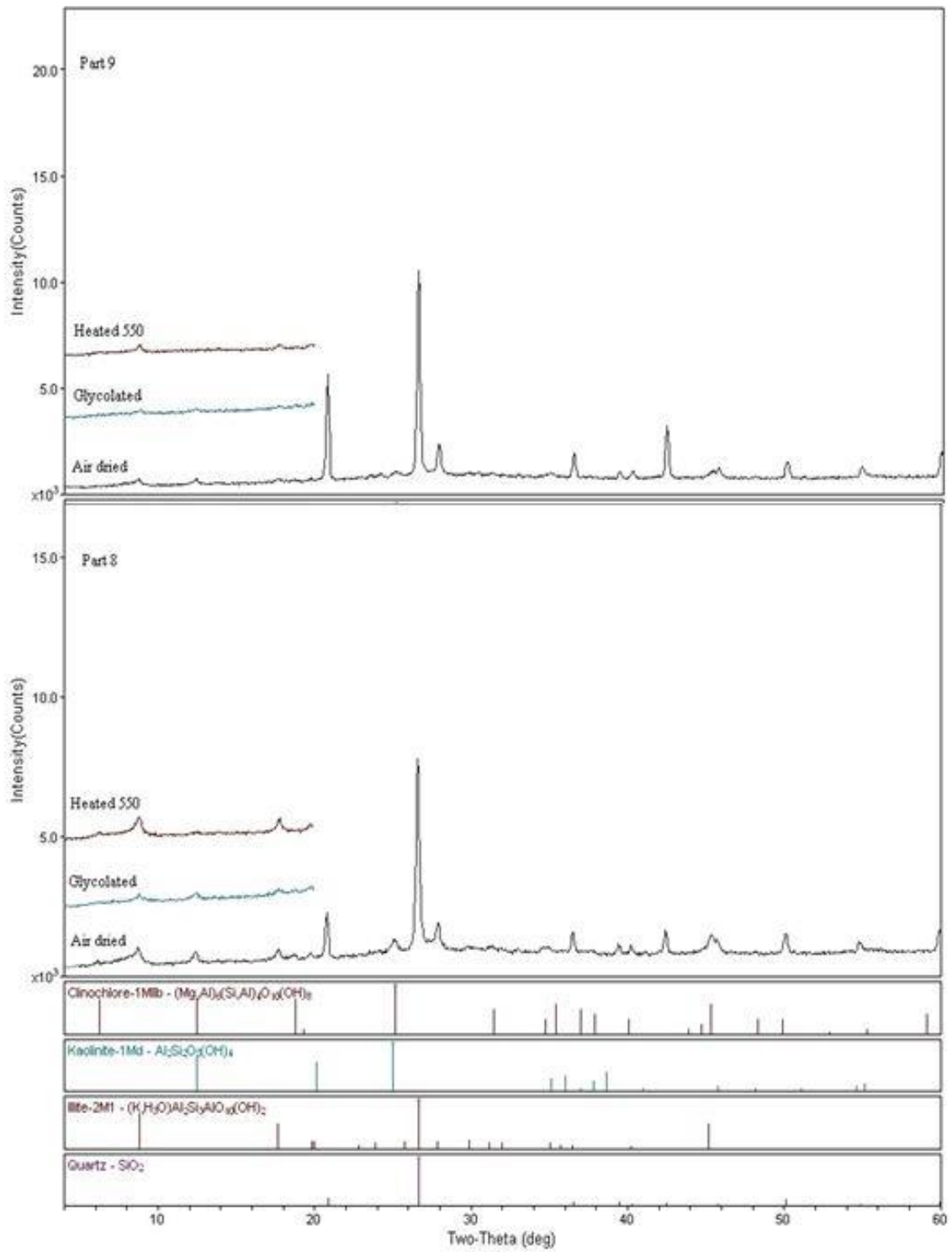


Figure 3.3 continued

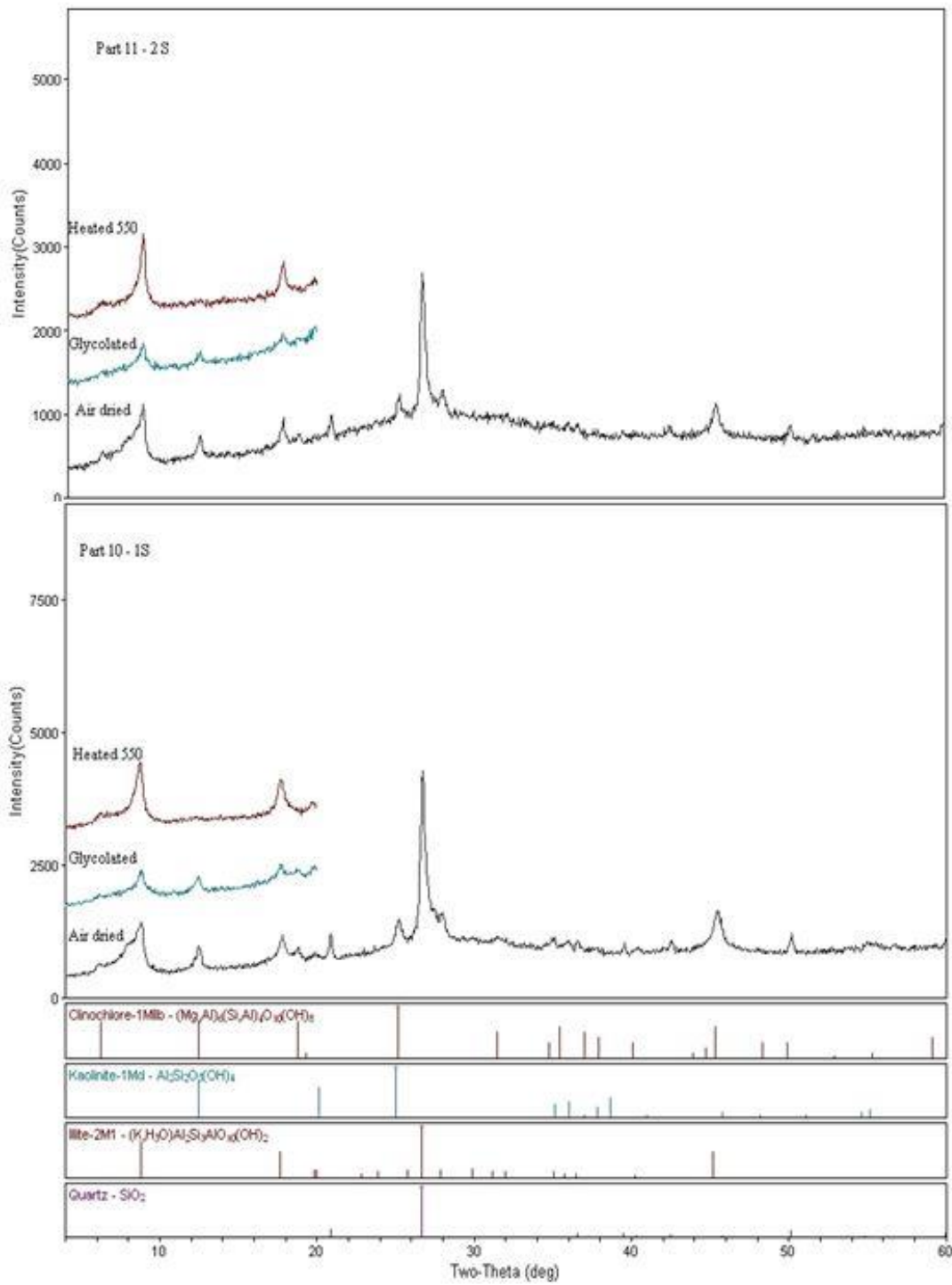


Figure 3.4. XRD pattern of clay oriented samples (Air dried, glycolated and heated to 550°) for Stark black shale unit

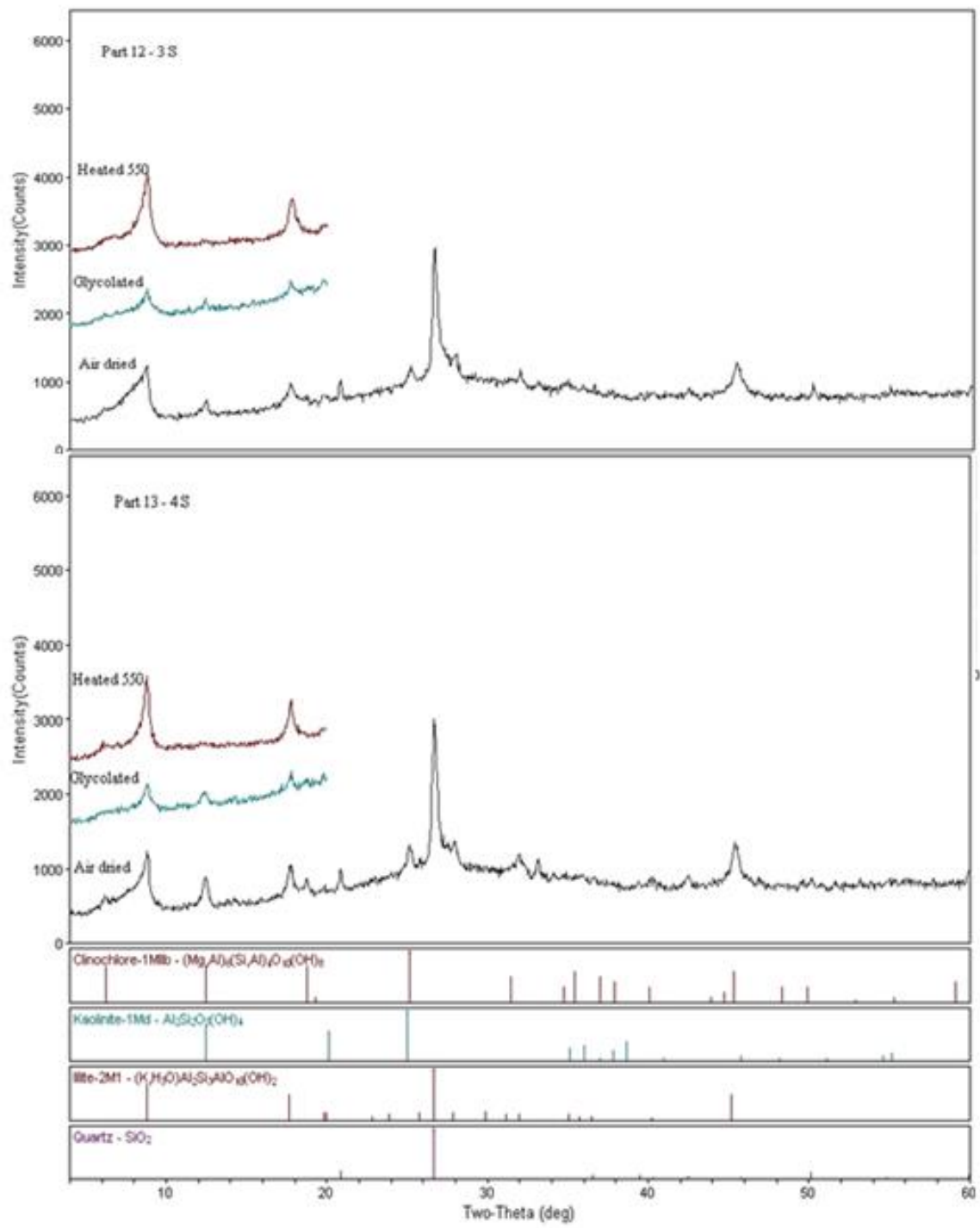


Figure 3.4 continued



## **Phosphate Minerals**

The phosphate mineral encountered in both black shale units is carbonate fluorapatite, which is traditionally called francolite. This mineral is always the sole constituent of phosphorites in unweathered or only slightly weathered sedimentary deposits, whatever their age or location (McClellan, 1980 and Prevot et al. 1989). Fluorapatite was identified by XRD as the major phosphate mineral in the studied samples. Although apatites commonly form hexagonal prisms, francolite in the studied shales occurs as very fine-grained crystalline aggregates in phosphate pellets as shown in Plates 1, 3, 4, 5, 6, 7, 8, 11, 12, 13, 18, 19, 20, 21 and 22. Some samples showed parts of conodonts (Plates 9 and 10). Figure 3.5 shows the XRD diagram and Figure 3.7 shows the EDS spectrum of fluorapatite.

## **Pyrite**

Pyrite is one of the most common minerals formed in reduced sedimentary environments. Pyrite forms in sediments as a consequence of the bacterial reduction of sea water sulphates (Berner 1982), thus highly pyritic shales must have formed under euxinic conditions where bacteriogenic  $H_2S$  exists at or above the sediment-water interface.  $H_2S$  will in turn react with  $Fe^{2+}$ , which was probably delivered into the basin as colloidal material adsorbed on clay minerals, to form iron sulphides. The presence of framboidal pyrite in black shale denotes the presence of a reducing environment during deposition. Such pyrite is commonly considered evidence of reducing environmental conditions during deposition of marine sediments and segregation between anoxic-euxinic and oxic environments in the water column (Wilkin et al, 1996; Suits & Wilkin, 1998; and Folk, R. L. 2005).

In this study, two types of pyrite were found, framboidal clusters and euhedral grains. The framboidal pyrites are widely scattered through the black shale (Plates 1, 3, 5, 7, 8, 9, 10, 13, 14, 19 and 20). The crystallites of the framboids have different sizes and are normally octahedral in shape (Plate 15). They are all loosely packed and readily disintegrate. The other type of pyrite occurs as few euhedral to subhedral grains embedded in the phosphate nodules (Plates 7, 11, 12, 13 and 20).

### **Sphalerite**

Sphalerite is considered to be the main ore mineral for zinc (Zn). It is formed under a wide range of low- to high-temperature hydrothermal conditions in different sedimentary rocks and incorporates iron (Fe), cadmium (Cd), and manganese (Mn) substituting for Zn, and selenium (Se) substituting for sulphur depending on temperature (Hibbard, 2002). The sphalerite observed in this study occurs as euhedral to subhedral grains within phosphate grains (Plate 17). It is always present exclusively near the edges of the phosphate grains (Plates 1, 3, 5, 6, 7, 8, 12, 13, 18, 19, 20, 21 and 22). Sometimes the sphalerite and clausthalite are found together in the phosphate grains as shown in Plates 3 and 5. Almost all the elemental maps indicate the presence of cadmium (Cd) in sphalerite. Figure 3.8 illustrates a typical sphalerite spectrum.

### **Clausthalite**

Clausthalite is a selenide mineral (PbSe) isostructural with galena (Pracejus, 2008). Many researchers have concluded that there is natural solid solution between clausthalite and galena and they form from low temperature hydrothermal solutions (Coleman, 1959; Tischendorf and Ungethum, 1964; and Healy and Petruk, 1992). Clausthalite in the black

shales exists as massive aggregates near the edges of, or filling the spaces between phosphate grains (Plates 3, 4 and 5). It was observed that there was a range of sulfur content within the clausthalite, indicating that the galena may be present with it in the form of solid solutions, as is evident from the elemental map (Plate 3 and 5). Also, it was noticed that the clausthalite was associated with sphalerite in phosphate grains as shown in Plates 3 and 5. Figure 3.6 shows the EDS spectrum for clausthalite.

### **Other Minerals**

Barite ( $\text{BaSO}_4$ ), chalcopyrite ( $\text{CuFeS}_2$ ), rutile ( $\text{TiO}_2$ ) and mica ( $\text{KAl}_2(\text{AlSi}_3\text{O}_{10})(\text{OH})_2$ ) were detected by SEM/EDS examination but not detected by XRD. Barite was found in the weathered samples, as aggregates and as single subhedral grains in black shale Plate 23. Barite precipitates within the marine sediments as an authigenic mineral. The release of barium ( $\text{Ba}^{2+}$ ) under reducing conditions within the sediments with seawater ( $\text{SO}_4^{2-}$ ) ions in solution to precipitate the diagenetic barite within the sedimentary rock sequences, often at the oxic-anoxic boundary (Bolz et al., 1974; Breheret and Brumsack, 2000). Under suboxic conditions, the diagenetic barite can be reprecipitated in sediments. Chalcopyrite was found in the Greenwood quarry samples. It was also detected by SEM/EDS in one sample as shown in Figure 3.9. Rutile was observed throughout the silicate-rich portions of the shales and its grains are smaller than quartz grains, and are likely detrital (Plates 3 and 5). Uncommon detrital mica grains were observed associated with clay particles as shown in Plate 24.

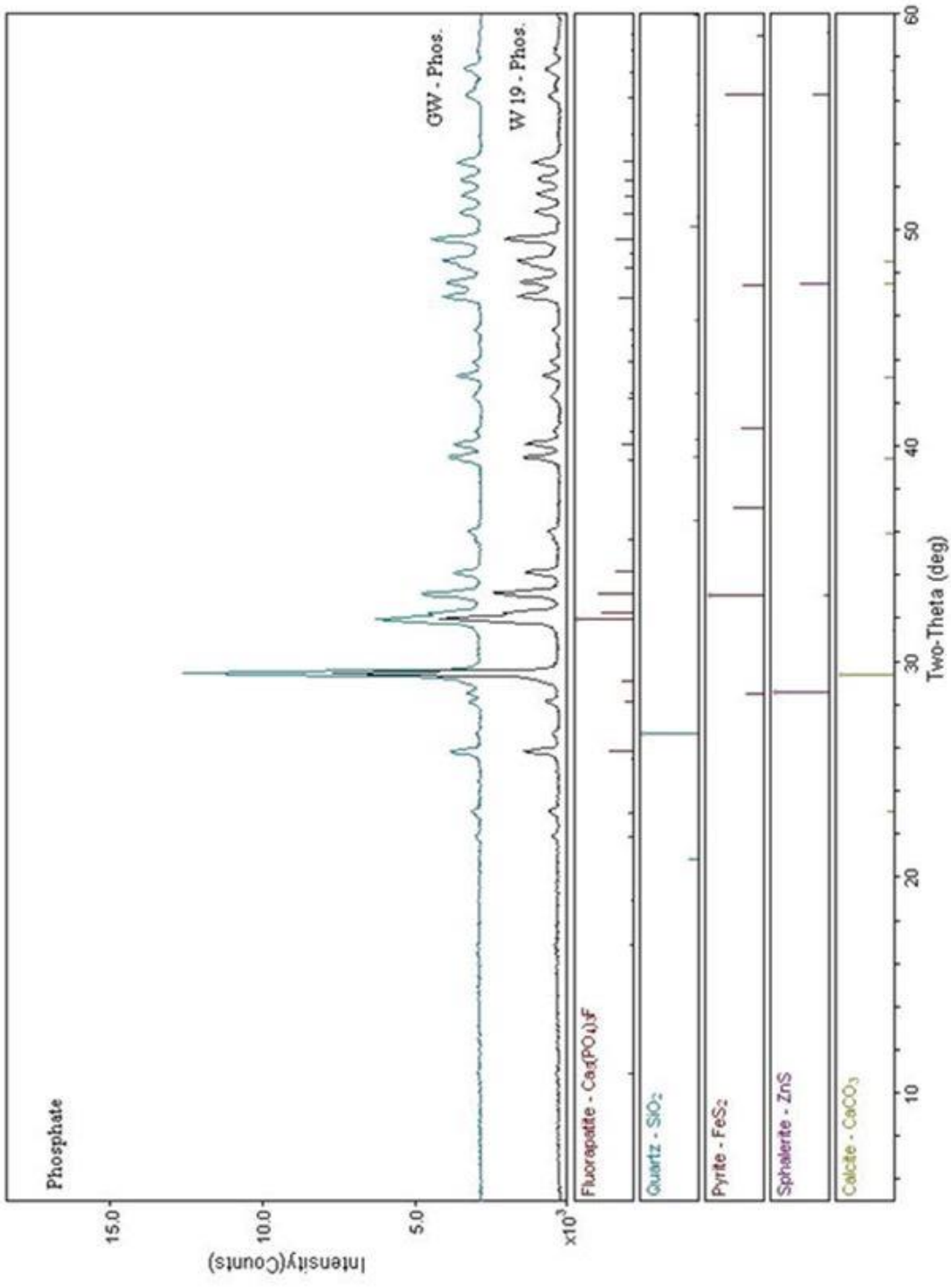
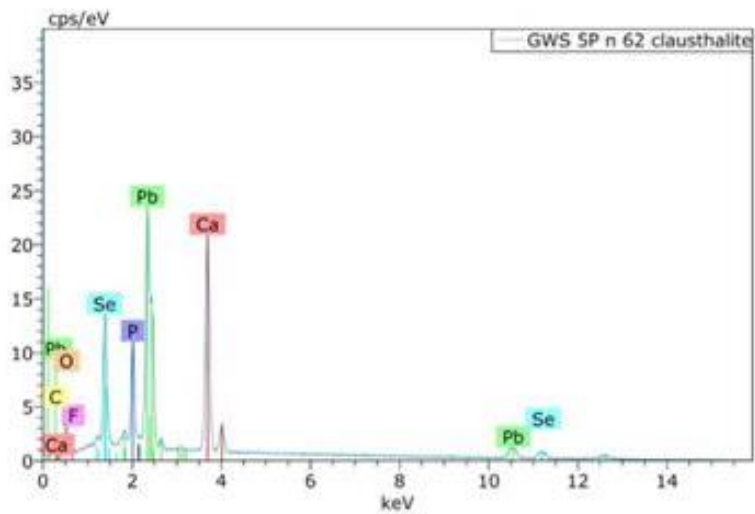
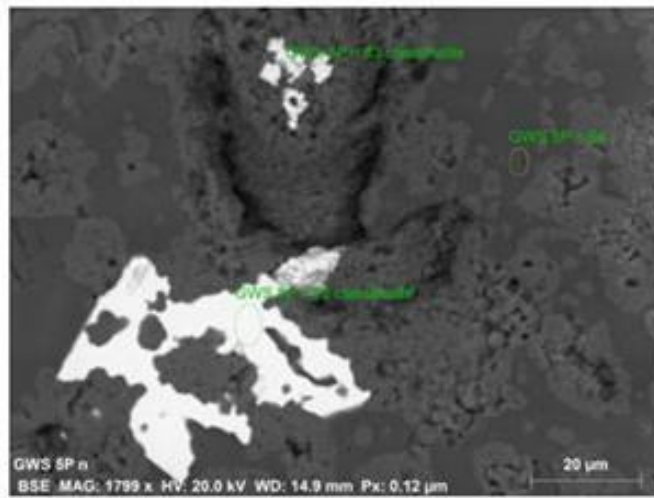


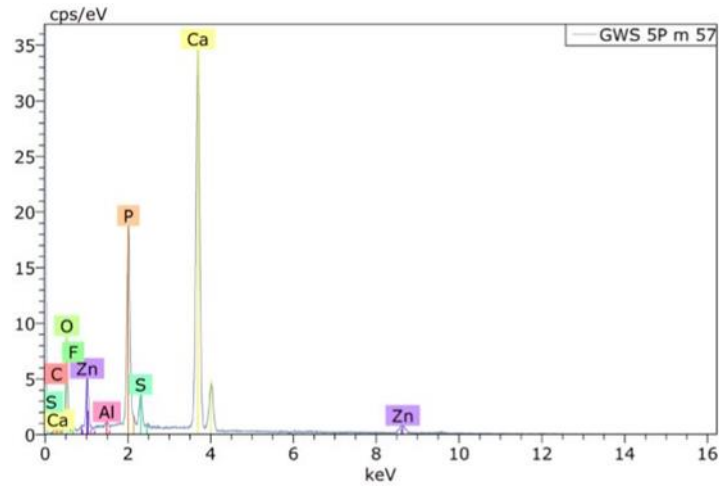
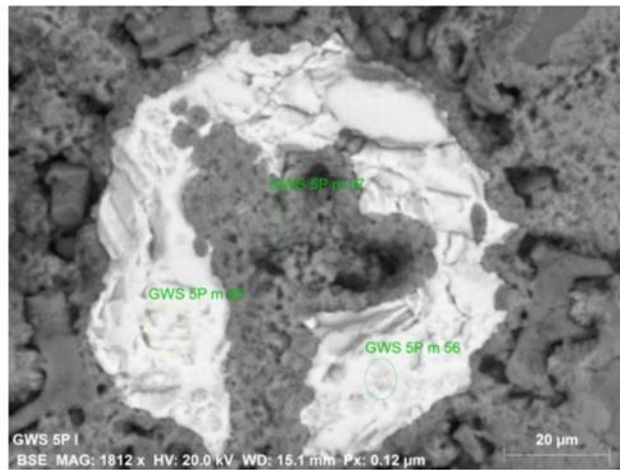
Figure 3.5. XRD powder diagram for the phosphate in Stark black shale unit



Spectrum: GWS 5P n 62 clausenthalite

El	AN	Series	unn. C [wt.%]	norm. C [wt.%]	Atom. C [at.%]	Error (1 Sigma) [wt.%]
C	6	K-series	4.86	6.52	19.30	0.69
O	8	K-series	12.74	17.07	37.97	1.57
F	9	K-series	0.97	1.31	2.45	0.19
P	15	K-series	4.61	6.18	7.10	0.20
Ca	20	K-series	19.06	25.54	22.67	0.58
Se	34	K-series	8.22	11.02	4.96	0.28
Pb	82	L-series	24.16	32.37	5.56	0.76
Total:			74.63	100.00	100.00	

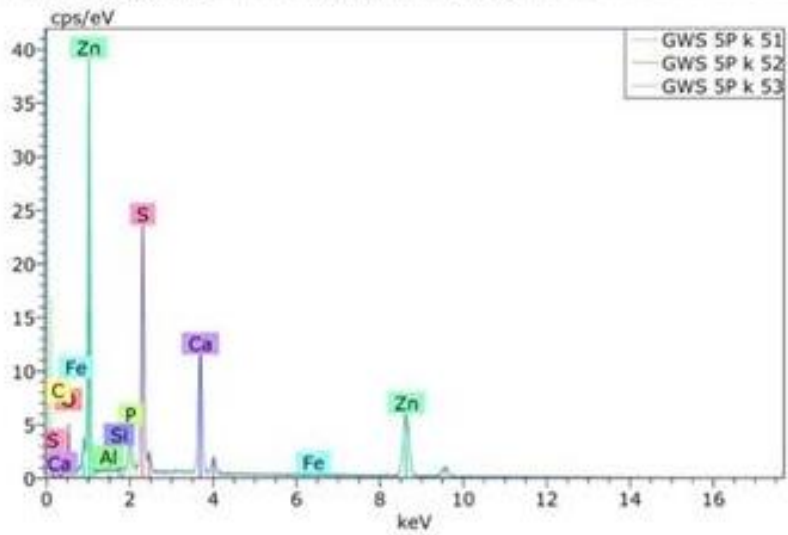
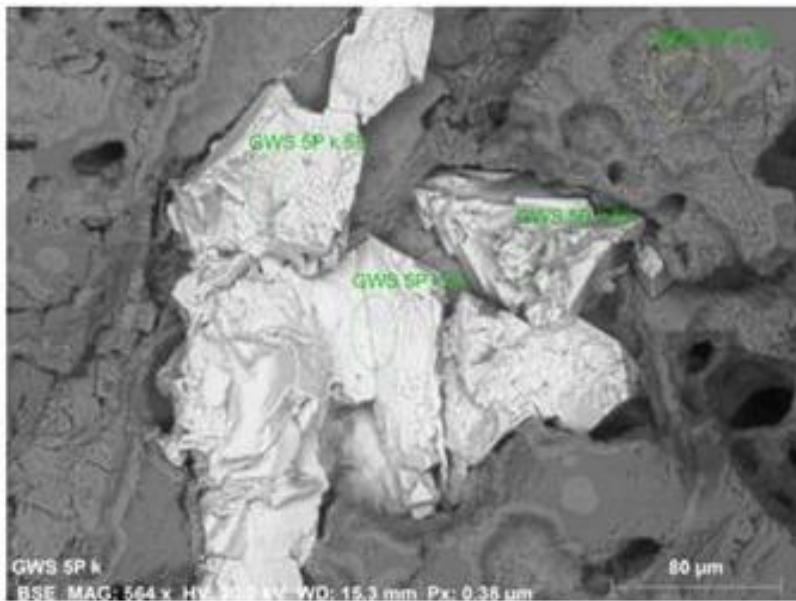
Figure 3.6. Clausenthalite EDS spectrum and composition in Stark black shale, Greenwood quarry, Greenwood, MO.



Spectrum: GWS 5P m 57

El	AN	Series	unn. C [wt.%]	norm. C [wt.%]	Atom. C [at.%]	Error (1 Sigma) [wt.%]
C	6	K-series	8.73	9.43	17.51	1.46
O	8	K-series	32.45	35.08	48.88	4.33
F	9	K-series	2.85	3.08	3.62	0.59
Al	13	K-series	0.22	0.23	0.19	0.04
P	15	K-series	8.76	9.47	6.82	0.37
S	16	K-series	1.64	1.77	1.23	0.09
Ca	20	K-series	33.50	36.21	20.14	1.01
Zn	30	K-series	4.36	4.72	1.61	0.17
Total:			92.51	100.00	100.00	

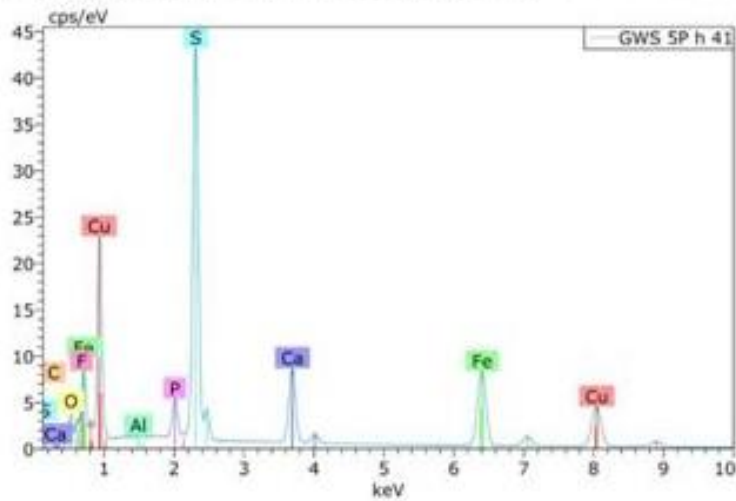
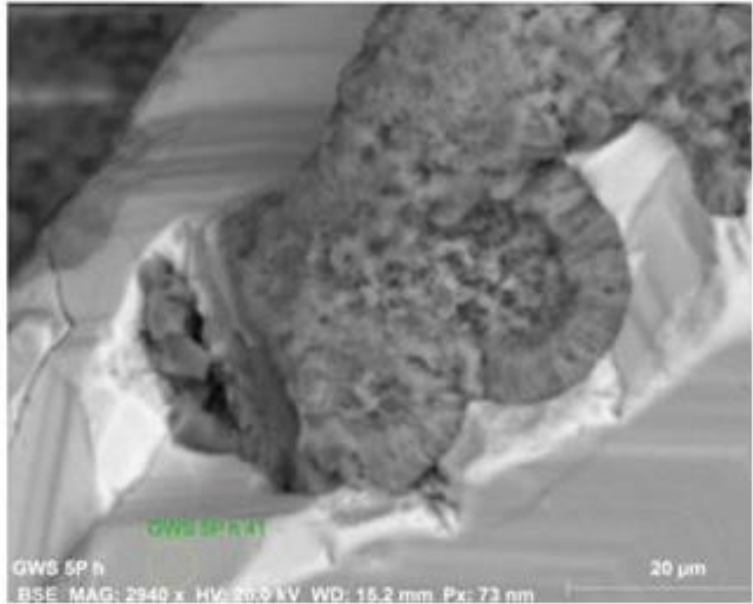
Figure 3.7. Fluorapatite EDS spectrum and composition, Stark black shale unit, Greenwood quarry, Greenwood, MO.



Atomic percent (%)

Spectrum	C	O	Al	Si	P	S	Ca	Fe	Zn
GWS 5P k 51	36.25	21.60	0.19	0.01	2.71	15.29	9.86	0.17	13.93
GWS 5P k 52	39.11	23.76	0.22	0.33	2.56	12.18	9.34	0.07	12.42
GWS 5P k 53	-	32.78	0.45	0.05	4.95	22.14	17.00	0.21	22.42
Mean value:	37.68	26.05	0.29	0.13	3.41	16.54	12.07	0.15	16.26
Sigma:	2.02	5.93	0.14	0.18	1.34	5.10	4.28	0.08	5.39
Sigma mean:	1.17	3.42	0.08	0.10	0.77	2.94	2.47	0.04	3.11

Figure 3.8. Sphalerite EDS spectrum and composition from Stark black shale unit, Greenwood quarry, Greenwood, MO.



Spectrum: GWS 5P h 41

El	AN	Series	unn. C [wt.%]	norm. C [wt.%]	Atom. C [at.%]	Error (1 Sigma) [wt.%]
C	6	K-series	11.56	13.78	33.09	1.48
O	8	K-series	7.72	9.20	16.59	0.95
F	9	K-series	0.27	0.32	0.49	0.07
Al	13	K-series	0.00	0.01	0.01	0.03
P	15	K-series	1.65	1.96	1.83	0.09
S	16	K-series	19.61	23.38	21.03	0.73
Ca	20	K-series	7.43	8.86	6.38	0.24
Fe	26	K-series	17.69	21.09	10.89	0.49
Cu	29	K-series	17.95	21.40	9.71	0.51

Total: 83.87 100.00 100.00

Figure 3.9. Chalcopyrite EDS spectrum in Stark black shale, Greenwood quarry, Greenwood, MO.



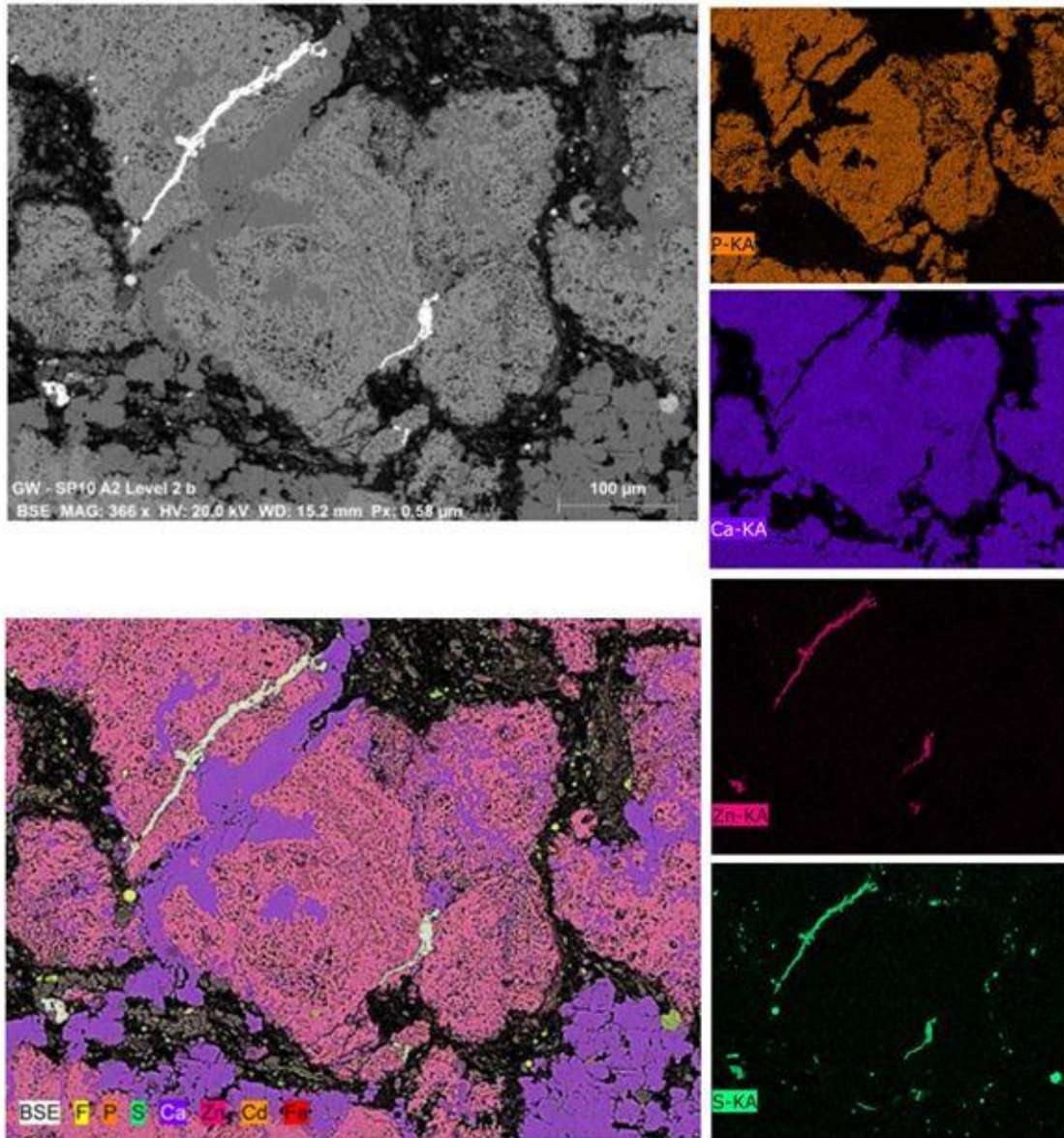


Plate1: EDS maps for Stark shale. Top left, backscattered electron image. Bottom left, composite elemental map with BSE image. Small images on right: individual elemental maps for P, Ca, Zn, and S showing distribution of secondary calcite (purple), P and Ca in phosphate clot, Zn and S in sphalerite. Sphalerite is filling the space between phosphate grains. Stark shale GW- SP10, Greenwood quarry, Greenwood, MO.

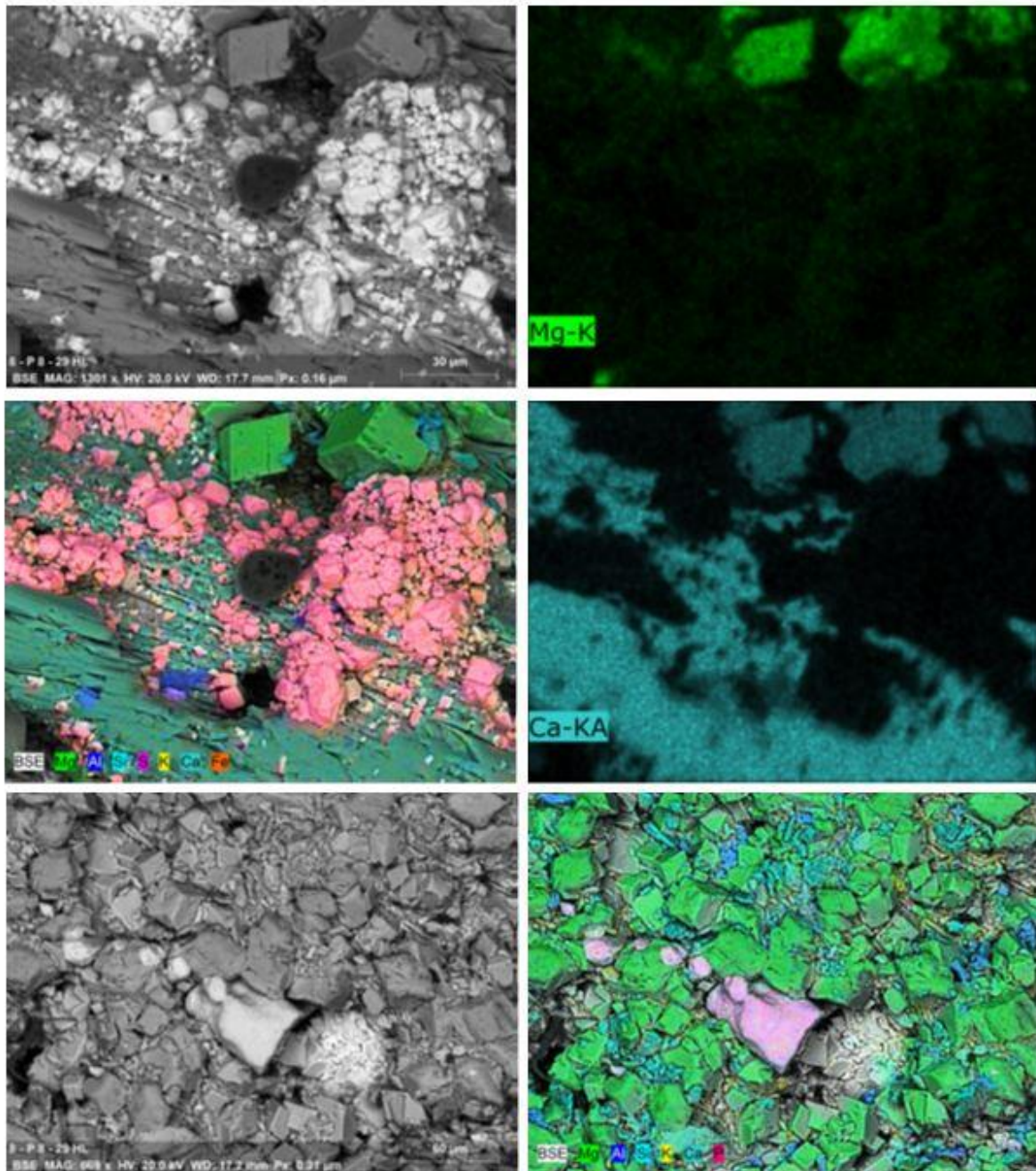


Plate 2: EDS maps for Hushpuckney shale. Top left, backscattered electron image. Middle left, composite elemental map with BSE image. Images on top and middle right: individual elemental maps Mg and Ca showing dolomite rhombs scattered in shale. Bottom left, backscattered electron image. Bottom right, composite elemental map with BSE image showing different size of dolomite rhombs. Hushpuckney shale BR8 – Kansas City, MO.

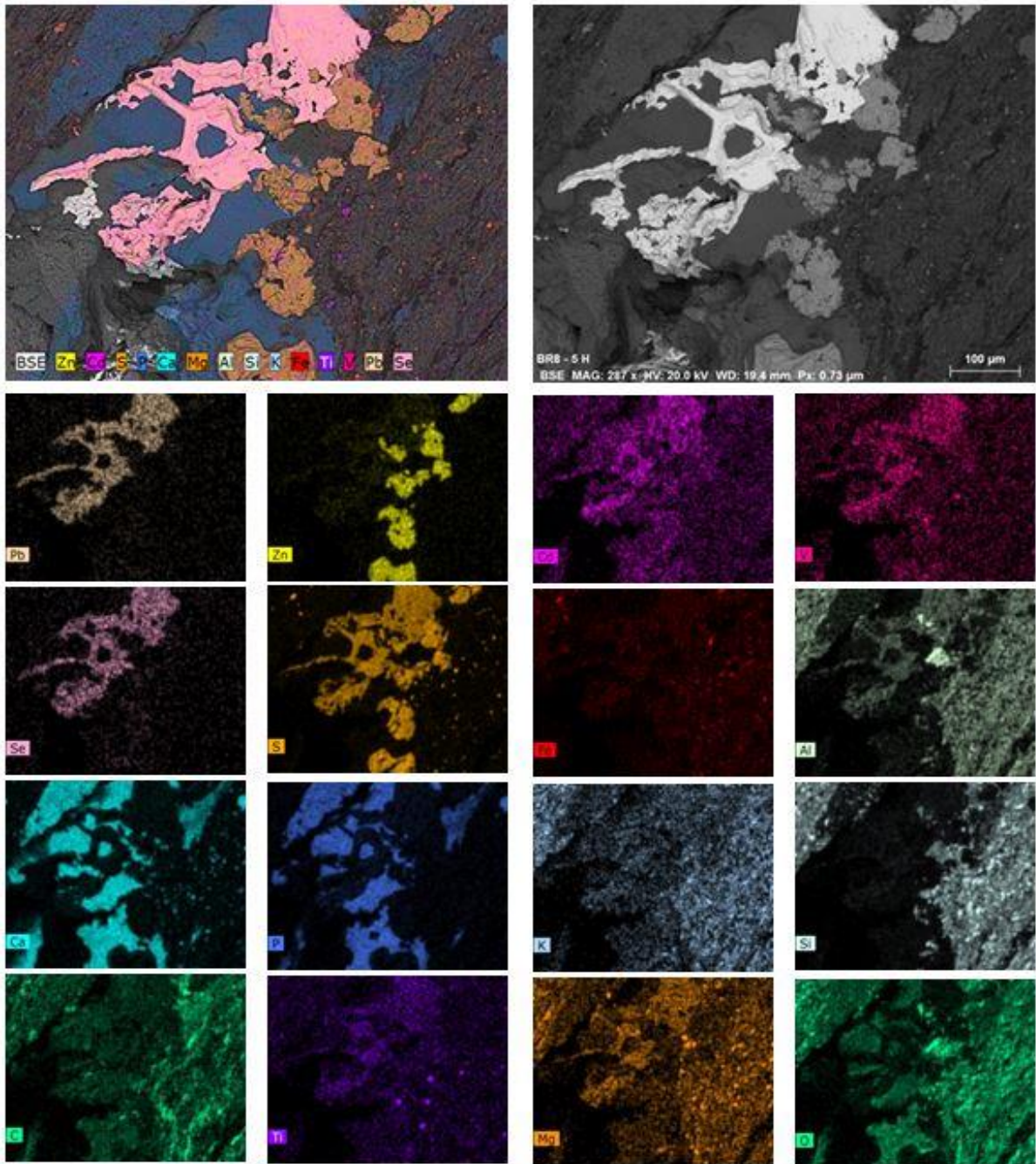


Plate 3: EDS maps for Hushpuckney shale. Top right, backscattered electron image. Top left, composite elemental map with BSE image. Small images: individual elemental maps for Pb, Zn, Cd, V, Se, S, Fe, Al, Si, K, P, Ca, C, Ti, Mg and O showing distribution of clausthalite (Pb, Se), sphalerite (Zn, S), framboidal pyrite (Fe, S), phosphate (P, Ca), clays (Al, Si, K),

quartz (Si, O), dolomite (Mg, Ca), organic matter (C), and Rutile (Ti, O). Sulfur elemental map shows association with Se and Pb. Cd and V elemental maps show association with sphalerite and clausthalite respectively. Hushpuckney shale sample BR8- 5H, Kansas City, Mo.

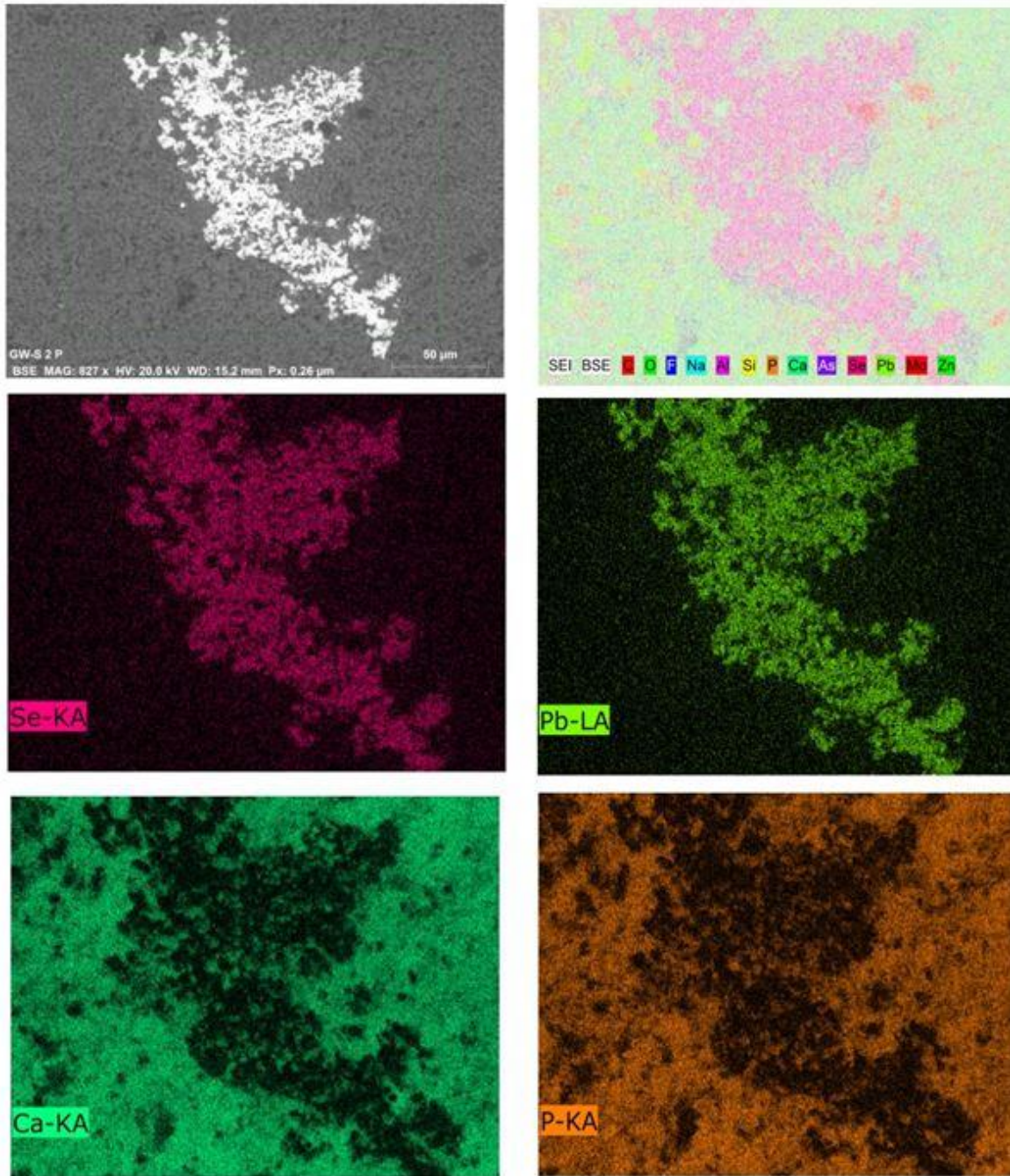


Plate 4: EDS maps for Stark shale. Top left, backscattered electron image. Top right, composite elemental map with BSE image. Individual elemental maps for Pb, Se, Ca, and P showing dissemination of clausthalite (Pb, Se) in phosphate (P, Ca). Stark shale sample GW- 5, Greenwood quarry, Greenwood, MO.

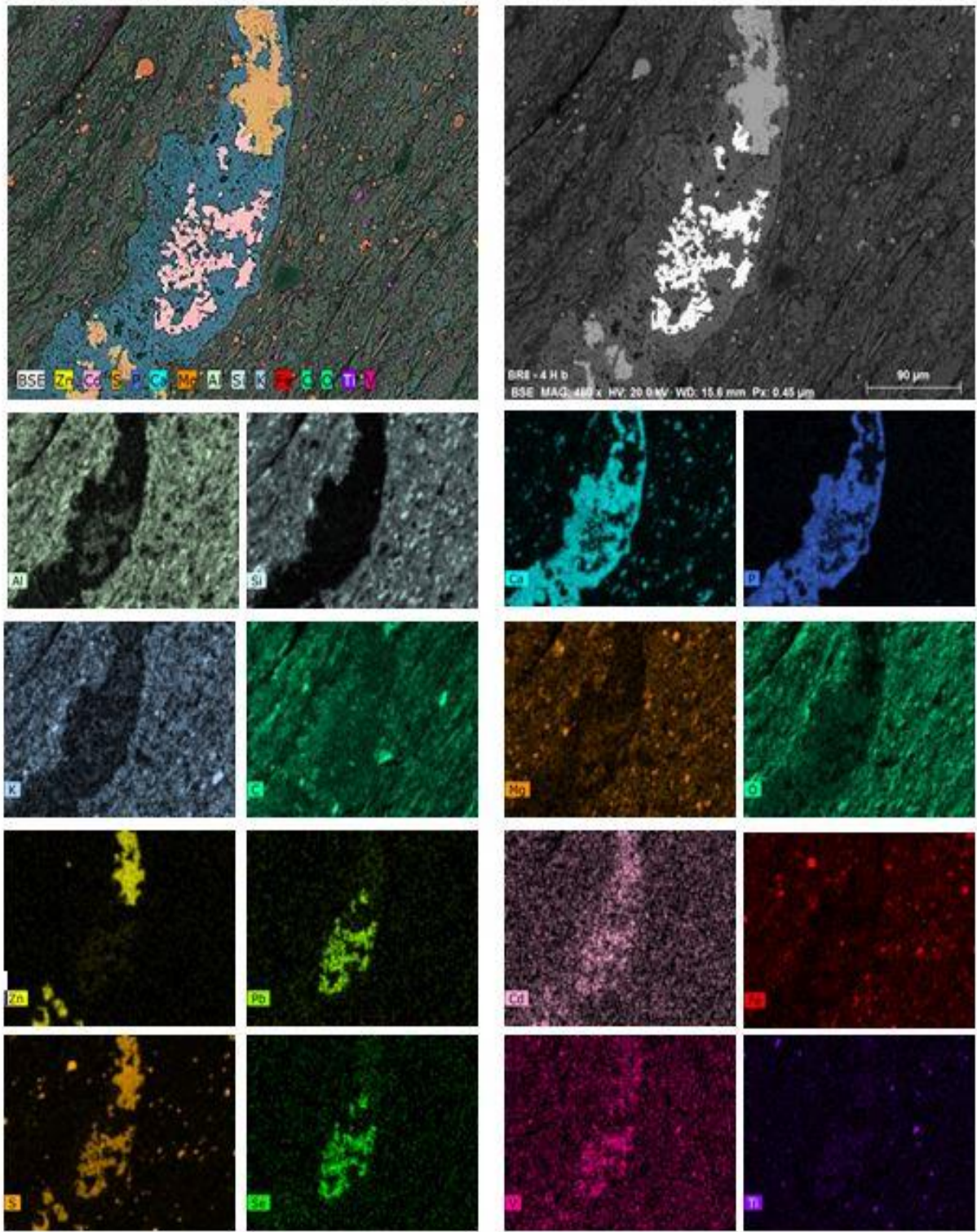


Plate 5: EDS maps for Hushpuckney shale. Top right, backscattered electron image. Top left, composite elemental map with BSE image. Small images: individual elemental maps for Al,

Si, Ca, P, K, C, Mg, O, Zn, Pb, Cd, Fe, S, Se, V and Ti showing distribution of clausthalite (Pb, Se), sphalerite (Zn, S), framboidal pyrite (Fe, S), phosphate (P, Ca), clays (Al, Si, K), quartz (Si, O), dolomite (Mg, Ca), organic matter (C), and Rutile (Ti, O). Sulfur elemental map shows association with Se and Pb. Cd and V elemental maps show association with sphalerite and clausthalite respectively. Hushpuckney shale sample BR8- 4H-b, Kansas City, MO.

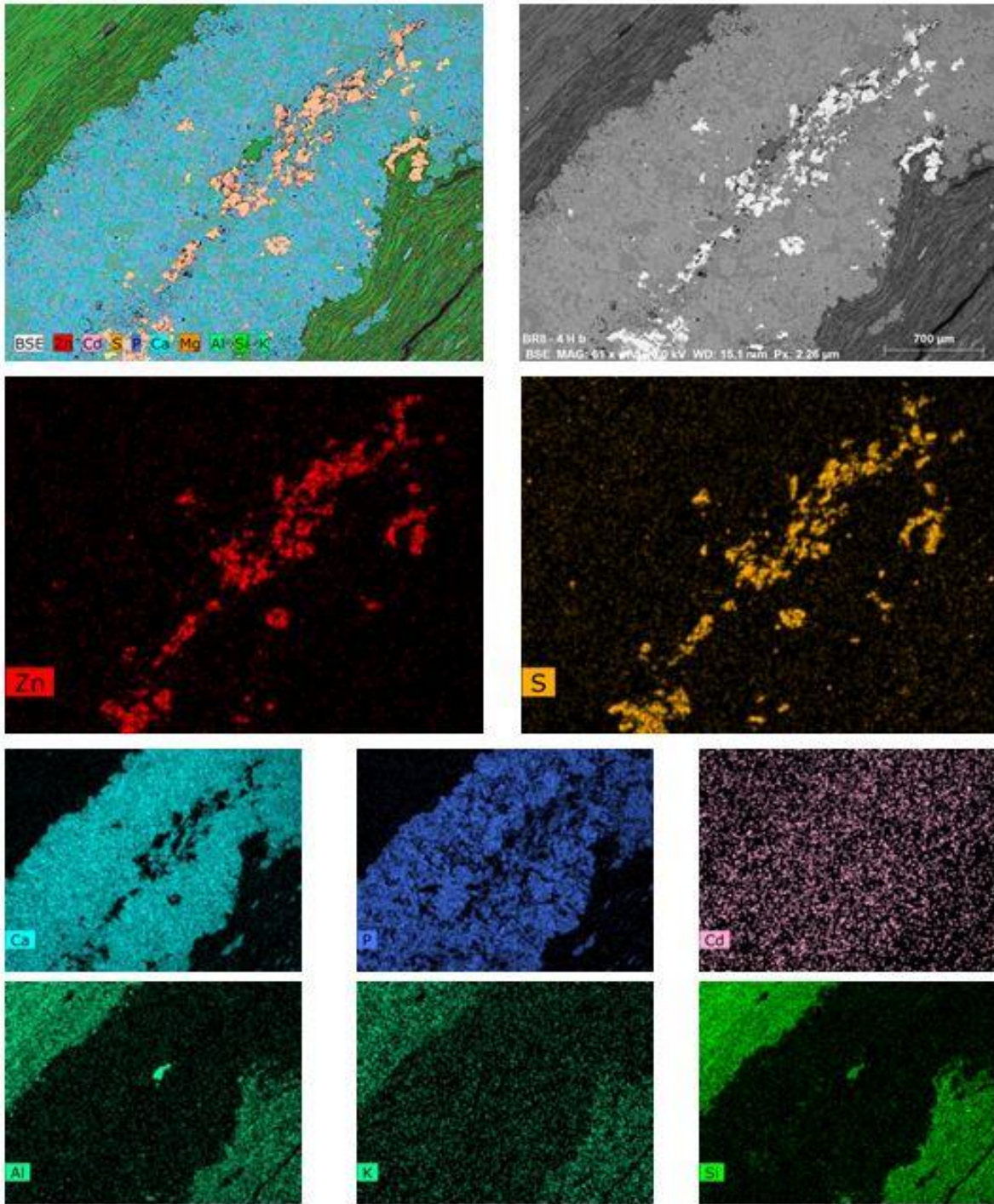


Plate 6: EDS maps for Hushpuckney shale. Top right, backscattered electron image. Top left, composite elemental map with BSE image. individual elemental maps for Zn, S, Cd, P, Ca, Al, Si, and K showing distribution of sphalerite (Zn, S), phosphate (P, Ca), clays (Al, Si, K).



Cd elemental map shows association with sphalerite and phosphate respectively. Calcium element map indicates more presence than phosphorus in phosphate nodules as secondary calcite. Al and Si element maps show the presence of possible dickite, a hydrothermal clay in the kaolinite group. Hushpuckney shale sample BR8- 4H-b, Kansas City, Mo.

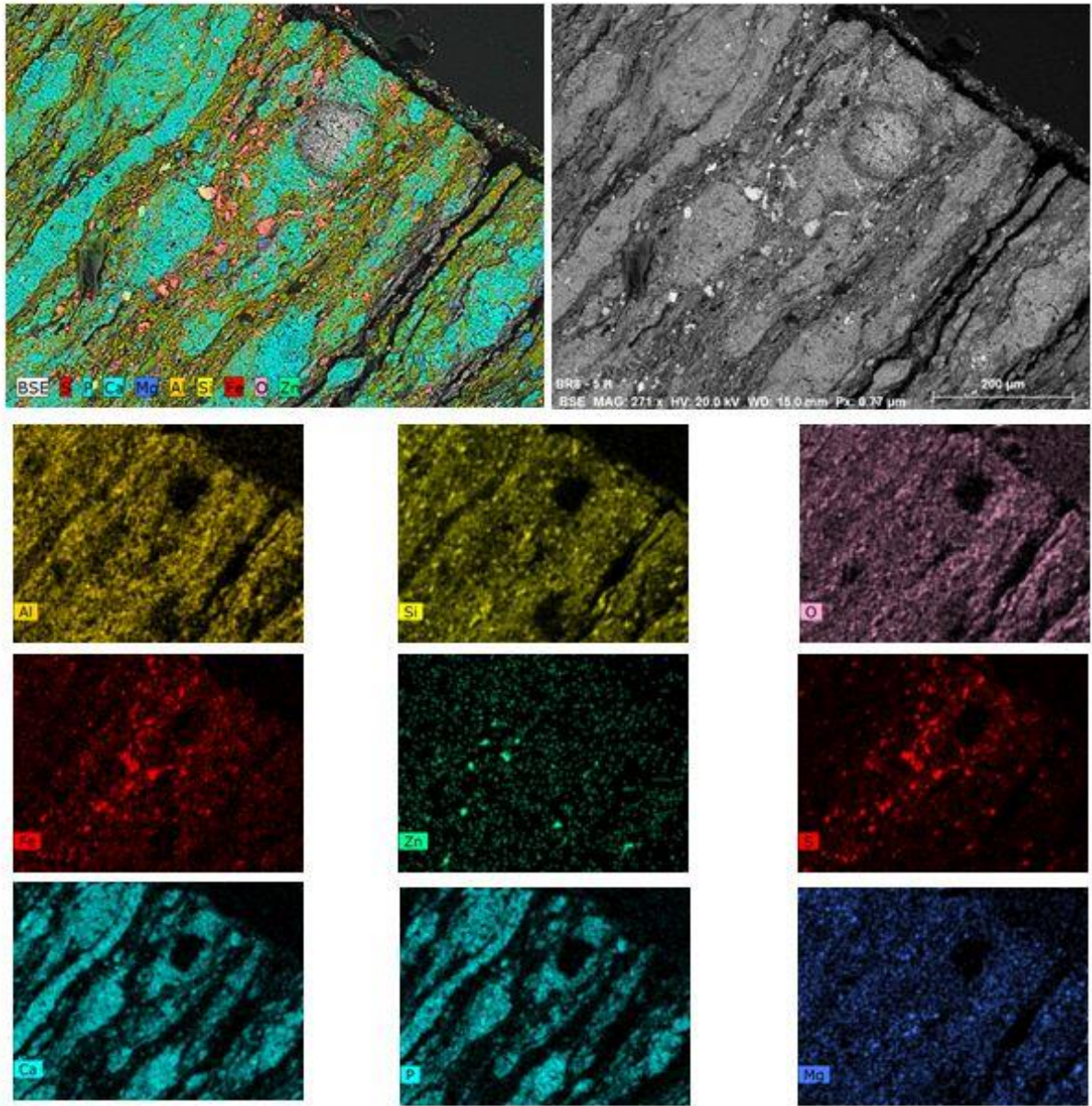


Plate 7: EDS maps for Hushpuckney shale. Top right, backscattered electron image. Top left, composite elemental map with BSE image. Small images: individual elemental maps for Al, Si, O, S, Zn, Fe, Ca, P and Mg showing distribution of sphalerite (Zn, S), framboidal pyrite and pyrite (Fe, S), phosphate (P, Ca), clays (Al, Si), dolomite (Mg, Ca), and quartz (Si, O). Framboidal pyrite scattered in shale whereas pyrite disseminated in phosphate. Hushpuckney shale sample BR8- 5H, Kansas City, MO.

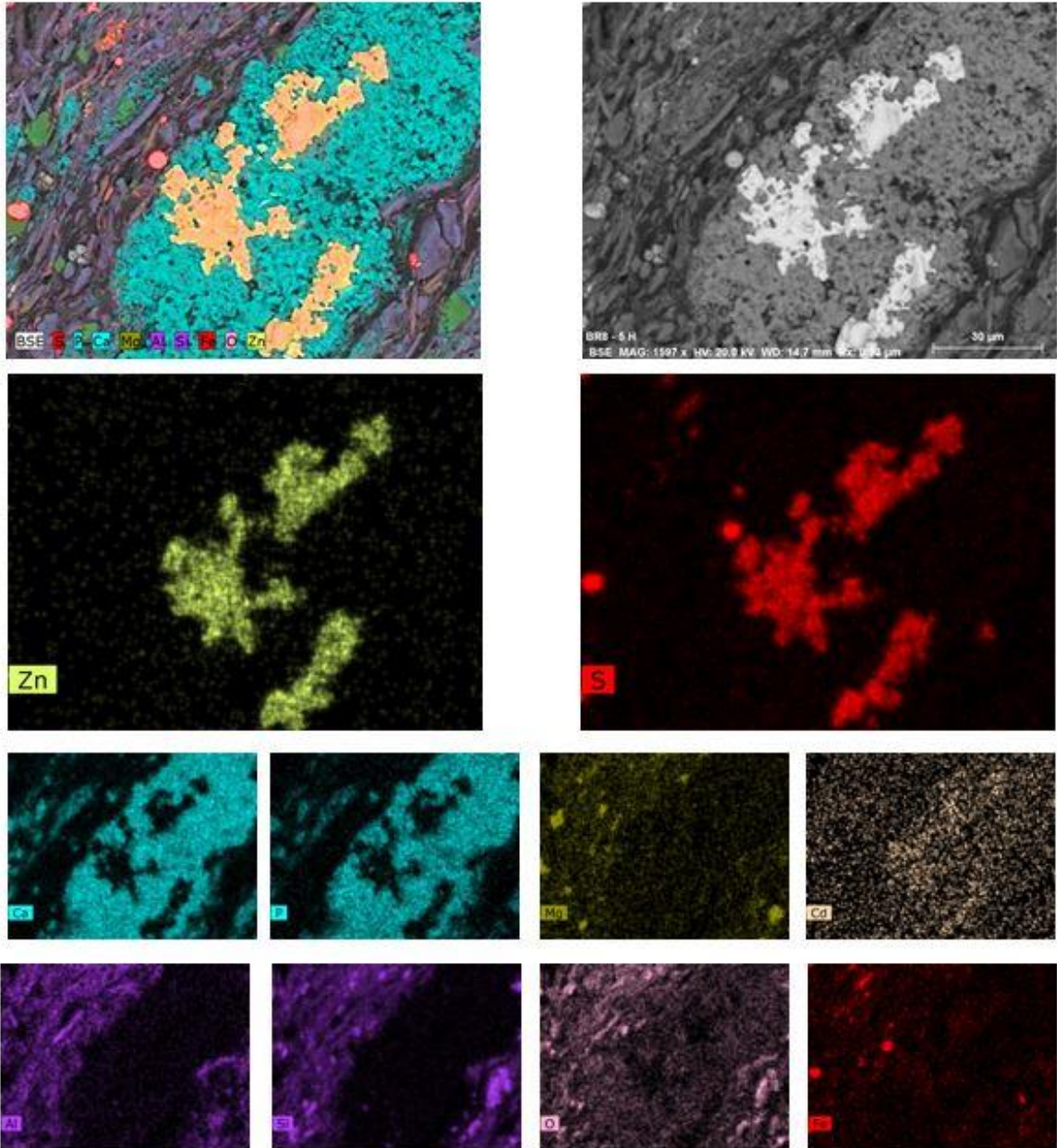


Plate 8: EDS maps for Hushpuckney. Top right, backscattered electron image. Top left, composite elemental map with BSE image. Small and large images: individual elemental maps for Zn, S, Cd, Mg, P, Ca, Al, Si, O and Fe showing distribution of sphalerite (Zn, S), framboidal pyrite (Fe, S), phosphate (P, Ca), clays (Al, Si), quartz (Si, O), and dolomite (Ca, Mg). Cd elemental map shows traces with sphalerite. Hushpuckney shale sample BR8- 5H, Kansas City, MO.

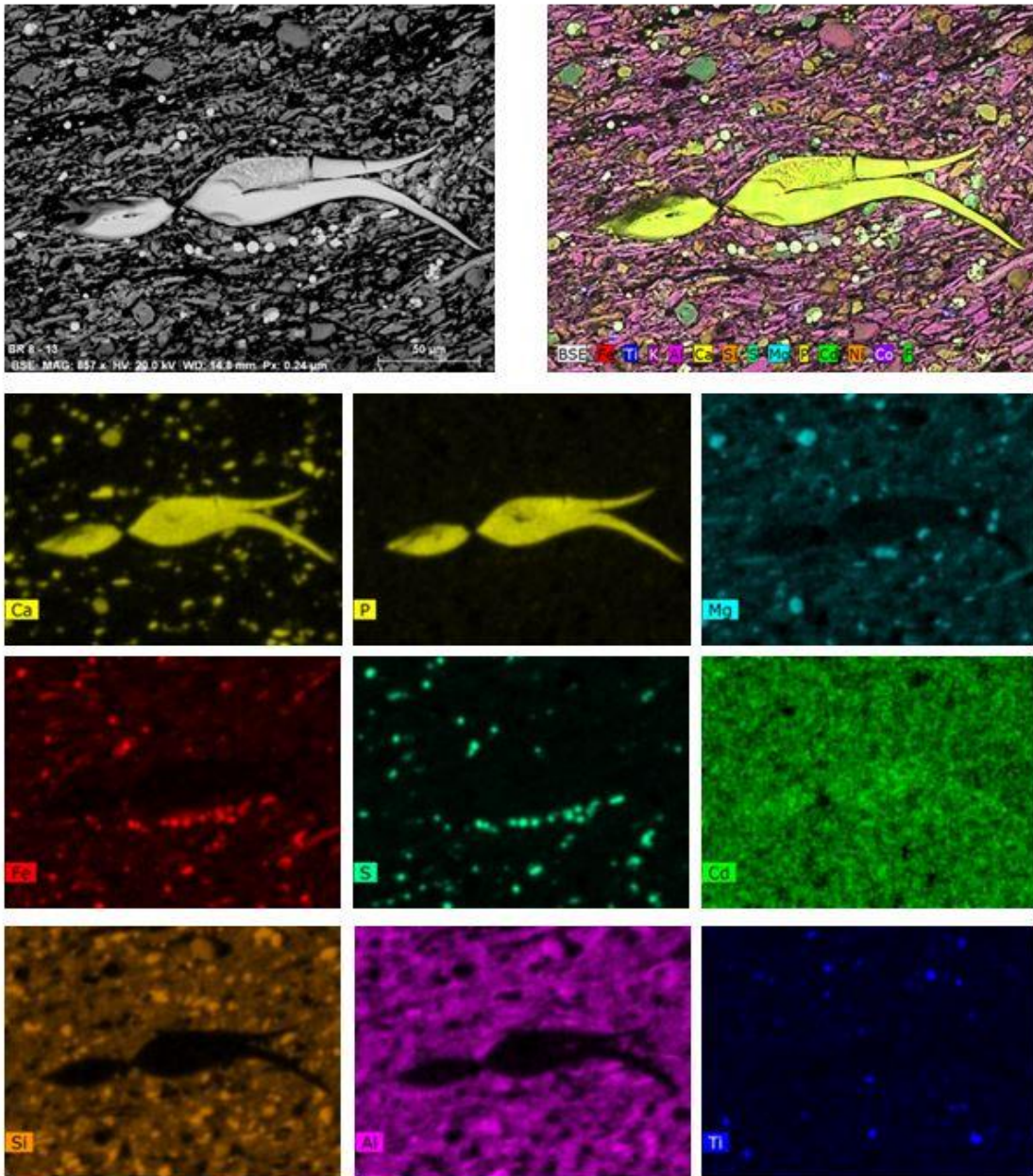


Plate 9: EDS maps for Hushpuckney shale. Top left, backscattered electron image. Top right, composite elemental map with BSE image. Small images: individual elemental maps for Ca, P, Mg, Fe, S, Cd, Si, Al and Ti showing distribution of apatite (Ca and Mg as conodont), Fe and S as framboidal pyrite, dolomite (Mg, Ca), clays (Al, Si) and rutile (Ti). Cd elemental map shows association with phosphate. Hushpuckney shale sample BR8 – 13, Kansas City, MO.

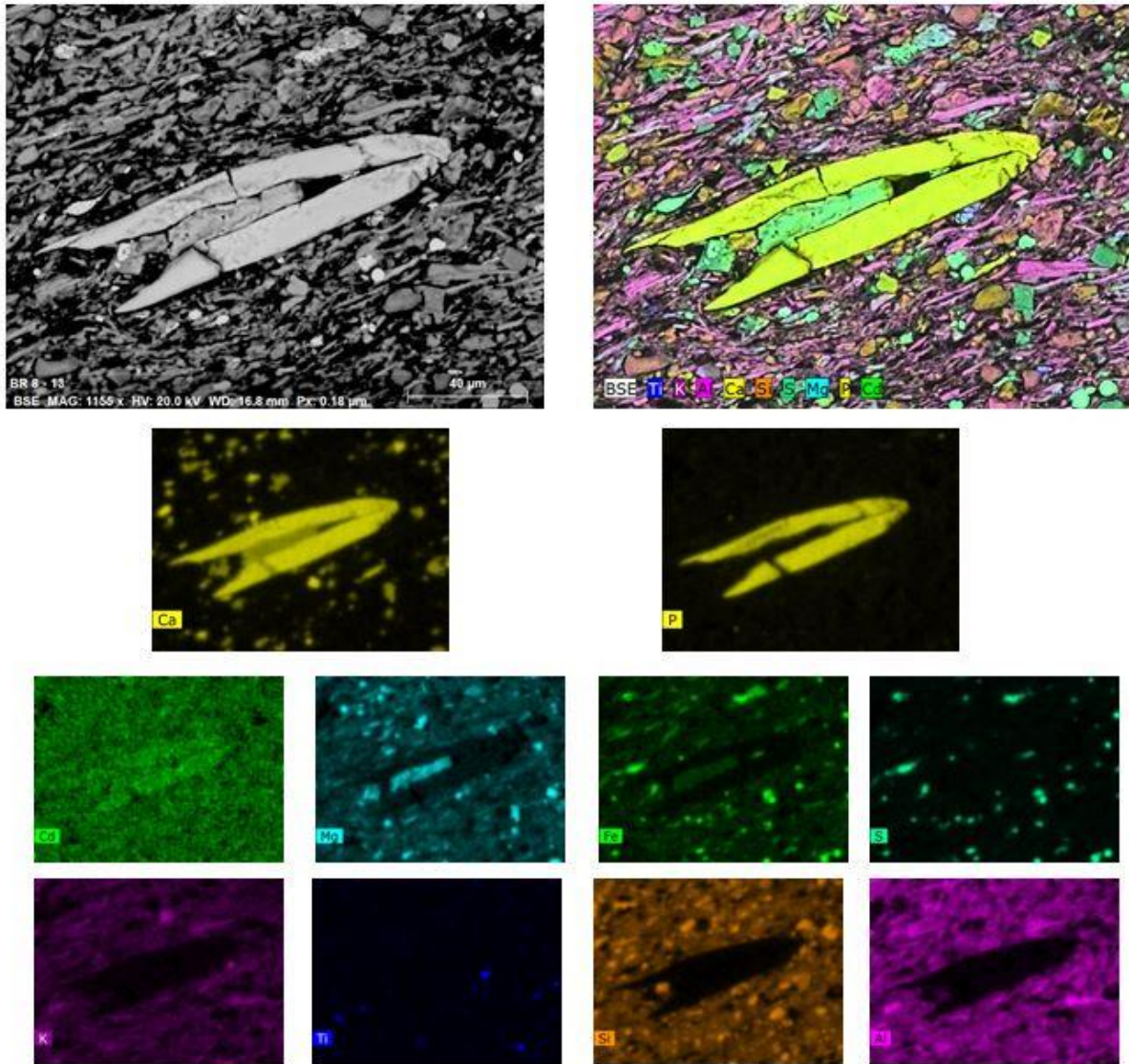


Plate 10: EDS maps for Hushpuckney shale. Top left, backscattered electron image. Top right, composite elemental map with BSE image. Small images: individual elemental maps for Ca, P, Cd, Mg, Fe, S, Si, Al, K and Ti showing distribution of apatite (Ca and Mg as conodont), Fe and S as framboidal pyrite, dolomite (Mg, Ca), clays (Al, Si) and rutile (Ti). Cd elemental map shows association with phosphate. Hushpuckney shale sample BR8 – 13, Kansas City, MO.

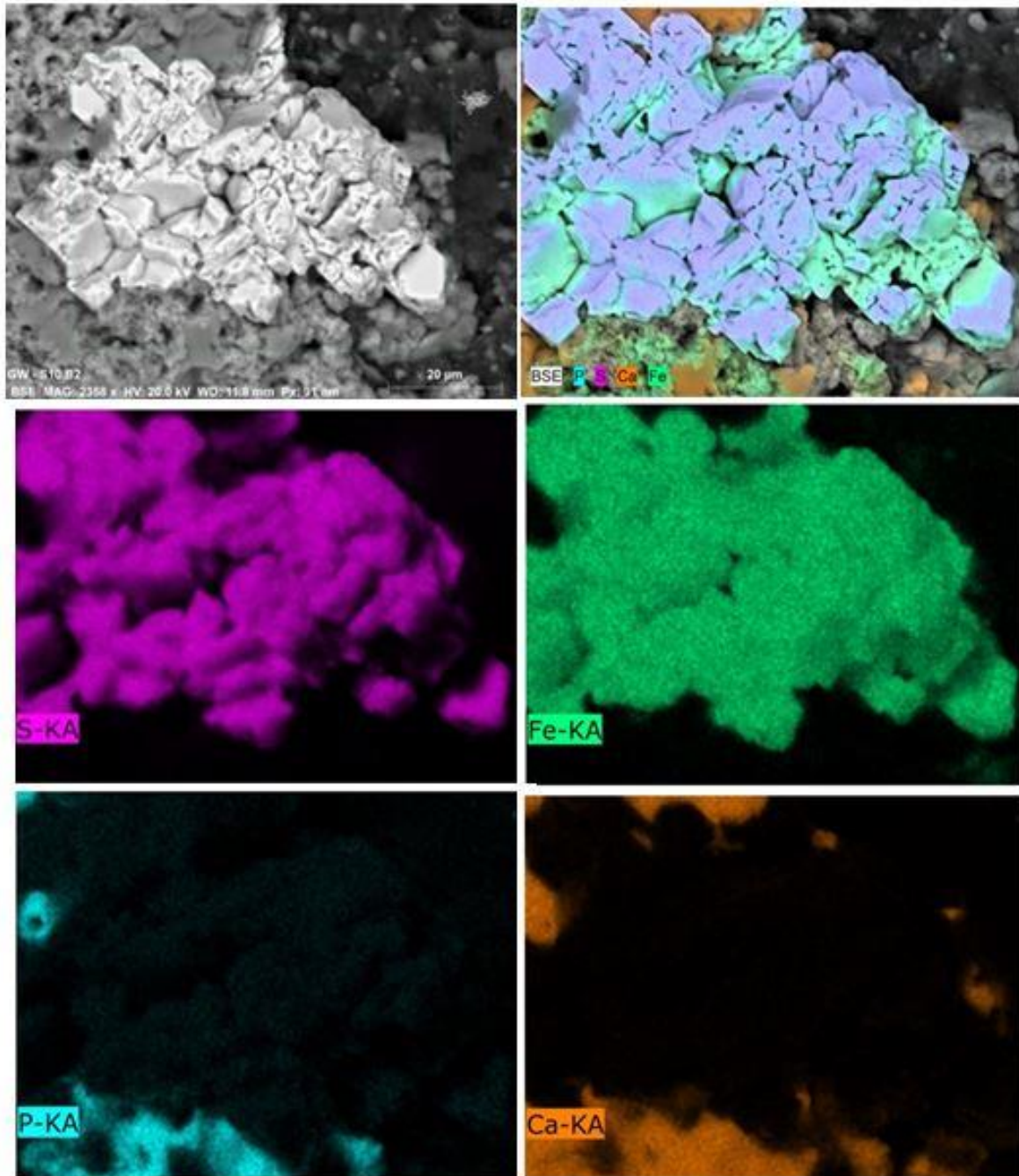


Plate 11: EDS maps for Stark shale. Top left, backscattered electron image. Top right, composite elemental map with BSE image. Individual elemental maps for Fe, S, Ca, and P showing distribution of euhedral pyrite (Fe, S) and phosphate (P, Ca). Stark shale sample GW- 5S, Greenwood quarry, Greenwood, MO.

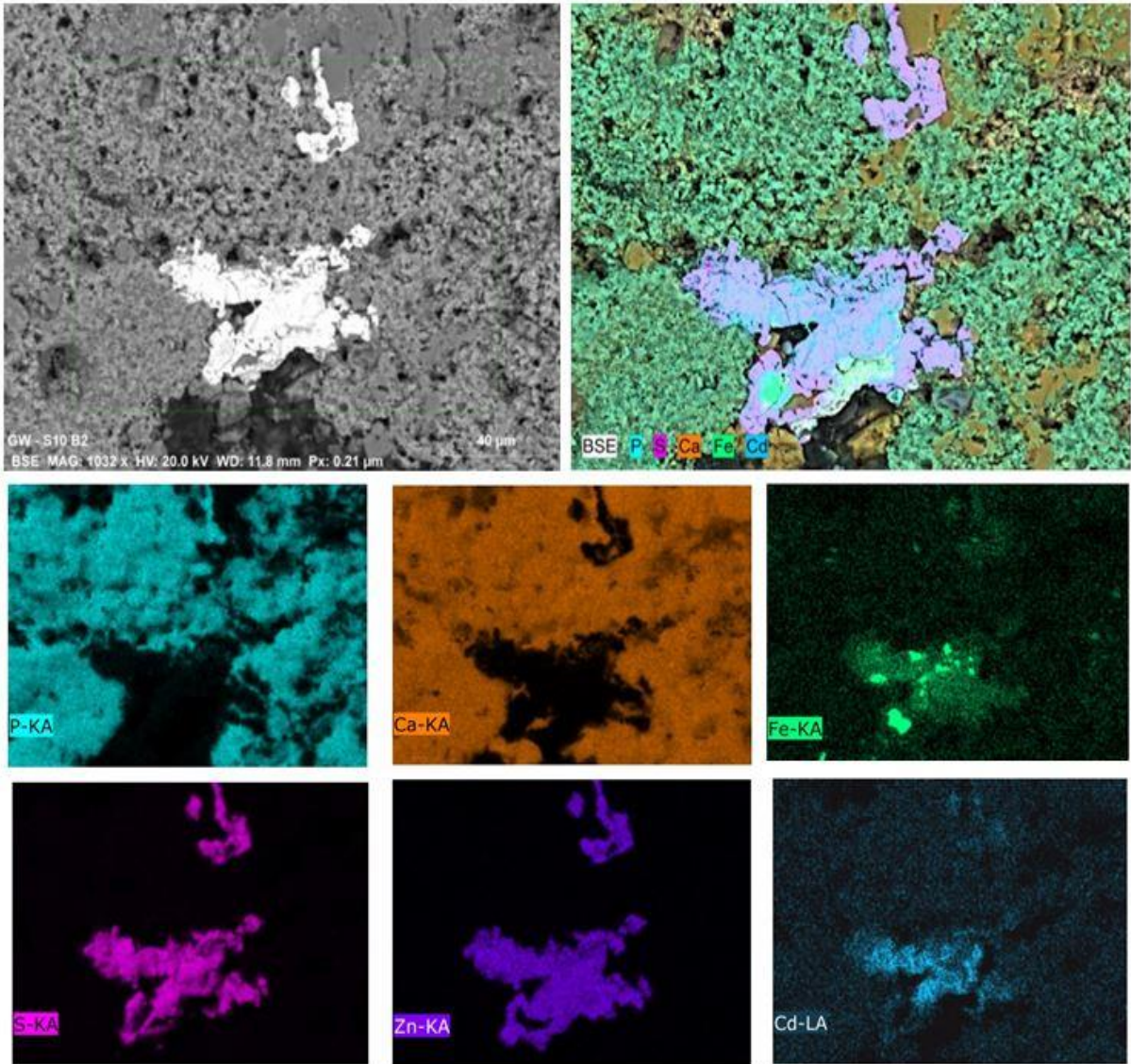


Plate 12: EDS maps for Stark shale. Top left, backscattered electron image. Top right, composite elemental map with BSE image. Small images: individual elemental maps for P, Ca, Fe, S, Zn and Cd showing distribution of sphalerite (Zn, S), pyrite (Fe, S) and phosphate (P, Ca). Cadmium associated with sphalerite as shown in Cd elemental map. Stark shale sample GW- S 10, Greenwood quarry, Greenwood, MO.

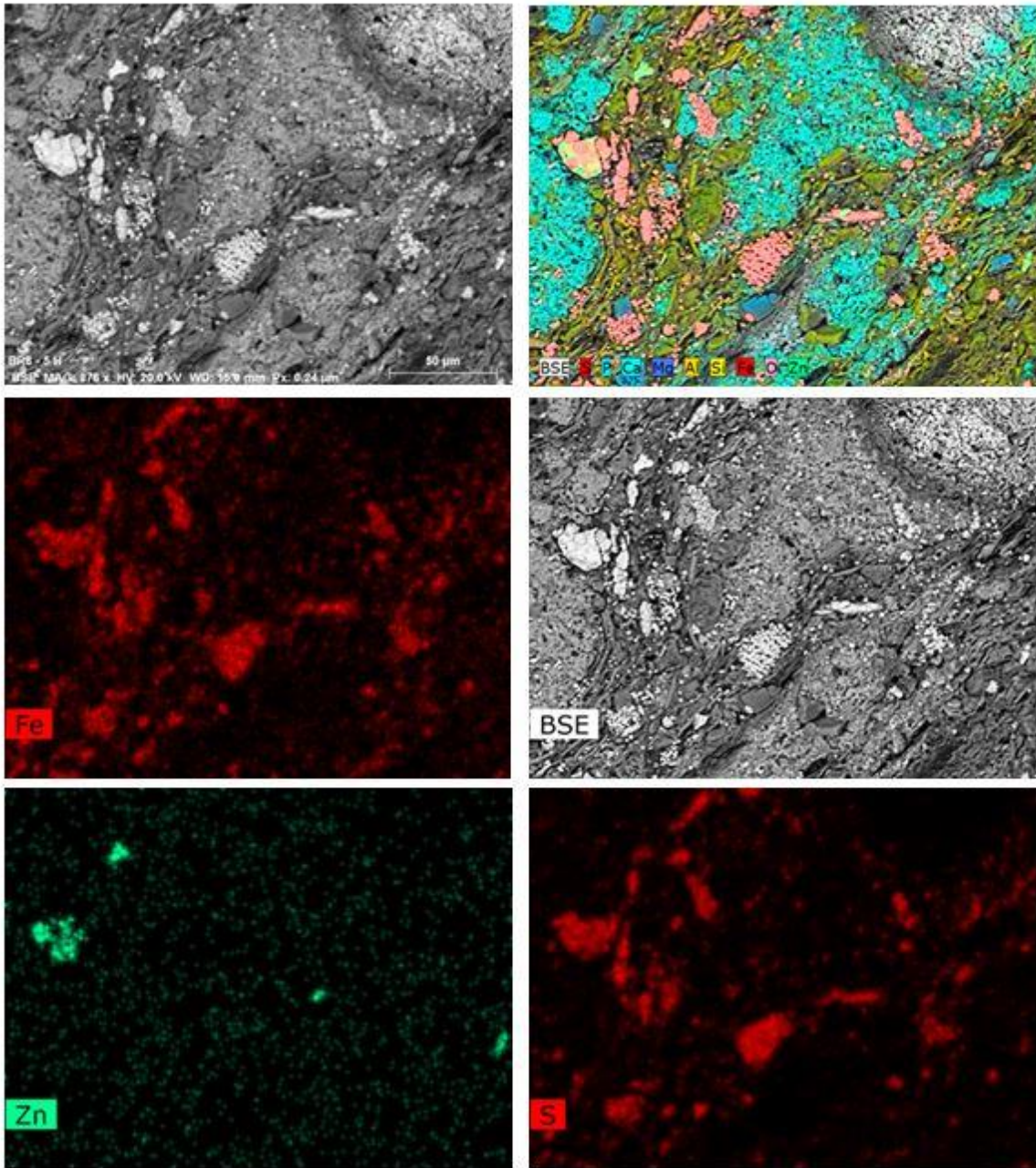


Plate 13:EDS maps for Hushpuckney shale.. Top left and middle right, backscattered electron image. Top right, composite elemental map with BSE image. Individual elemental maps for Fe, S and Zn showing distribution of framboidal pyrite and pyrite (Fe, S) and sphalerite (Zn, S). Hushpuckney shale sample BR8 – 5H, Kansas City,



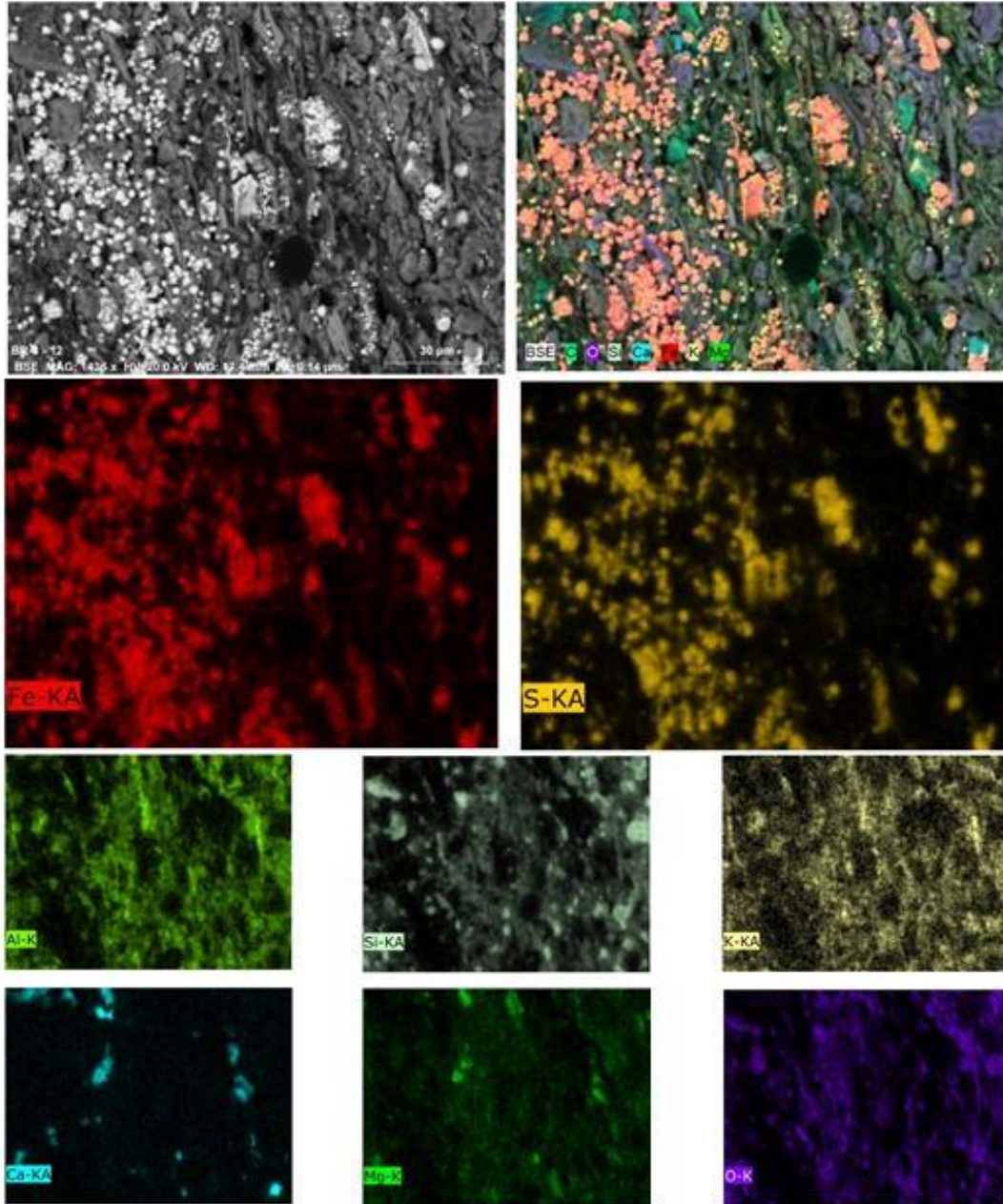


Plate 14: EDS maps for Hushpuckney shale. Top left, backscattered electron image. Top right, composite elemental map with BSE image. Individual elemental maps for Fe, S, Al, Si, K, Ca, Mg and O showing distribution of framboidal pyrite (Fe, S), clays (Al, Si, K), quartz (Si, O) and dolomite (Mg, Ca). the framboids are disintegrated and scattered between clay particles. Hushpuckney shale sample BR8- 12, Kansas City, MO.

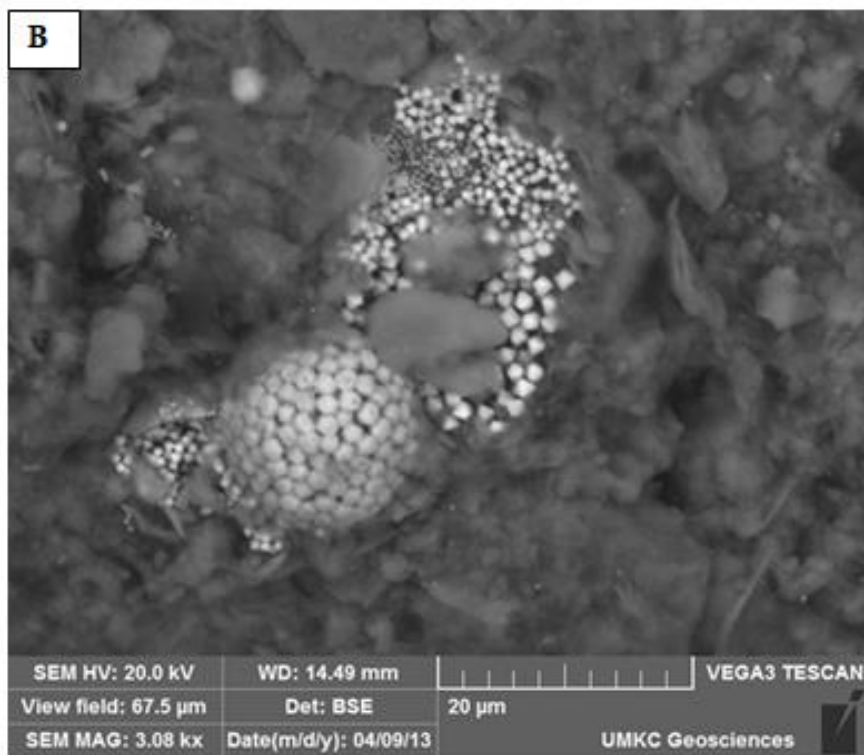
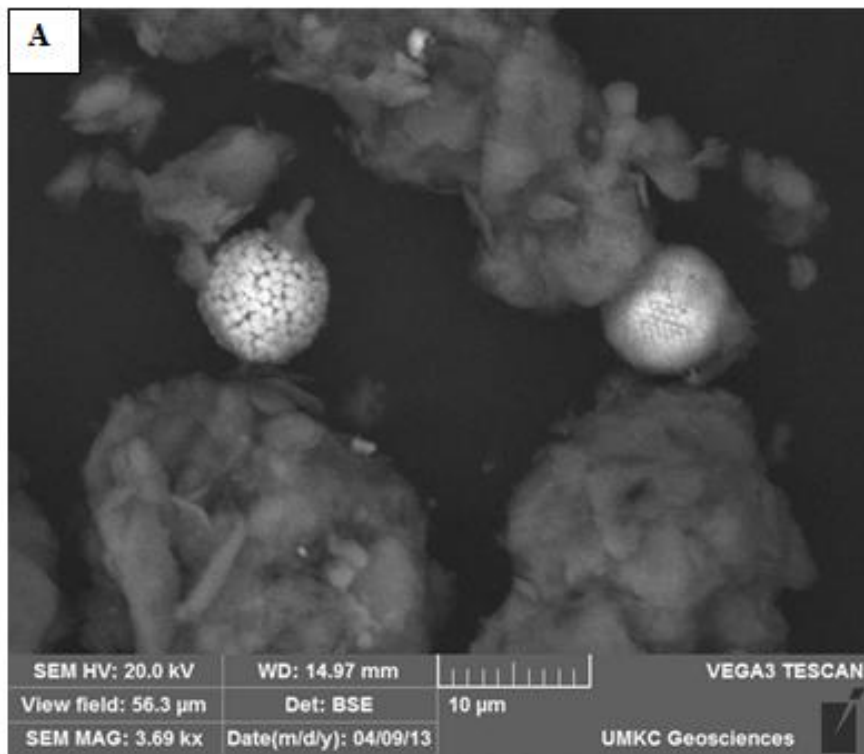


Plate 15: SEM photomicrograph for Stark shale. A- Different sizes of framboids.  
 B- Spheres of framboids show different stages of growth and disaggregation. Stark weathered sample, BBS section, Kansas City, MO.

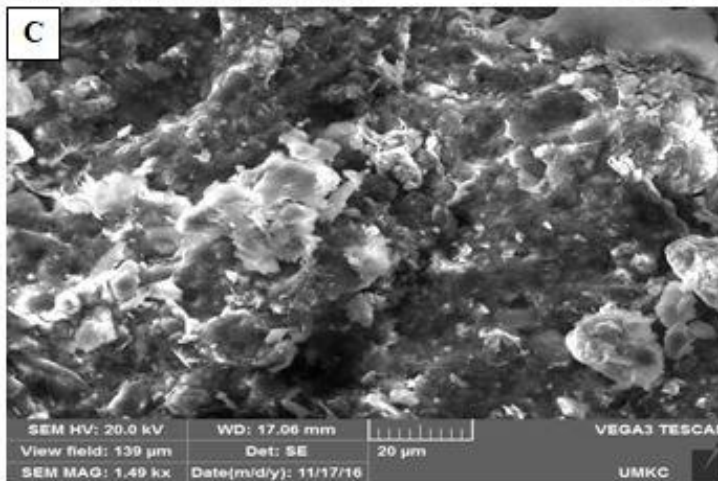
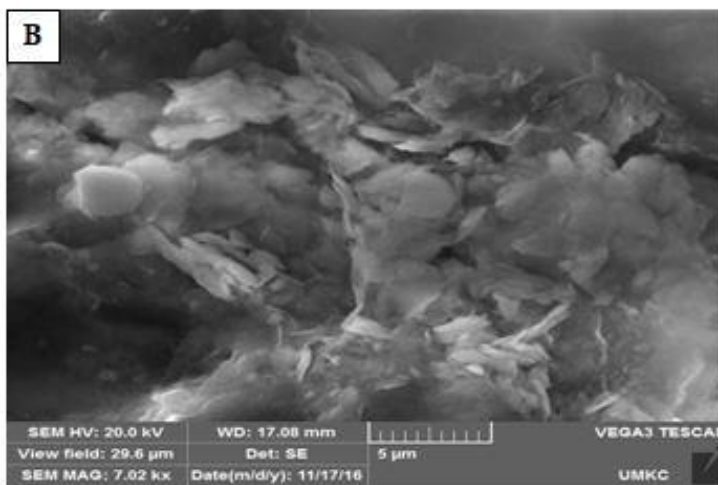
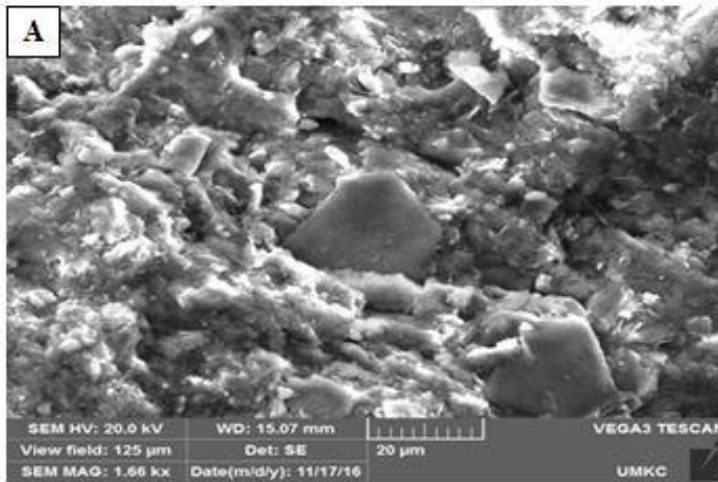


Plate 16: SEM images for Hushpuckney and Stark shale. A- Detrital clay particles from Hushpuckney shale sample. B and C- Detrital clay particles from Stark shale sample. Kansas City, MO.

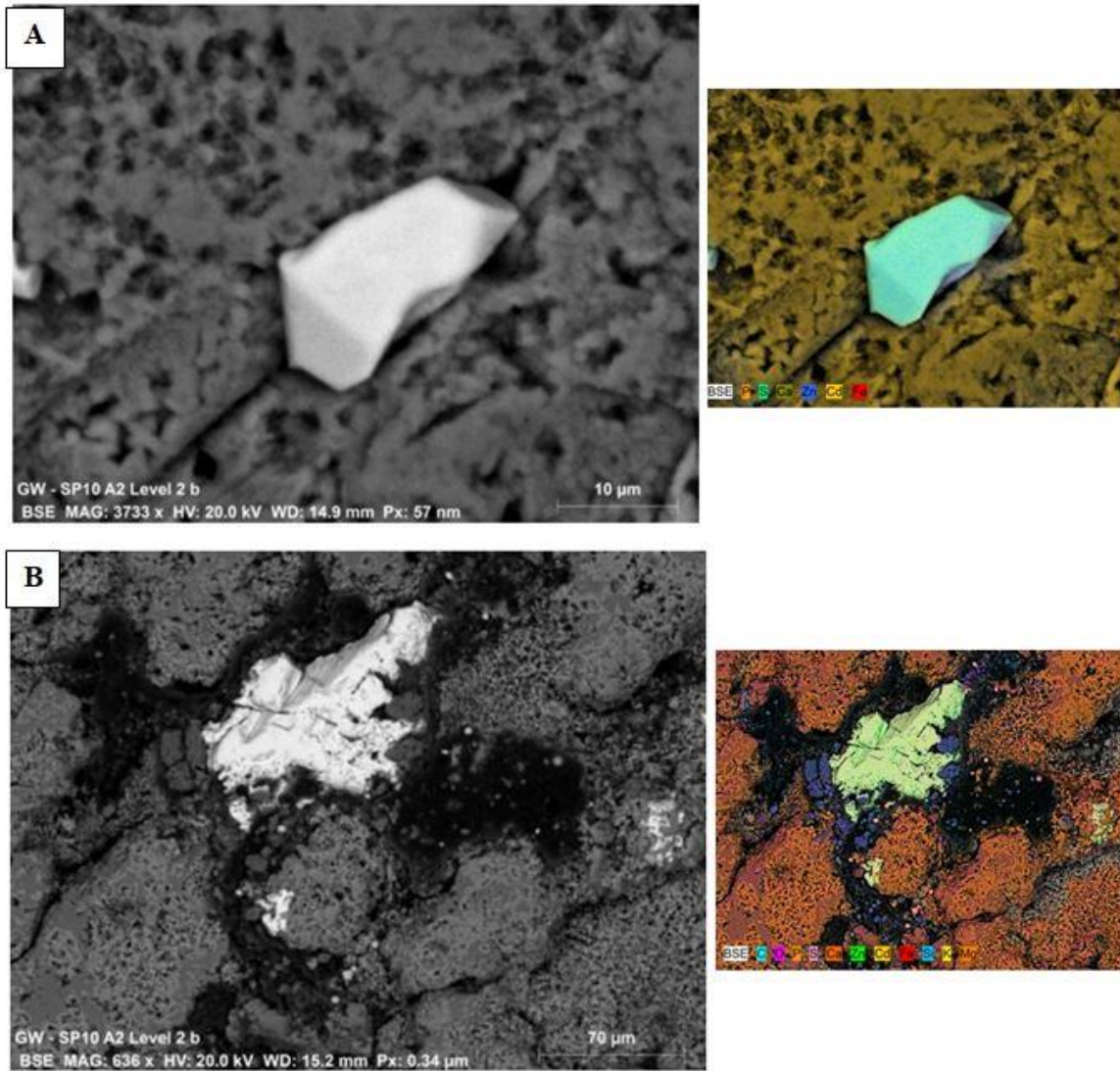


Plate 17: EDS maps for Stark shale. Top and bottom left, backscattered electron images. Top and bottom right, composite elemental map with BSE image showing shape features for sphaerite embedded in phosphate. A- Euhedral. B- Subhedral. Stark shale sample, GW-SP10, Greenwood quarry, Greenwood, MO.

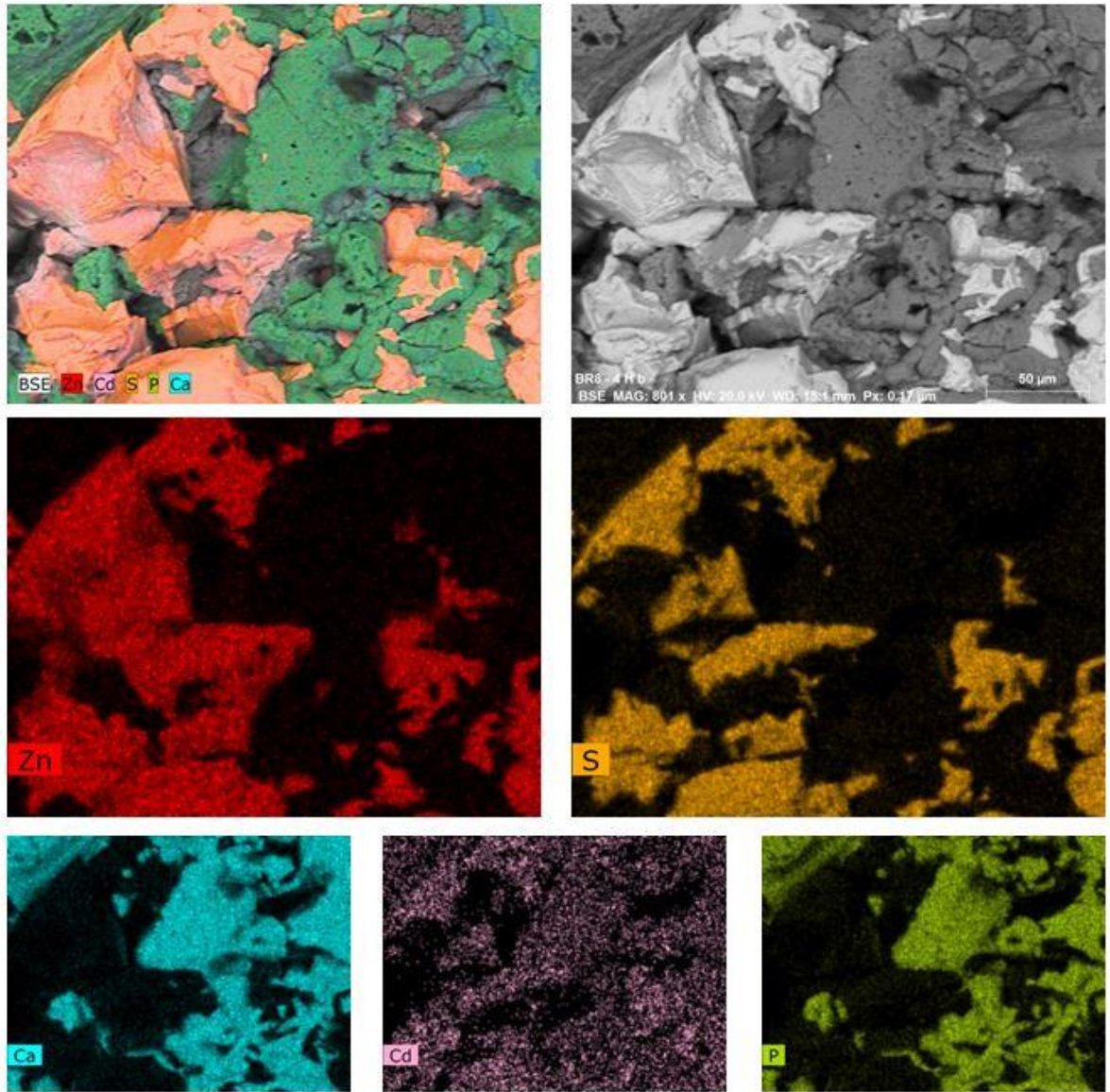


Plate 18: EDS maps for Hushpuckney shale. Top right, backscattered electron image. Top left, composite elemental map with BSE image. Individual elemental maps for Zn, S, Ca, P and Cd showing distribution of sphalerite (Zn, S) and phosphate (P, Ca). Cd element map shows association in sphalerite and phosphate. Hushpuckney shale sample BR8-4H b, Kansas City, MO

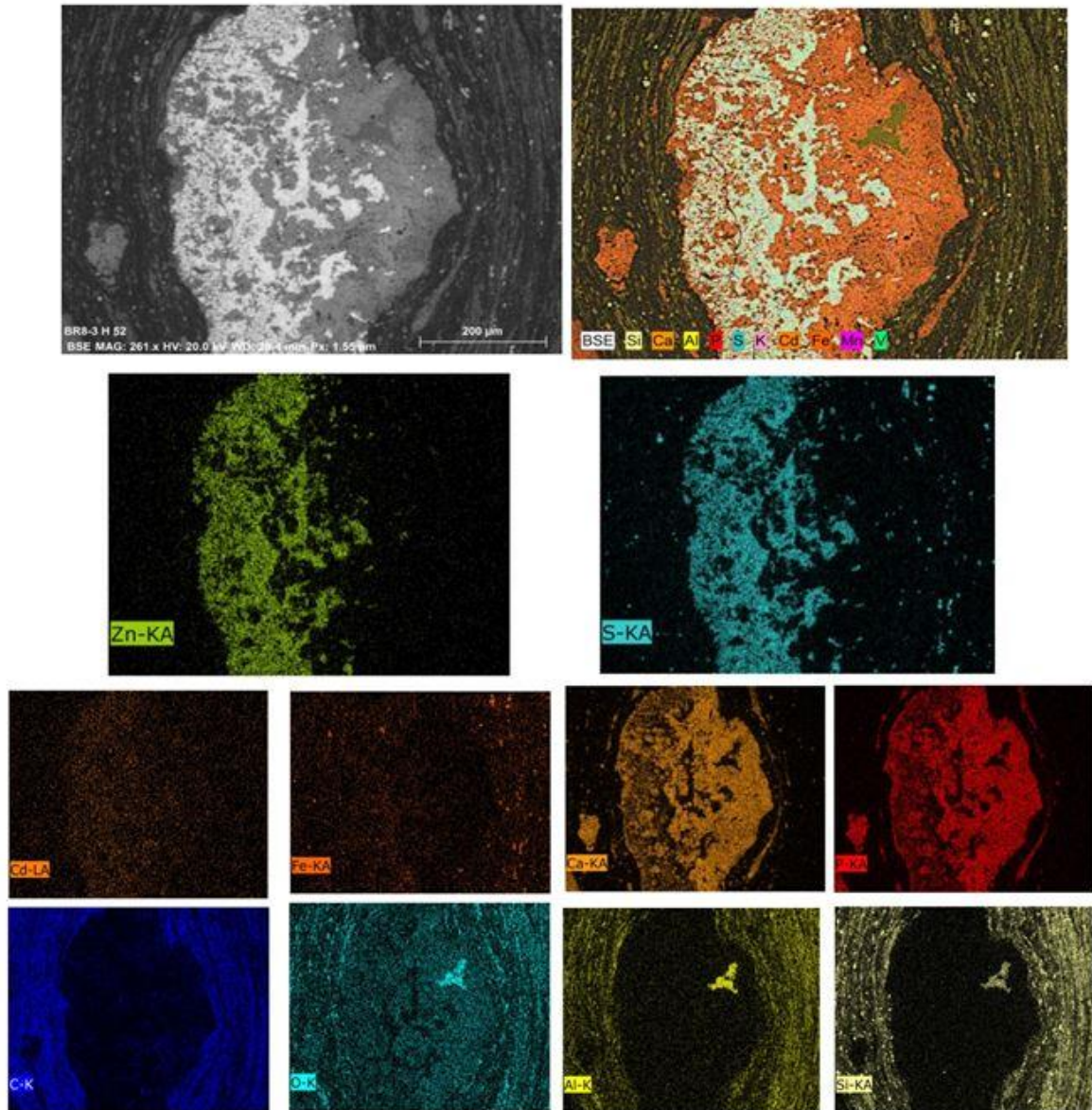


Plate 19: EDS maps for Hushpuckney shale. Top left, backscattered electron image. Top right, composite elemental map with BSE image. Small images: individual elemental maps for Zn, S, Cd, Fe, Ca, P, Si, Al, O and C showing distribution of sphalerite (Zn, S), framboidal pyrite (Fe, S), phosphate (P, Ca), clays (Si, Al) and organic matter(C). O, Al, and Si maps show possible dickite ( $\text{Al}_2\text{Si}_2\text{O}_5(\text{OH})_4$ ), a hydrothermal clay in the kaolinite group. Hushpuckney shale sample BR8 – 3H, Kansas City, MO.

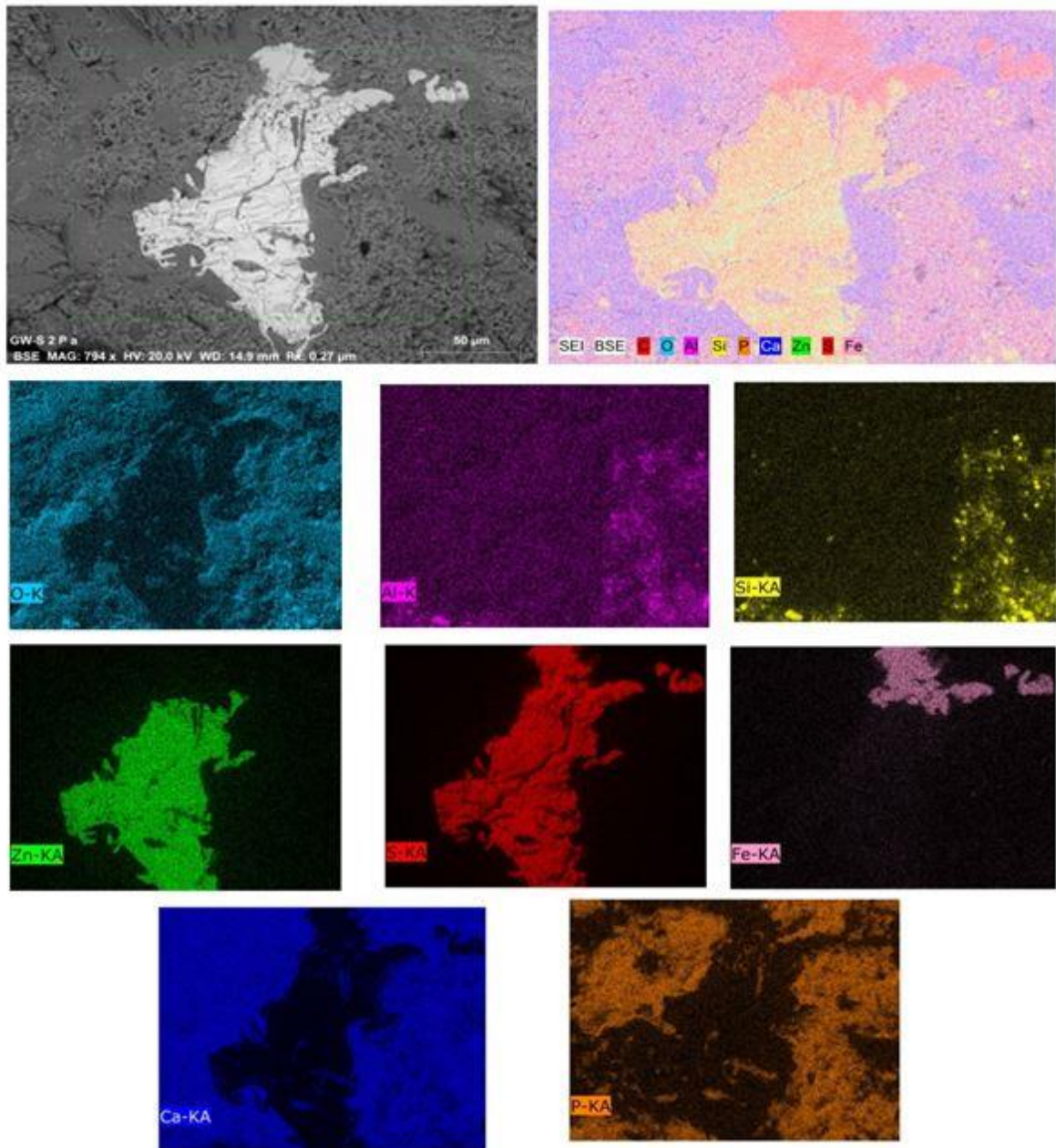


Plate 20: EDS maps for Stark shale. Top left, backscattered electron image. Top right, composite elemental map with BSE image. Small images: individual elemental map for Si, Al, O, Zn, S, Fe, Ca and P showing distribution of sphalerite (Zn, S), pyrite (Fe, S), phosphate (P, Ca), clays (Si, Al) and calcite (Ca) purple. Sphalerite and pyrite disseminated in phosphate. . Stark shale sample GW- S 2P, Greenwood quarry, Greenwood, MO.

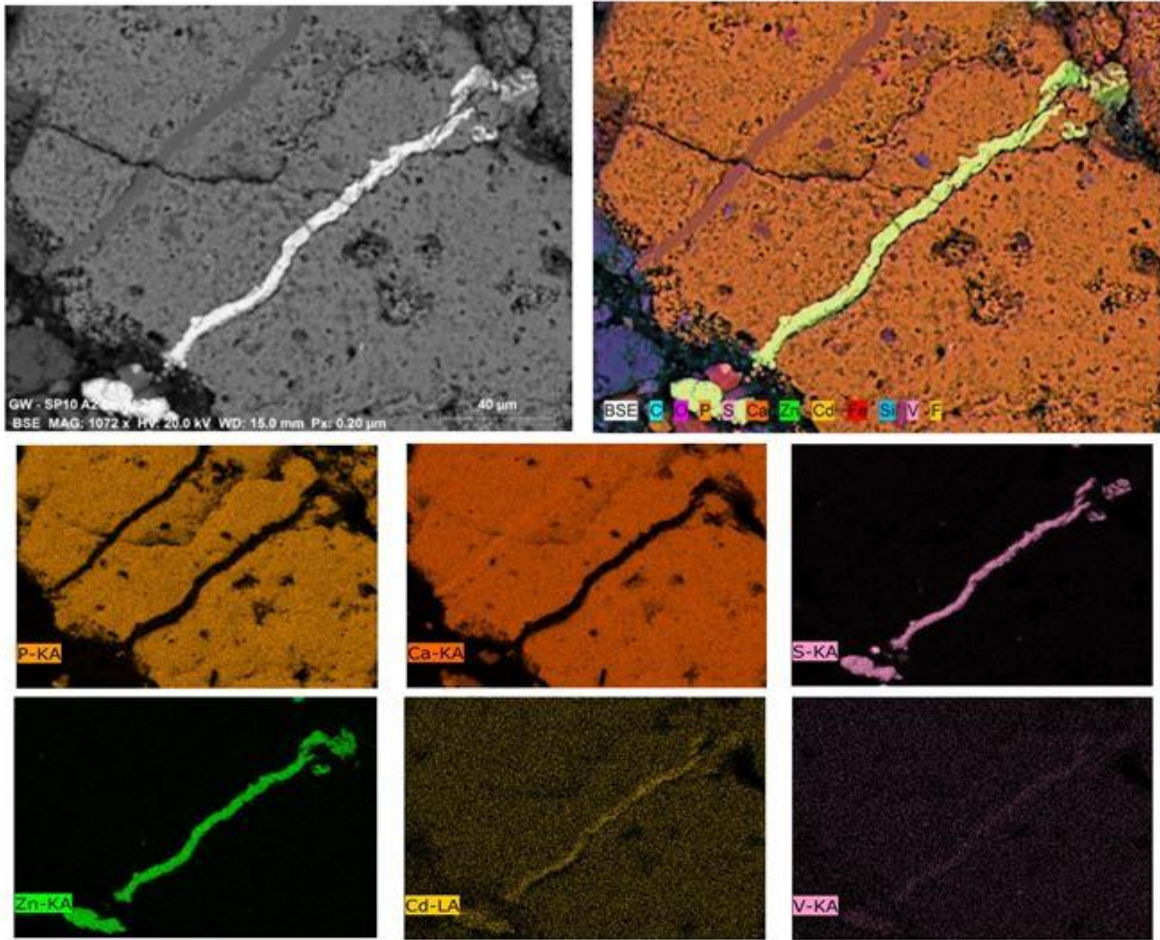


Plate 21: EDS maps for Stark shale. Top left, backscattered electron image. Top right, composite elemental map with BSE image. Small images: individual elemental map for P, Ca, S, Zn and Cd showing distribution of sphalerite (Zn, S), phosphate (P, Ca). Cadmium and V show association with sphalerite. These maps showing dissolution for phosphate and reprecipitated Calcite then sphalerite. Stark shale sample GW- SP10A, Greenwood quarry, Greenwood, MO.



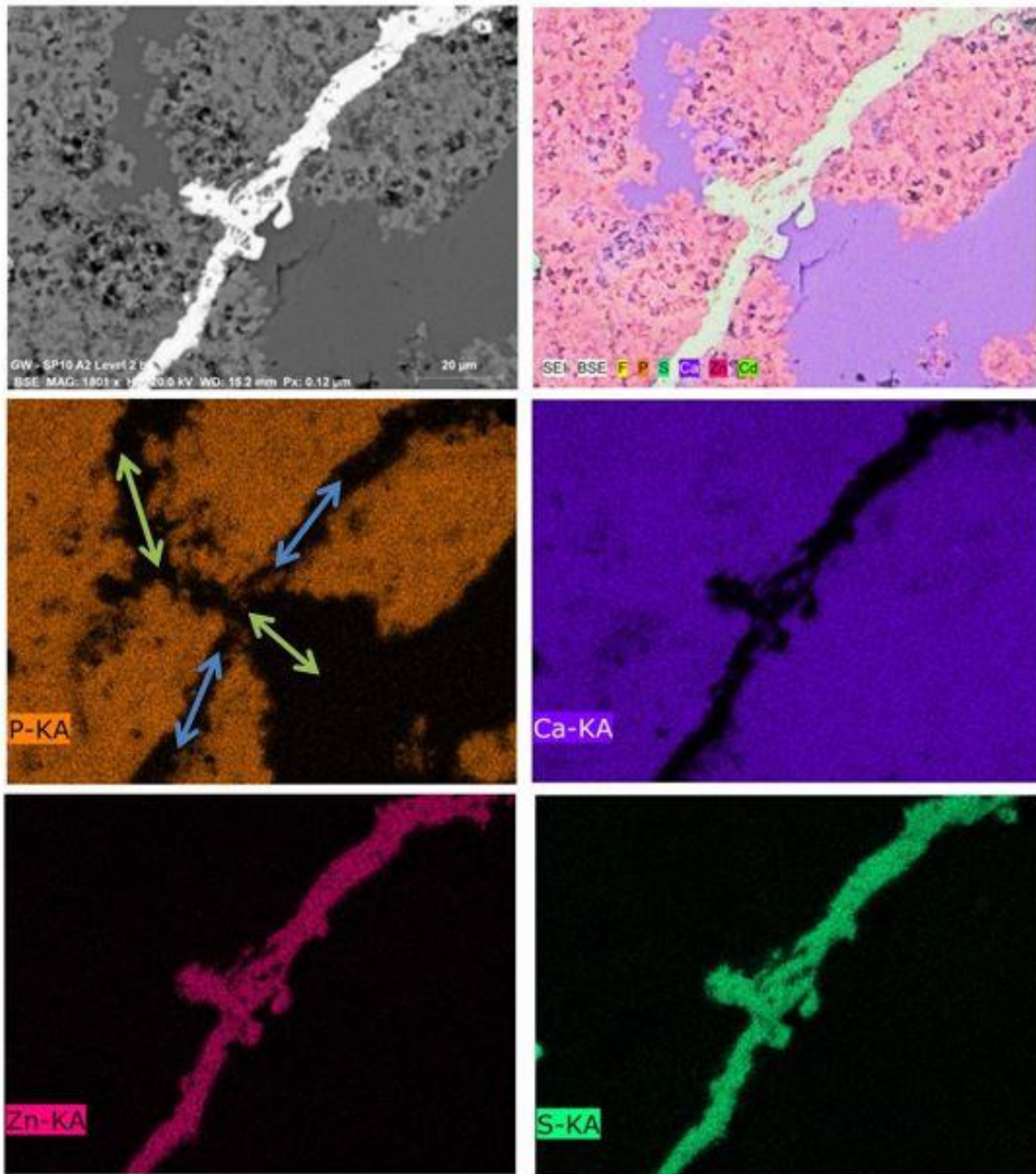


Plate 22: EDS maps for Stark shale. Top left, backscattered electron image. Top right, composite elemental map with BSE image. Individual elemental maps for Zn, S, Ca and P showing distribution of sphalerite (Zn, S), calcite (Ca) and phosphate (P, Ca). This plate enlarged from plate 1. These maps clearly show that calcite filled the space first as indicated with green arrows then sphalerite filled it later (blue arrows). Stark shale sample GW-SP10A2, Greenwood quarry, Greenwood MO.

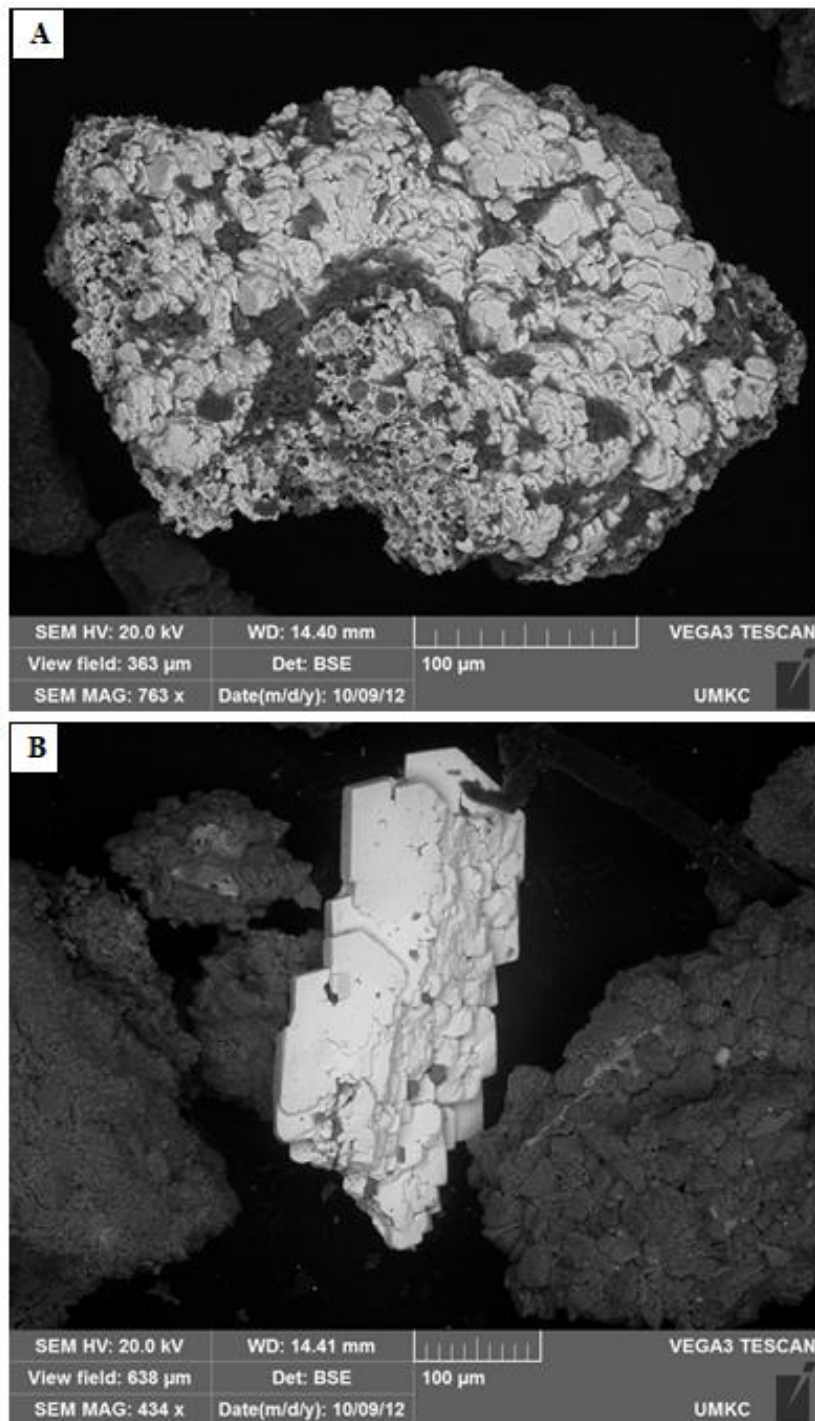


Plate 23: SEM images for barite in Hushpuckney shale. A- Aggregate of barite grains. B- Single barite grain. Hushpuckney shale sample, 87<sup>th</sup> H, Kansas City, MO.

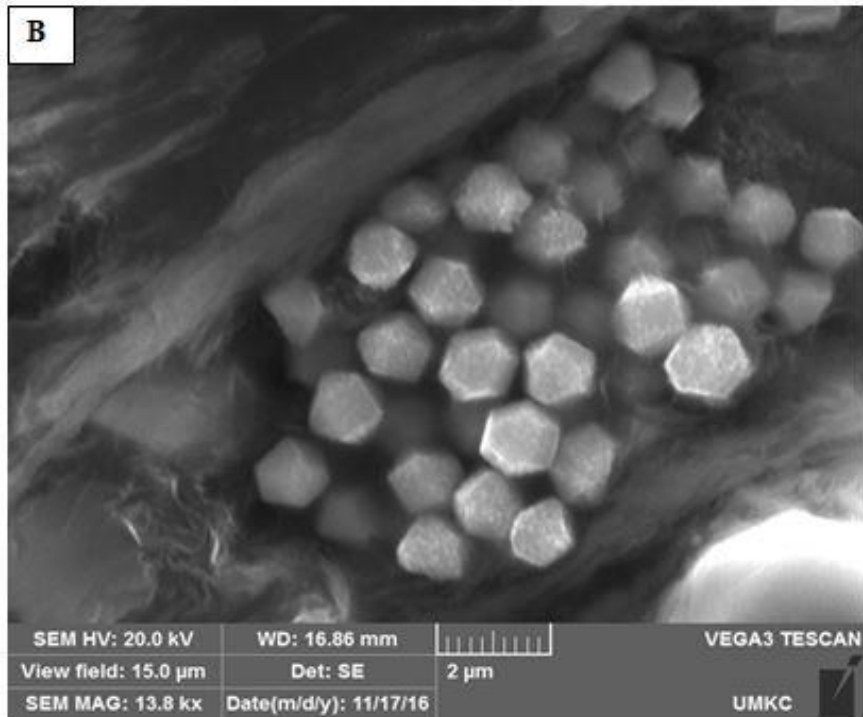
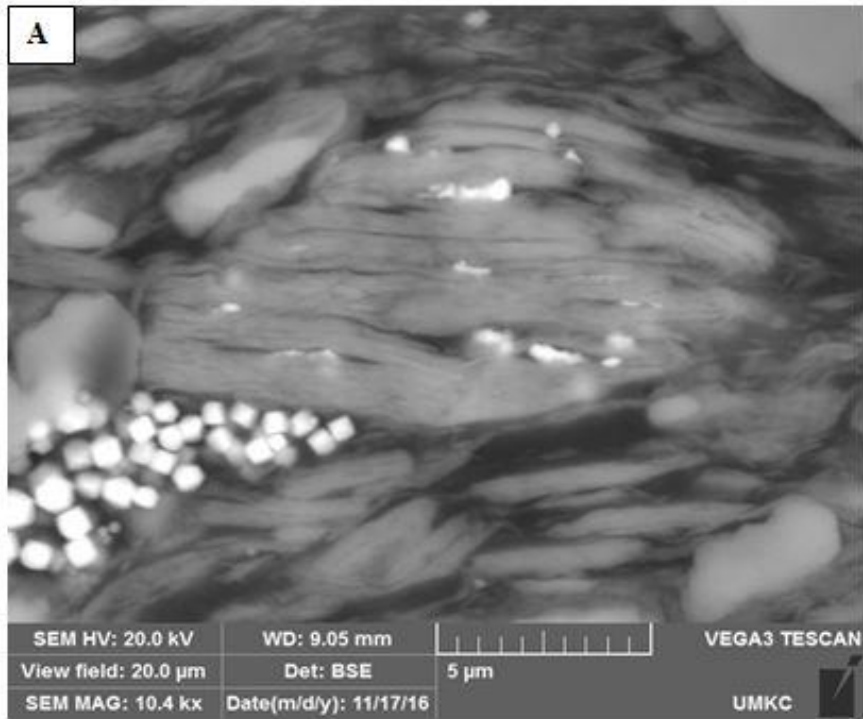


Plate 24: SEM photomicrograph for Hushpuckney shale. A- Detrital mica grain and octahedral framboidal pyrite grains in clay. B- Enlarged photo from A for framboidal pyrite. Hushpuckney shale sample, BR8, 13, Kansas City, MO.

## CHAPTER 4

### GEOCHEMISTRY

Elemental analysis of the studied two shale units (major, minor, trace and metals) and elemental correlation and distribution were determined using two techniques: SEM/EDS and XRF. The EDS spectrum used to identify individual minerals by their spectra shows all the elements in the mineral and their concentration, but such analyses are limited to a specific points and do not cover the full viewed area.

#### **Element Maps and XRF Data**

Element maps are showing the different minerals with their elemental components as a whole map in addition to individual elemental map for all the mineral composition. It shows the relation between the elements like: Si, Al and K for clay minerals and the excess of Si to quartz. Ca and Mg are chosen for dolomite. Ca and P are for phosphate. Zn and S are for sphalerite. Pb and Se are for clausthalite. Fe and S are for pyrite. Ba and S are for barite. This technique is giving good results about the presence of elements and covered all the viewed section but it does not give the concentrations and their percent. These results are very well matched with the XRD results.

Each element within the XRF's detection range fluoresces at unique energies allowing for counts to be made of various elements. The Scanning XRF uses X-rays to excite the electrons of atoms within the sediments and force them into higher energy states. When the electrons move back into their lower energy state, energy is released in the form of fluorescence. Each element within the XRF's detection range fluoresces at unique energies allowing for counts to be made of various elements (Rothwell, 2006). The results given for

this analysis are counts for each element then which was converted to weight percent by using a special formula. In this study, scanning XRF detected the following elements provided as counts: Al, Si, , K, Ca, Mg, Fe, P, S, Ti, Mn, V, Co, Ni, Cu, Zn, Pb, Se, Rb, Sr, Cl, Ar, Sc, Y, Zr, Cd, Sn, Sb, Ba, La, Ce, Pr, Pm, Sm, Tb, Tm, Yb, Lu, Hf, Ta, W, Ir, Pt, Au, Hg, Bi and At.

Unfortunately, the standard elements analyzed at the University of Minnesota - Duluth used in the mathematical equation (formula) to convert the counts to the percentage concentrations are only the following elements: Si, Al, Fe, Mg, Ca, K, P, Ba, S, Co, Cu, Ni, Sr, V, Zn, Pb, Sc, La, Ti, Se, Rb and Sb. The concentrations of the elements are plotted relative to depth for both units (Figures 4-1, 2, 3 and 4).

Weight percentages were used for the major elements and parts per million (ppm) were used for minor and trace elements. These concentrations or percentages are shown in Tables 4-1 and 2, these tables listed the presence of major, minor and trace elements in both black shale units. Also, they are comprised the maximum, minimum and average values of each element. There is an exception only by placing the zinc element in weight percent instead of ppm because of its presence more than 2%. The two tables show that there are very slight differences in the proportions of the major, minor and trace elements in both black shale units. These differences may be due to the quantity of processed detrital materials from source area (abiotic) or as a result of biological activities that occurred during sedimentation (biotic) (Tribovillard et al., 2006).

A comparison made for these two units with other shales that have different places and age. The objective of this comparison is to illustrate the amounts of natural

concentrations of elements in the shale rocks and to indicate the rate of enrichment of some elements in them as it shown in (Table 4-3). These two units show less concentration of aluminum (Al), less in iron (Fe), phosphate (P) rich, less in titanium (Ti), zinc (Zn) and lead (Pb) rich, barium (Ba) rich, rich in vanadium (V), less in magnesium (Mg) and somehow above the range in antimony (Sb).

Vanadium in the unaltered black shale is primarily in the organic matter and adsorbed on or incorporated in illite and kaolinite (Gehring et al., 1993; Meunier, 1994; and Peacor et al., 2000). The two black shale units contain abundant vanadium associated with zinc. This can be explained by hydrothermal leaching as the fluid passes through the clay and organic matter, extracting vanadium, redepositing it with the sulfides.

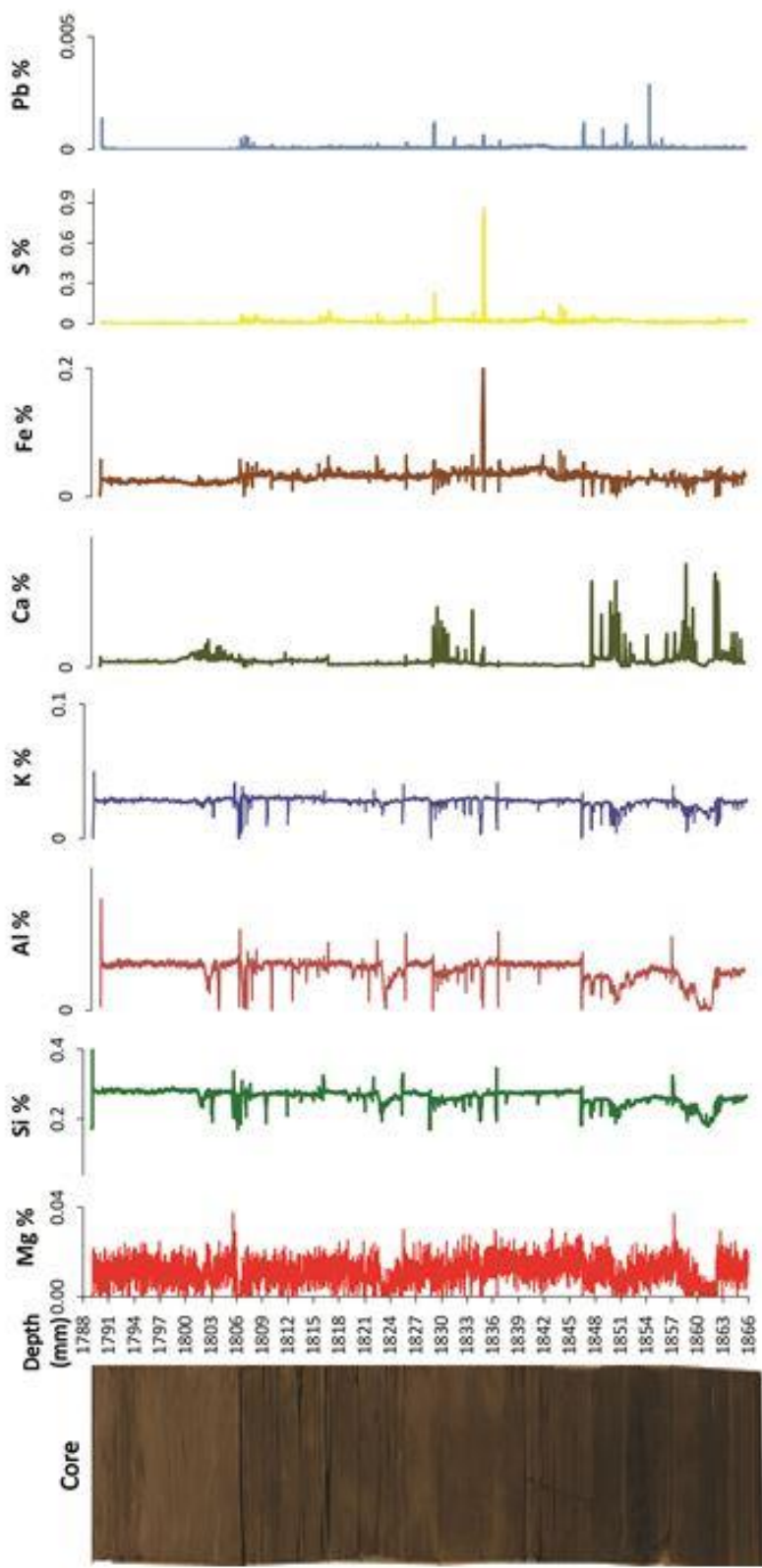


Figure 4.1. Vertical distribution of major elements along the Hushpuckney black shale.

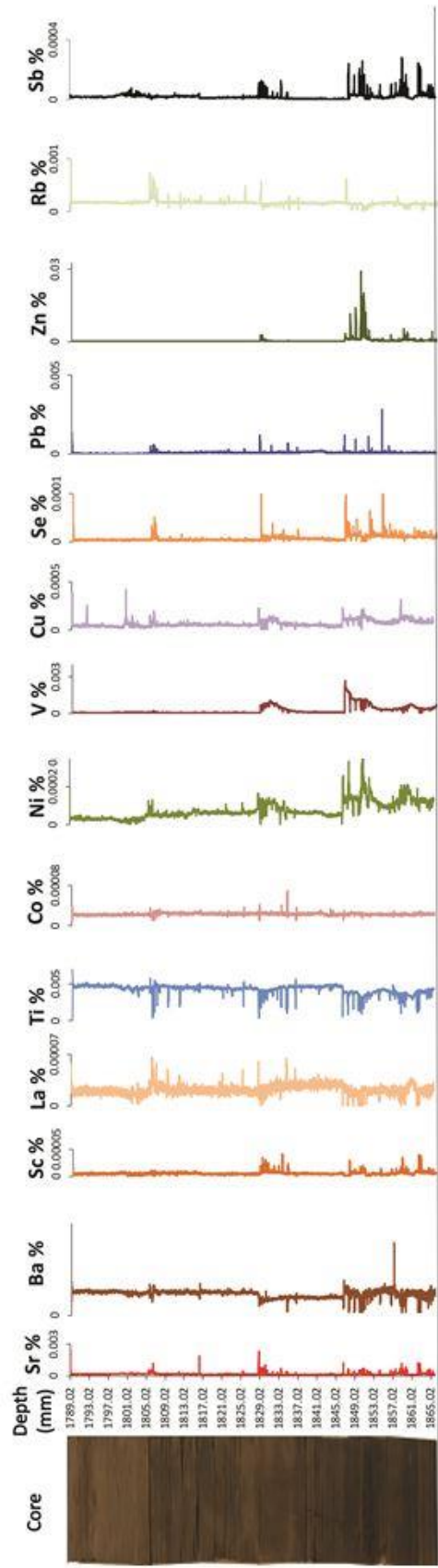


Figure 4.2. Vertical distribution of minor and trace elements along the Hushpuckney black shale.



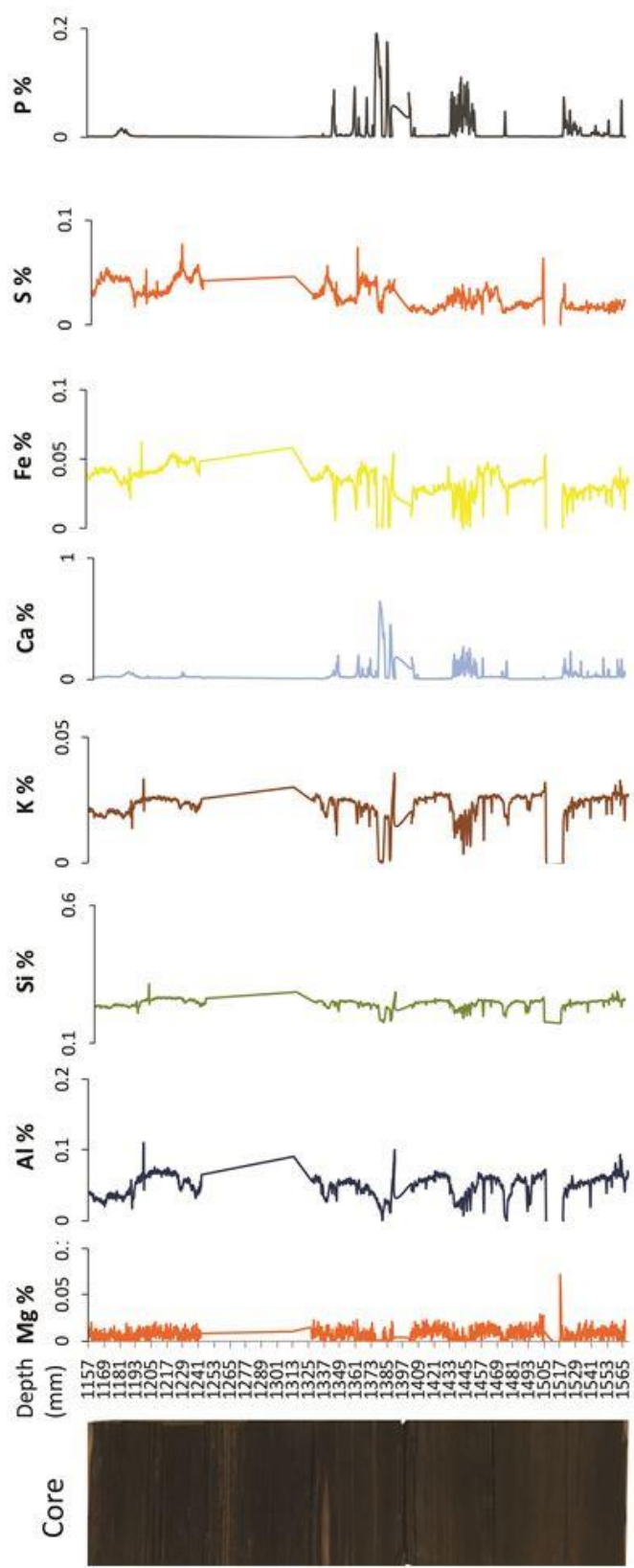


Figure 4.3. Vertical distribution of major elements along the unweathered part of Stark black shale.

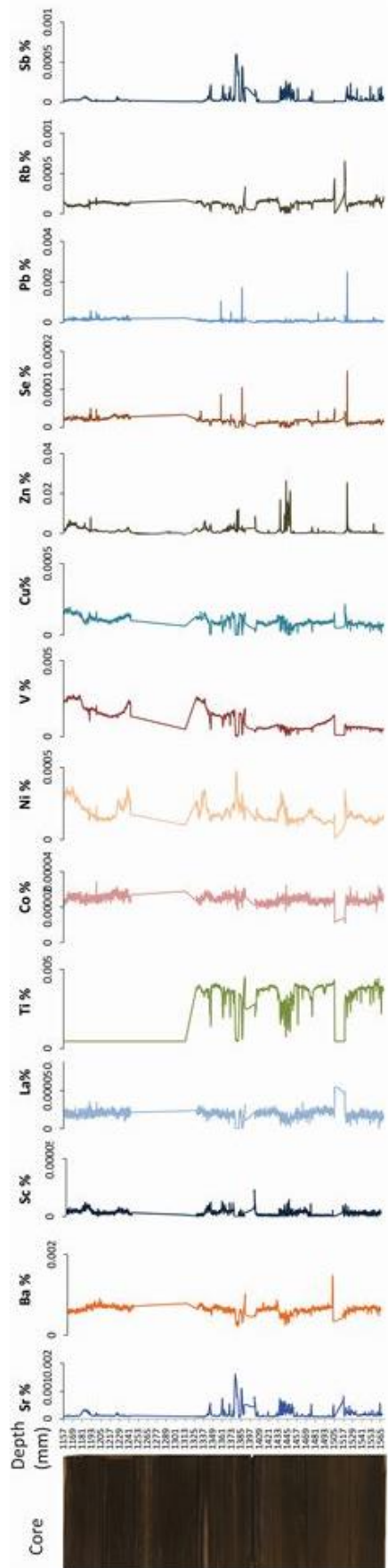


Figure 4.4. Vertical distribution of minor and trace elements along the unweathered part of Stark black shale.

Table 4.1. Major elements compositions weight percent (%) for Hushpuckney and Stark shale units

Element	Major elements weight percent (%)											Unit
	Mg	Al	Si	K	Ca	Fe	S	P	Zn			
Maximum	3.774%	19.371%	40.111%	5.000%	31.478%	30.330%	84.648%	12.841%	2.925%			Hushpuckney black shale
Minimum	0.080%	0.000%	17.023%	0.007%	0.175%	0.002%	0.001%	0.050%	0.010%			
Average	1.144%	7.029%	26.370%	2.721%	2.310%	2.973%	1.602%	0.381%	0.045%			
Maximum	7.125%	10.965%	31.272%	3.571%	64.052%	6.256%	7.623%	18.998%	2.635%			Stark black shale
Minimum	0.080%	0.027%	17.193%	0.001%	0.186%	0.009%	0.102%	0.000%	0.000%			
Average	0.806%	5.424%	24.870%	2.368%	3.358%	3.753%	3.105%	0.833%	0.137%			

Table 4.2. Minor and trace composition (PPM) for Hushpuckney and Stark units

Element	Minor & trace elements (PPM)														Unit	
	V	Cu	Se	Sr	Ba	Sc	La	Pb	Ti	Co	Ni	Rb	Sb			
Maximum	2700	412	182	2455	2360	41	66	2830	6324	69	352	3397	280			Hushpuckney black shale
Minimum	4	0	0	22	100	0	0	0	429	11	2	16	2			
Average	253	68	7	166	688	6	22	71	4218	23	76	169	22			
Maximum	2743	212	148	1606	1475	23	55	2484	4501	34	471	650	603			Stark black shale
Minimum	0	0	0	49	228	0	0	0	429	11	14	0	2			
Average	1091	92	20	153	662	3	20	124	2176	25	174	135	35			

Table 4.3. Comparison of average abundances of elements in different shales with the two black shale units.

Element	Krauskopf 1982 shale	Frost et al., 1985 New Albany shale group	Rimmer 2004 Upper Cleveland black shale (Average)	Li & Schieber 2015 Chattanooga shale (CM-K1)	This study 2017 Average concentration	
					Hushpuckney black shale	Stark black shale
Si	238000	566000	660500	518600	263700	248700
Al	92000	137000	151500	120800	70290	54240
K	25000	45000	41100	42700	27210	23680
Ca	25000	11000	8200	3200	23100	33580
Mg	14000	15000	13700	15200	11440	8060
Fe	47000	52000	69200	52100	29730	37530
P	750	700	3200	1400	3810	8330
S	2500	23000	29800	30700	16020	31050
Ti	4500	7100	8200	7000	4218	2176
Zn	90	150	539	1176	450	1370
Pb	20	37	89	-	71	124
Se	0.6	7	-	-	7	20
Ba	600	480	-	307	688	662
V	130	210	843	1972	253	1091
Sr	400	92	-	-	166	153
Rb	140	150	-	-	169	135
Ni	80	84	144	186	76	174
Cu	50	79	121	207.1	68	92
La	40	38	-	33.1	22	20
Co	20	23	19	12.5	9	25
Sc	15	17	-	-	6	3
Sb	1.5	3.9	-	-	22	35

## **Element Correlation**

The correlation coefficient ( $R^2$ ) was utilized for the analyzed data. It is a statistical investigation method to determine the linear association between pairs of data. The value of the linear relationship ranges from -1.0 to +1.0. The negative sign indicates negative correlation, whereas the positive value is positive correlation and zero shows no relation (Davis, 1973; Steiner, 2008).

The studied samples were black shale bearing phosphates and this phosphate embraces sphalerite and the clausthalite on the edges of the grains or among them as is evident from the SEM images (Chapter 3). A linear relationship was made between the phosphorus element with the other major, minor and trace elements separately to establish the relationship between them. This relationship was plotted and a correlation coefficient calculated as shown in Figure 4.5. Another attempt was made to establish a relationship between the aluminum and the other elements to clarify the detrital origin of these rocks, considering that the aluminum is used as a proxy for the clastic origin (Tribovillard et al., 2006; Soua, 2011; and Gertsch et al., 2011) (Figures 4.6). In addition, linear relationships were drawn between some metals and elements to find any relationship between them. Linear relationships were drawn between lead versus selenium and sulfur; iron versus sulfur, copper and zinc; copper versus sulfur; barium versus sulfur; and calcium versus magnesium and strontium. The data which were used from XRF scanning are 3849 readings for Hushpuckney unit and 1854 readings for Stark unit. The scattered graphs of these relationships were plotted as shown in (Figures 4.5, 6 and 7), which in the same time shows a comparison between the two black shale units. The results of these correlations were summarized in Tables 4.4- 6.

The phosphorus relations with the other elements in the Hushpuckney unit indicate: very strong positive correlation with calcium and antimony; moderate positive correlation with scandium; weak and very weak positive correlation with zinc, copper and nickel respectively; while it has weak and very weak negative correlation with titanium, lanthanum, barium, iron and rubidium respectively. Almost no relation noticed with vanadium, lead and cobalt. The Stark unit shows slightly different correlation. It indicates weak negative correlation with copper and cobalt, while the other correlation almost the same as in Hushpuckney unit.

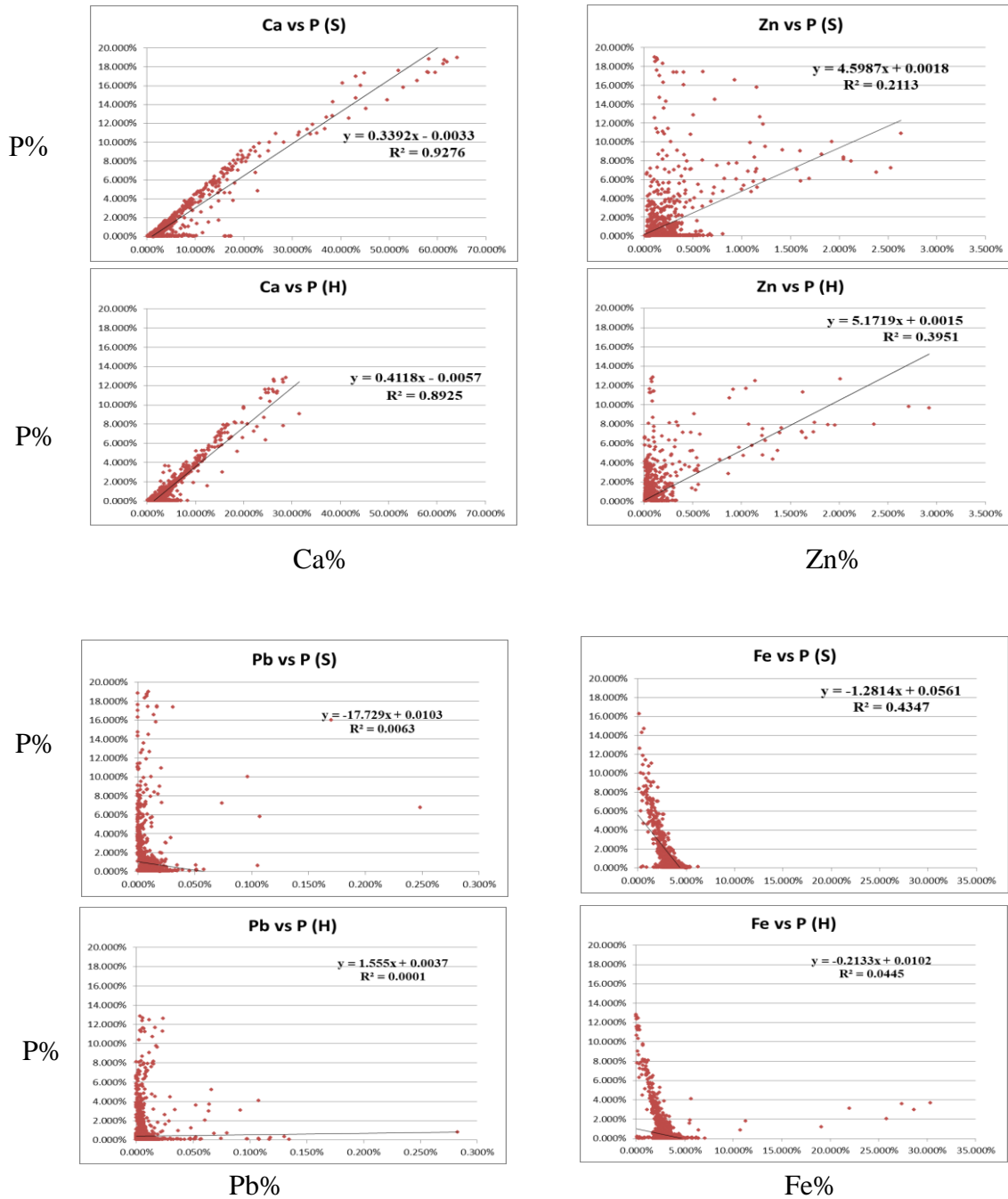


Figure 4.5. Correlation between P and other elements (Ca, Zn, Pb, Fe, Cu, V, Ti, Rb, Sc, La, Co, Ni, Ba and Sb) in Hushpuckney (H) and Stark (S) black shales. Strong P-Ca correlation is expected if fluorapatite is present. A strong negative P-Fe correlation is seen in both shales, and no P-Pb correlation was observed.

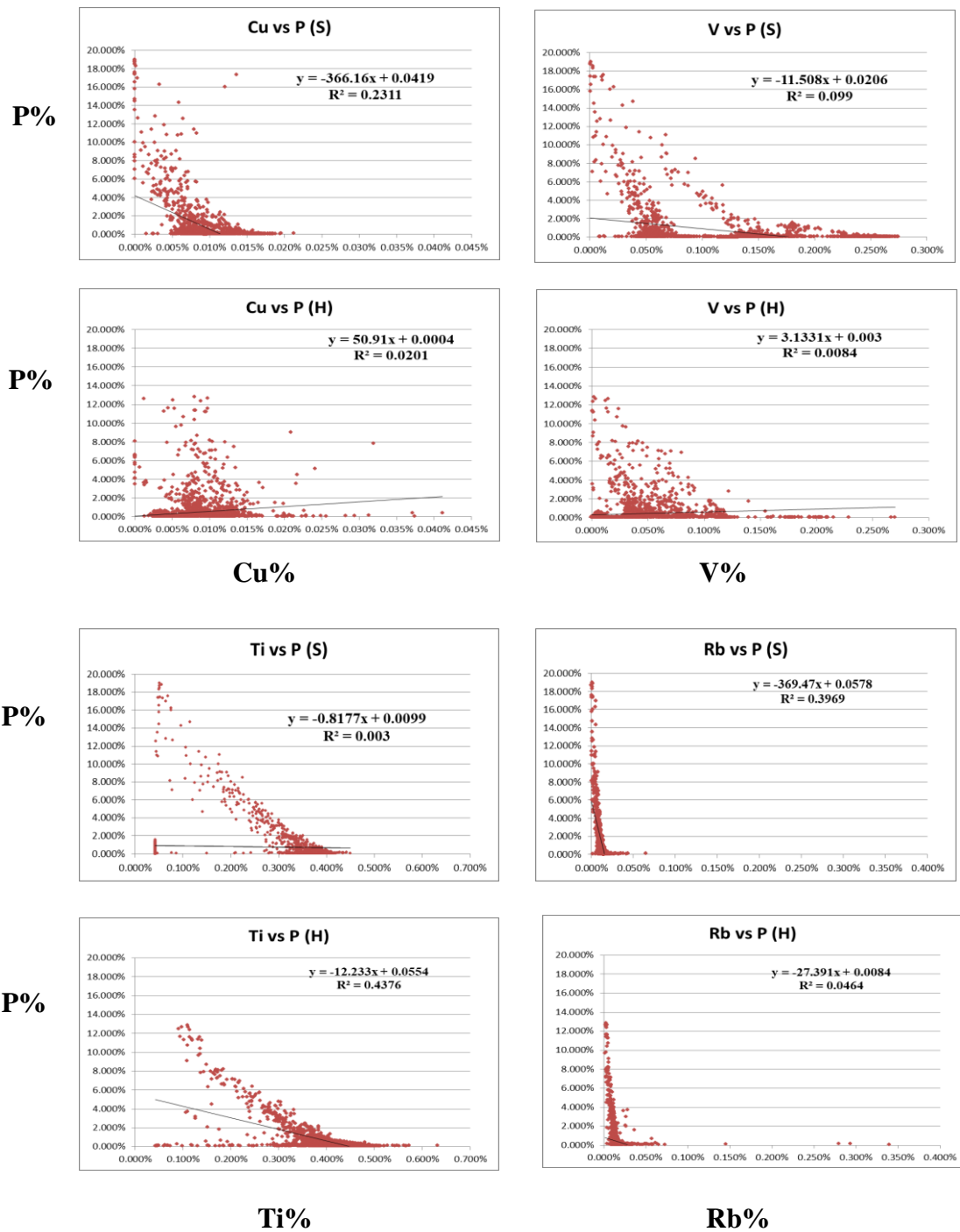


Figure 4.5 continued



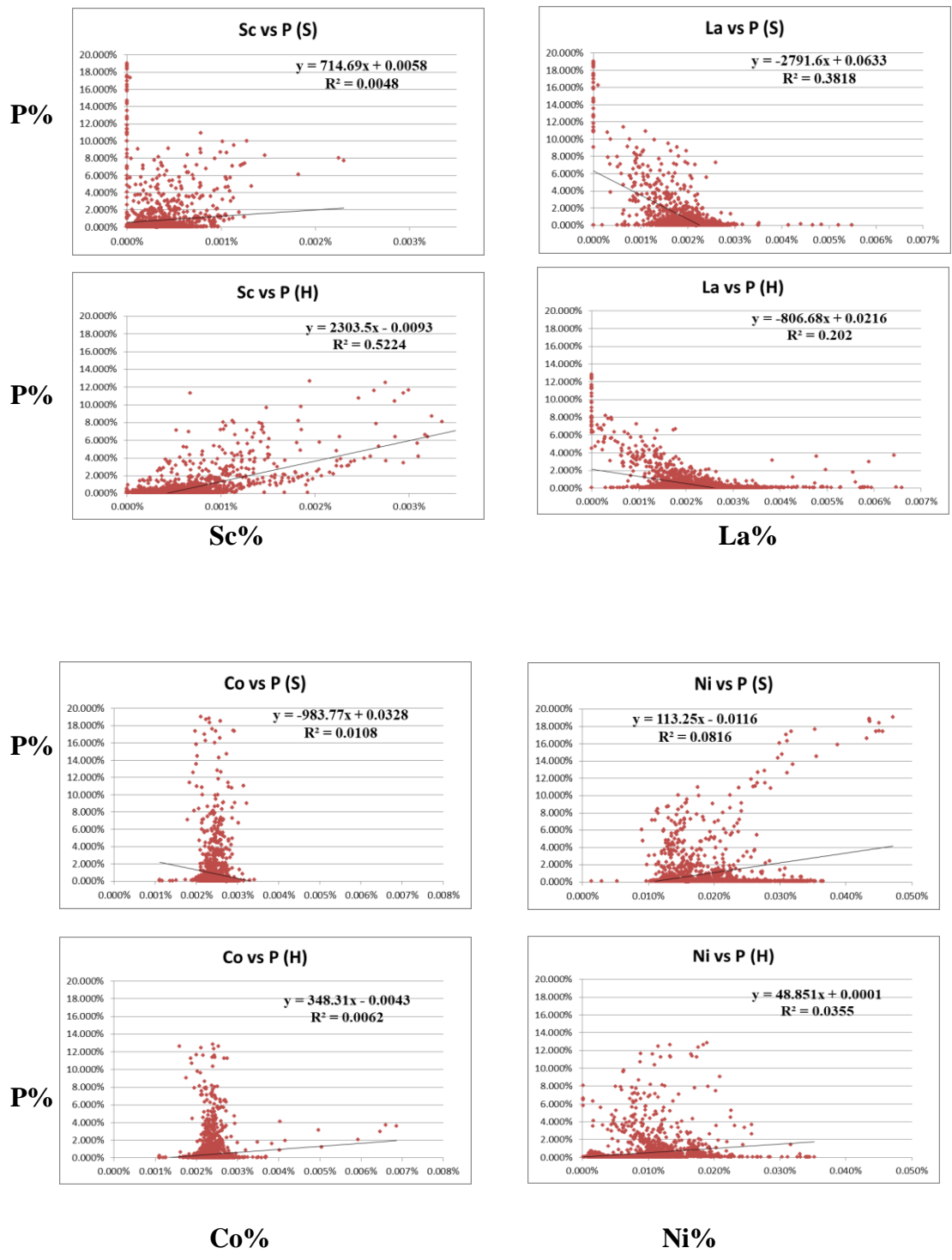
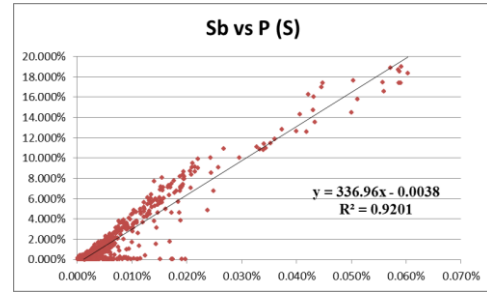
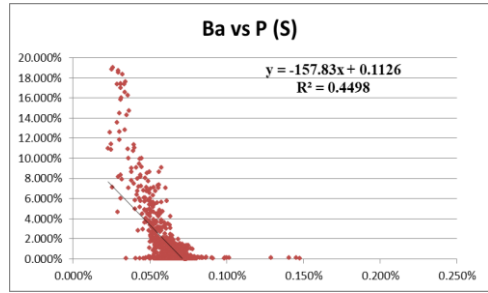
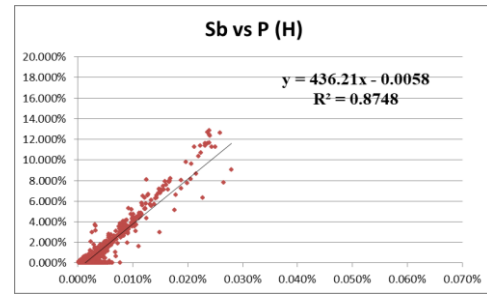
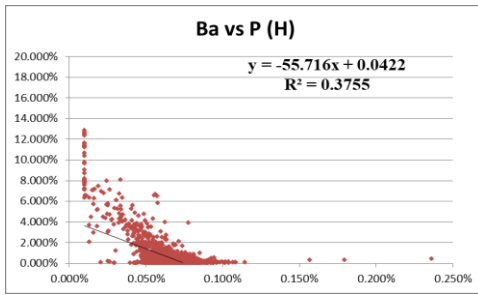


Figure 4.5 continued

**P%**



**P%**



**Ba%**

**Sb%**

Figure 4.5 continued



Figure 4.6. Correlation between Al and other elements (Si, K, Ti, V, Ni, Co, Cu, P, Zn, Pb, Sc, La and Sb) in Hushpuckney (H) and Stark (S) black shales. Strong Al-Si correlation is expected if clay minerals are present. A strong positive Al-K correlation is expected if illite is present.



Figure 4.6 continued

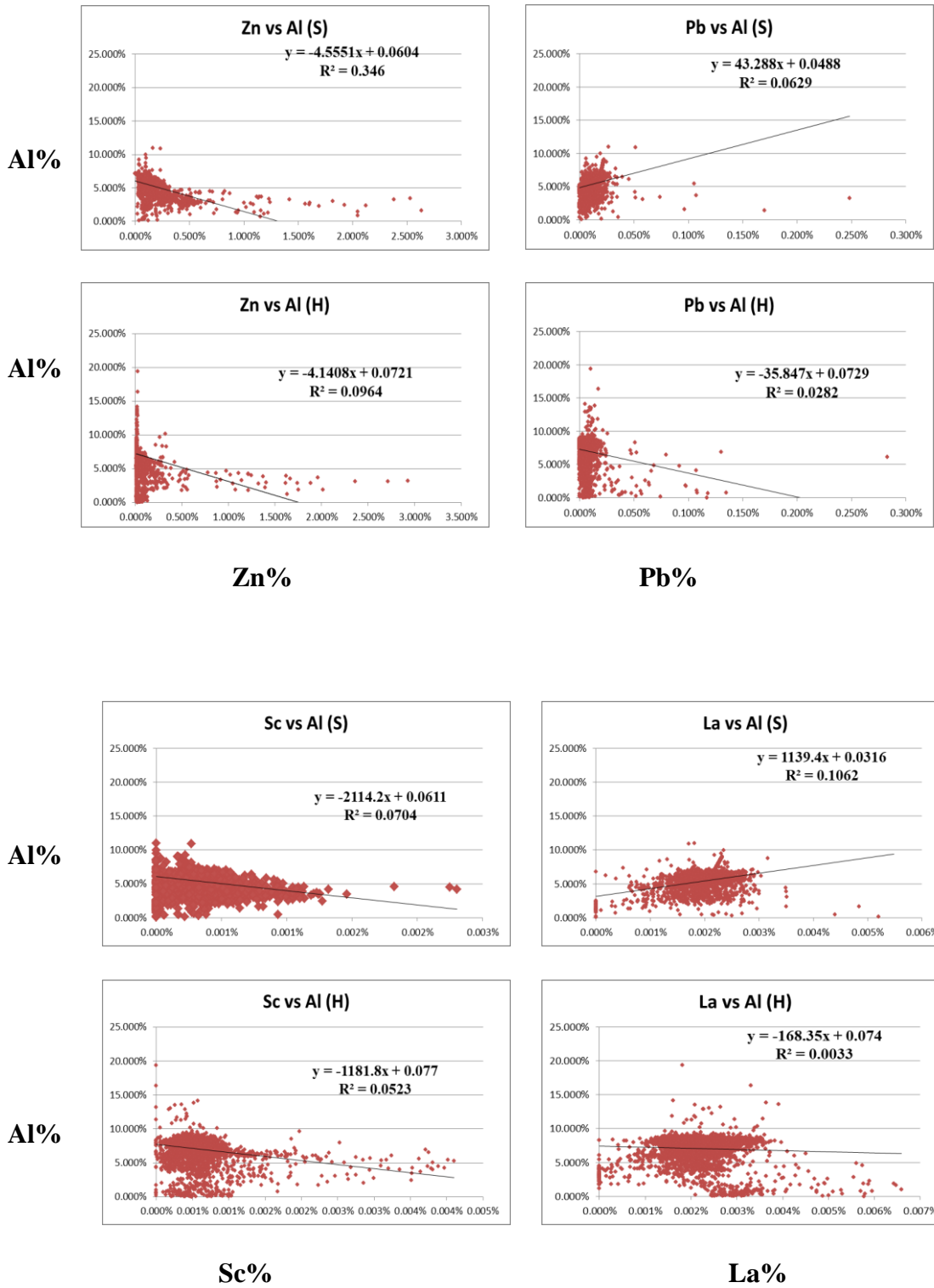


Figure 4.6 continued

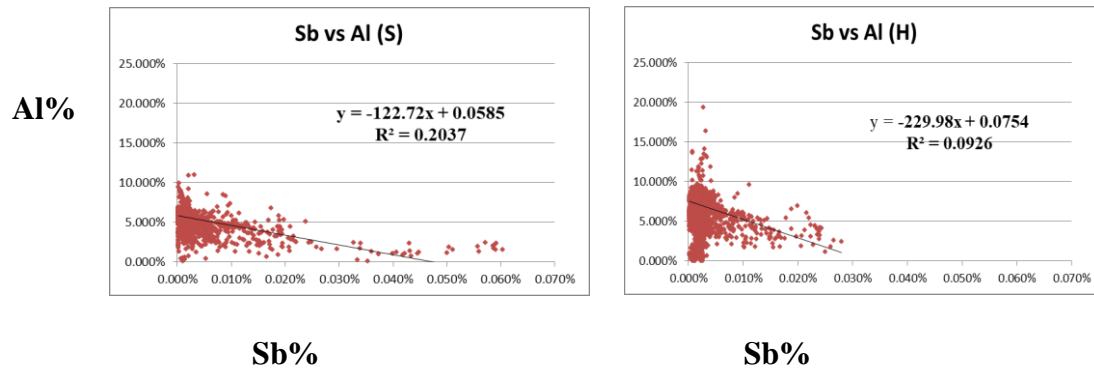


Figure 4.6 continued

The aluminum correlation relationships with the other elements explained in the Hushpuckney unit: there is a very strong and strong positive correlation with silicon, potassium and titanium respectively; weak positive correlation with cobalt; weak and very weak negative correlation with nickel, copper, vanadium, phosphorus, zinc, lead, scandium and antimony respectively; and almost no relation with lanthanum. The Stark unit has the same correlation coefficients, except the titanium with aluminum has very weak negative correlation.

Other correlations in this work are lead versus selenium and sulfur which indicate strong positive relation for selenium in Stark, while in Hushpuckney shows positive moderate correlation and weak and very weak positive correlation with sulfur in Stark and Hushpuckney units respectively. The iron has moderate positive correlation with sulfur in Stark and strong positive relation in Hushpuckney; very weak positive relation with copper in Stark and almost no relation in Hushpuckney; and weak negative correlation with zinc in Stark while in Hushpuckney very weak negative relation. The relation between zinc and antimony in Stark is very weak positive correlation and weak positive in Hushpuckney; while there is almost no relation between zinc and copper in Stark and very weak positive in Hushpuckney. Sulfur has very weak positive correlation with copper in both units, while it has very weak positive relation with barium in Stark and very weak negative in Hushpuckney. Calcium versus magnesium has very weak negative relation in Stark while in Hushpuckney there is almost no relation. Calcium and strontium have very strong positive relation in Stark but weak positive relation in Hushpuckney. Finally, there is moderate positive relation between rubidium and potassium in Stark while it is almost no relation in Hushpuckney.

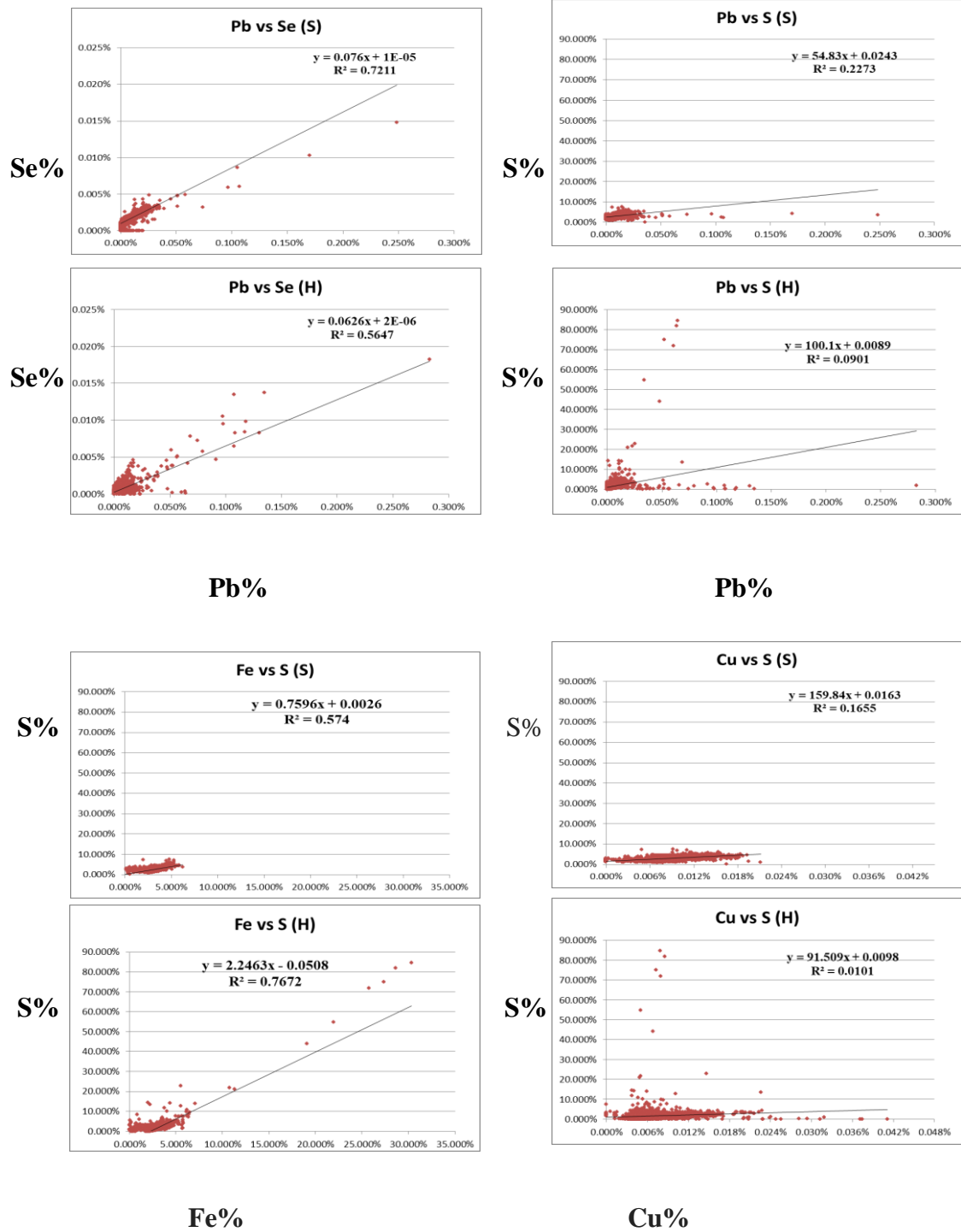


Figure 4.7. Linear correlation among selected elements as it indicates to each relationship in Hushpuckney (H) and Stark (S) black shale units.



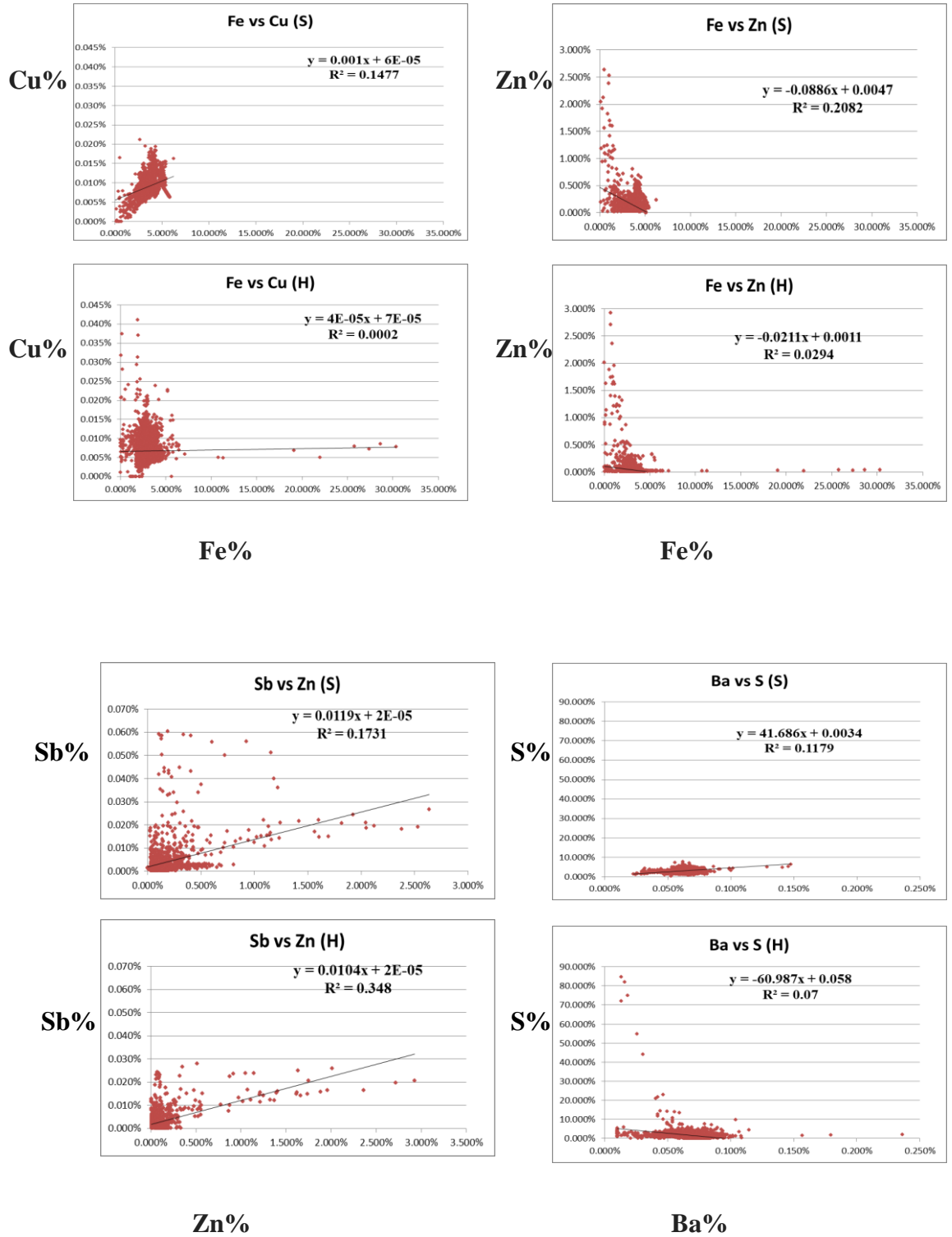
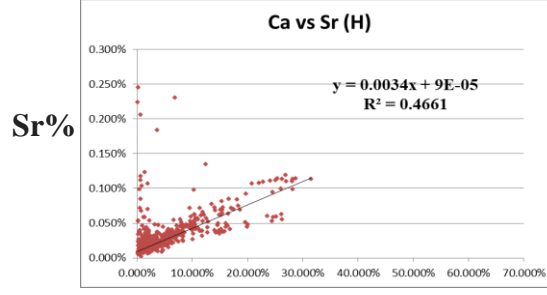
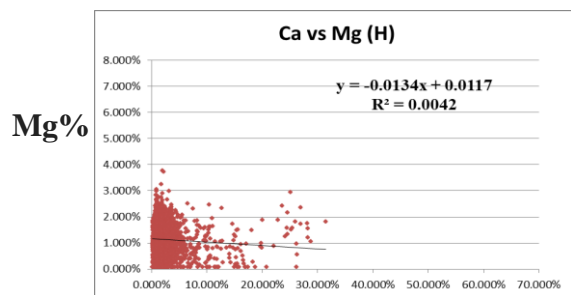
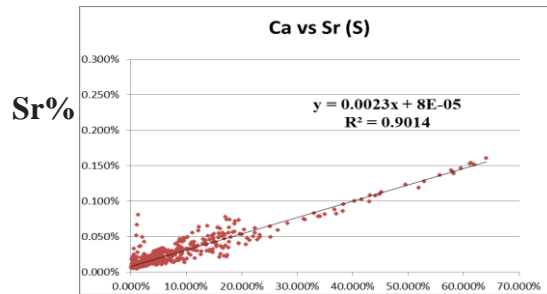
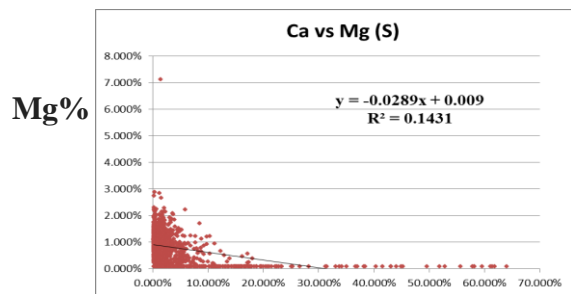
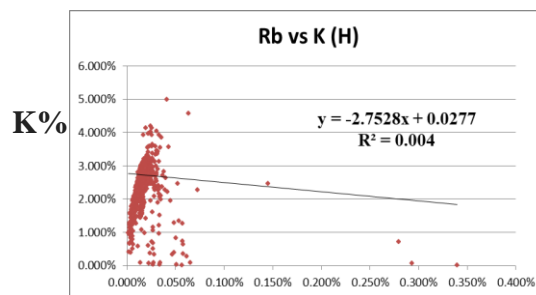
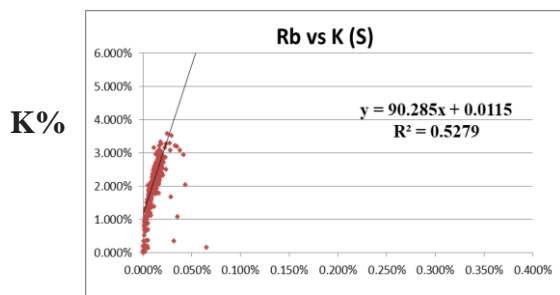


Figure 4.7 continued



Ca%

Ca%



Rb%

Rb%

Figure 4.7 Continued

## **Linear Correlation Discussion**

Correlation coefficients showed some clear relationships in the two black shale units, as for phosphorus with calcite, which supports the presence of fluoroapatite mineral. Also, this relationship showed the possibility there are two phases or two stages of phosphate minerals in both units. The relationship between phosphorus and zinc is weak positive and this is giving the impression that phosphates are not the source of zinc enrichment. Although the relation between phosphorus and vanadium is very weak negative in Stark unit and almost no relation in Hushpuckney unit, it showed there are might be two stages or phases of phosphate minerals again. The relationship between phosphorus and other elements did not show any obvious relationship. This can be explained by the fact that the sources of these elements may be from the transferred clay minerals or the organic matter present in the black shale.

There are positive correlations between Al and Si and K in both units strongly suggesting the occurrence of these elements in common phases as detrital clay minerals and in addition of existing free silica as quartz. The relationship of titanium with aluminum is different in both units where there is a negative relationship in the stark, while a strong positive relationship in the Hushpuckney. This can be explained by the different type and quantities of sediments and their source area. Very weak positive correlation found between Al and Co, Pb and La which may explained by accompaniment the clay minerals .The correlation relationships between the aluminum and other metals listed in Table 4.5 showed that there were insignificant relationships. This can be explained by the fact that these metals may came from organic matter or from limited activity hydrothermal solutions during the shale deposition.

The relationship between lead on one hand and selenium and sulfur on the other hand showed a strong positive relationship with selenium. This corresponds to the presence of the clausthalite. The relationship with sulfur, although weak but positive, can be explained by the presence of very small quantities of galena may exist with clausthalite as solid solutions as previously mentioned in Chapter 3 as it shows some traces of sulfur in the elemental map. Positive strong to moderate correlation between iron and sulfur, this is natural for the presence pyrite and framboidal pyrite. Correlation between iron and copper was done, this relation showed very weak positive relation in Stark while almost no relation in Hushpuckney. This matter may explain the existence of chalcopyrite in Stark unit while it is not detected in Hushpuckney unit. The relation between iron and zinc in both units is weak to very weak negative relation and this may explain by substitution between them. The relations between zinc versus copper, antimony versus zinc, copper versus sulfur and barium versus sulfur are not significant although it is positive relation but very weak. Calcium makes very weak negative correlation with magnesium in Stark unit and negative but almost no relation in Hushpuckney unit. This negative relation is due to the presence of dolomite. Strontium makes very strong positive relation with calcium in Stark unit but weak positive relation in Hushpuckney unit. This positive relation is confirming accommodation in the calcite lattice; in addition, calcium carbonate when it formed in sea water always contains some Sr (Krauskopf, 1982). The relation between rubidium and potassium is moderate positive in Stark unit while it is almost no relation in Hushpuckney unit. Rubidium is a member of the alkali metal group 1 of the periodic table, along with Li, Na, K and Cs. Rubidium is a lithophile metallic element that does not form any minerals of its own, but it is present in several common minerals in which it substitutes for potassium (Krauskopf, 1982).

**Table 4.4. Correlation relations of major, minor and trace elements versus phosphorus (P)**

Element vs P	Stark black shale unit		Hushpuckney black shale unit		Limits for correlation type
	Correlation value	Correlation type	Correlation value	Correlation type	
Ca	Positive / 0.9276	Very strong	Positive / 0.8925	Very strong	$\leq 0 - 0.01$ Almost no relation
Zn	Positive / 0.2113	Weak	Positive / 0.3951	Weak	0.01 - 0.2 Very weak
Cu	Negative/0.2311	Weak	Positive / 0.0201	Very weak	0.2 - 0.5 Weak
V	Negative /0.099	Very weak	Positive/ 0.0084	Almost no relation	0.5 - 0.6 Moderate
Fe	Negative/0.4347	Weak	Negative/0.0445	Very weak	0.6 - 0.8 Strong
Pb	Negative/0.0063	Almost no relation	Positive / 0.0001	Almost no relation	0.8 - 0.99 Very strong
Ti	Negative /0.003	Almost no relation	Negative/0.4376	Weak	$\neq 1$ Perfect
Rb	Negative/0.4699	Weak	Negative/0.0464	Very weak	
Sc	Positive / 0.0048	Almost no relation	Positive / 0.5224	Moderate	
La	Negative/0.3818	Weak	Negative / 0.202	Weak	
Co	Negative/0.0108	Very weak	Positive / 0.0062	Almost no relation	
Ni	Positive / 0.0816	Very weak	Positive / 0.0355	Very weak	
Ba	Negative/0.4498	Weak	Negative/0.3755	Weak	
Sb	Positive / 0.9201	Very strong	Positive / 0.8748	Very strong	

**Table 4.5. Correlation relations of major, minor and trace elements versus Aluminum (Al)**

Element vs Al	Stark black shale unit		Hushpuckney black shale unit		Limits for correlation type
	Correlation value	Correlation type	Correlation value	Correlation type	
Si	Positive/0.9245	Very strong	Positive/0.9325	Very strong	$\leq 0 - 0.01$ Almost no relation $0.01 - 0.2$ Very weak $0.2 - 0.5$ Weak $0.5 - 0.6$ Moderate $0.6 - 0.8$ Strong $0.8 - 0.99$ Very strong $\pm 1$ Perfect
K	Positive/0.739	Strong	Positive/0.6898	Strong	
Ti	Negative/0.0217	Very weak	Positive/0.6332	Strong	
V	Negative/0.0364	Very weak	Negative/0.1814	Very weak	
Ni	Negative/0.394	Weak	Negative/0.3163	Weak	
Co	Positive/0.1791	Very weak	Positive/0.0194	Very weak	
Cu	Negative/0.0383	Very weak	Negative/0.2632	Weak	
P	Negative/0.1972	Very weak	Negative/0.1067	Very weak	
Zn	Negative/0.346	Weak	Negative/0.0964	Very weak	
Pb	Positive/0.0629	Very weak	Negative/0.0282	Very weak	
Sc	Negative/0.0704	Very weak	Negative/0.0523	Very weak	
La	Positive/0.1062	Weak	Positive/0.0033	Almost no relation	
Sb	Negative/0.2037	Weak	Negative/0.0926	Very weak	

Table 4.6. Correlation coefficients relationship between some elements

Element vs Element	Stark black shale unit		Hushpuckney black shale unit		Limits for correlation type
	Correlation value	Correlation type	Correlation value	Correlation type	
Pb vs Se	Positive/0.7211	Strong	Positive/0.5647	Moderate	$\leq 0 - 0.01$ Almost no relation $0.01 - 0.2$ Very weak $0.2 - 0.5$ Weak $0.5 - 0.6$ Moderate $0.6 - 0.8$ Strong $0.8 - 0.99$ Very strong $\pm 1$ Perfect
Pb vs S	Positive/0.2273	Weak	Positive/0.0901	Very weak	
Fe vs S	Positive/0.574	Moderate	Positive/0.7672	Strong	
Fe vs Cu	Positive/0.1477	Very weak	Positive/0.0002	Almost no relation	
Fe vs Zn	Negative/0.2082	Weak	Negative/0.0294	Very weak	
Zn vs Cu	Positive/0.0079	Almost no relation	Positive/0.0433	Very weak	
Sb vs Zn	Positive/0.1731	Very weak	Positive/0.348	Weak	
Cu vs S	Positive/0.1655	Very weak	Positive/0.0101	Very weak	
Ba vs S	Positive/0.1179	Very weak	Negative/0.07	Very weak	
Ca vs Mg	Negative/0.1431	Very weak	Negative/0.0042	Almost no relation	
Ca vs Sr	Positive/0.9014	Very strong	Positive/0.4661	Weak	
Rb vs K	Positive/0.5353	Moderate	Negative/0.004	Almost no relation	

## CHAPTER 5

### DEPOSITIONAL ENVIRONMENT

Black shales were deposited in many places and at many times during the geologic history. They can be generally defined as laminated or fissile rocks containing clay- and silt-sized detrital and/or authigenic minerals grains, rich in organic matter, rich in iron sulfide, sometimes rich in metals, occasionally having phosphate nodules or laminations, and they formed in reduced redox environments. Some black shales have been recognized as reservoirs for gaseous hydrocarbons and others as syngenetic hosts for metal deposits. Many investigators have felt that all shales of this type may be related to a single depositional environment, whereas others have hypothesized a diversity of origins.

#### **Paleoenvironment**

Geochemical data for elements in sediments and sedimentary rocks can be correlated with each other to determine the factors that affected the quality of sediments, and can be used to interpret the influential geological events during deposition in marine environments through the geological time. These correlation factors are indices for the assessment of paleoredox conditions, provenance and tectonic setting. The immobile major and trace elements such as Al, Si and Ti can be used to identify the source area that produced the detrital materials of sediments in marine basin and its tectonic regime (Kronberg and Nesbitt, 1981; Gertsch et al., 2011; Soua, 2011 and Sari and Koca, 2012). Redox-sensitive trace elements in sea water such as V, U, Mo, Ni, Cr and Co are powerful tools to determine the paleoredox conditions (Rimmer, 2004; Brumsack, 2006; Tribovillard et al., 2006 and Soua, 2011). Paleoredox conditions give information about how the oxygen level fluctuated



throughout the past geologic time and its effect on the quality of marine sediments. It was defined as the prevailing conditions whether oxidizing or reducing during accumulation of sediments in marine environments (Tribovillard et al., 2006). Marine depositional environments have been classified into four categories (Alego and Maynard, 2004 and Tribovillard et al., 2006): (1) oxic environments in which oxygen is present, (2) anoxic environments which are characterized by a very low oxygen concentration and the absence of free H<sub>2</sub>S (non-sulfidic anoxic conditions), (3) suboxic (dysoxic) environments which are transitional between oxic and anoxic environments, and finally (4) the euxinic environments which have free H<sub>2</sub>S (sulfidic anoxic condition) and oxygen is effectively absent.

Trace elements can be utilized as proxies for the reconstruction of paleoredox conditions because of different behaviors in their solubility and oxidation state. Many redox-sensitive trace elements are insoluble under reducing environments, while they are soluble under oxidizing conditions (Tribovillard et al., 2006). Concentration ratios of some of these redox-sensitive elements, such as Ni/Co and V/ (V + Ni), can be used as indicators of paleoredox conditions. These two ratios are used to distinguish oxic and anoxic bottom water (Hatch and Leventhal, 1992; Jones and Manning, 1994; Souza, 2011 and Gertsch et al., 2011). Nickel, cobalt and vanadium under reducing environments are less soluble, and this may help to form organo-metallic compounds which lead to retention and enrichment of these elements (Alego and Maynard, 2004 and Tribovillard et al., 2006). These ratio values can be used as redox proxies to identify the ranges for oxidation reduction environments (Table 5.1).

These ratios are applied for the two black shales units as listed in Table 5.2. The values of the three trace elements are listed in Table 5.2.

## Paleoredox Discussion

The results listed in Table 5.2 reveal interference and fluctuation between oxidized and reduced environments. The Ni/Co ratio of the Hushpuckney shale indicates that the shale was deposited in oxic zone environment whereas the  $V/(V + Ni)$  ratio shows that deposition occurred within the range of reduced environments from anoxic to euxinic environment. This variation is due to diagenetic processes and/or minor post-depositional oxidation because these rocks are not far from the surface where its depth is about 19 meters. In addition, lithology for the Hushpuckney is composed of two parts: a black shale lower part and a gray shale at the top. In general, one can conclude that the Hushpuckney black shale started to form in an anoxic condition with accumulation of organic matter in the lower part but then the depositional environment gradually became more oxidizing with bioturbation appearing in the upper part of the gray shale (Table 5-2). The results obtained from the use of such element ratios for the unweathered part of the Stark are more consistent; both the Ni/Co and  $V/(V + Ni)$ , indicate anoxic – euxinic depositional conditions in agreement with the abundance of organic matter and framboidal pyrite.

Table 5.1. Redox proxy values and their ranges for oxic, dysoxic, anoxic and euxinic environments

<b>Proxy</b>	<b>Oxic</b>	<b>Dysoxic</b>	<b>Anoxic</b>	<b>Euxinic</b>
<b>Ni/Co<sup>(1)</sup></b>	<b>&lt; 5</b>	<b>5-7</b>	<b>&gt; 7</b>	
<b>V/(V + Ni)<sup>(2)</sup></b>	<b>&lt; 0.46</b>	<b>0.46 – 0.60</b>	<b>0.54 – 0.82</b>	<b>&gt; 0.84</b>

(1) Jones and Manning, 1994; (2) Hatch and Leventhal, 1992

Table 5.2. Maximum, minimum and average values ratios for the two studied black shales

<b>Units</b>	<b>Value</b>	<b>Ratios</b>	
		<b>Ni/Co</b>	<b>V/(V + Ni)</b>
<b>Stark black shale</b>	<b>Maximum</b>	<b>13.85</b>	<b>0.85</b>
	<b>Minimum</b>	<b>1.27</b>	<b>0.0</b>
	<b>Average</b>	<b>6.96</b>	<b>0.86</b>
<b>Hushpuckney black shale</b>	<b>Maximum</b>	<b>5.10</b>	<b>0.88</b>
	<b>Minimum</b>	<b>0.18</b>	<b>0.66</b>
	<b>Average</b>	<b>3.30</b>	<b>0.77</b>

## **Sphalerite and Clausthalite**

Sphalerite (ZnS) is the predominant zinc mineral in the shales. Clausthalite (PbSe) is a selenide phase and it is a member of the galena group. Both minerals can form under a wide range of low to high temperature hydrothermal solutions. They are clearly observed around the phosphate nodules edges which in turn are disseminated in both black shale units.

Sphalerite is formed under a wide range of low- to high-temperature hydrothermal conditions; in coal, limestone, and other sedimentary deposits. Coveney (1979) suggested that the sphalerite type in Hushpuckney and Stark black shales may have implications concerning the origin of Mississippi Valley-Type mineralization. Mississippi Valley-Type (MVT) lead-zinc deposits are found throughout the world but the largest and more intensely researched deposits occur in North America. The ores consist mainly of sphalerite, galena, and lesser amounts of iron sulfides. The most important characteristics of MVT ore deposits are: hosted mainly by dolostone and limestone in platform carbonate sequences and usually located at flanks of basins; they have no spatial or temporal relation to igneous rocks, which distinguishes them from skarn or other intrusive rock-related Pb-Zn ores; deposits form districts that are localized by geologic features, including breccias, depositional margins of shale units (shale edges), faults, and basement highs that permit upward migration of ore fluids; ore deposition temperatures are low (50° C to 200° C) and high salinities 15-25 wt% NaCl equivalent, but typically higher than those attributable to local basement-controlled thermal gradients; and associated alteration consists mainly of dolomitization, brecciation, host-rock dissolution, and dissolution / crystallization of feldspar and clay (Jensen and Bateman, 1981; Anderson, 1982; Guilbert, 1986; and Evans, 1993).

Another type of sphalerite formation occurs during the seepage of hydrothermal solutions at the seafloor. The formation of sphalerite is accomplished through circulation of seawater, which penetrates deeply into the oceanic crust at seafloor spreading centers; it is converted to a hydrothermal fluid with low pH, low Eh and high temperature during water-rock interaction above a high-level magma chamber. This fluid is capable of leaching large amounts of metals and other elements from the rocks. Metal sulfides, including pyrite, sphalerite and chalcopyrite which are precipitated from the hydrothermal fluids, gradually accumulate at and just below the seafloor where they can form large sulfide deposits in the form of sediments and chimneys (known as “black smokers”) (Evans, 1993 and Herzig and Hannington, 2006).

Zinc may be hosted in the apatite lattice substituting for calcium within a limited range due to the significant difference in ionic radii between Zn and Ca. In their experiments Walczyk et al., (2016), found that zinc can embed in calcium phosphate enhancing bone formation. In addition, incorporation of Zn improves antifungal and antibacterial properties. They concluded that enhancement with various ions (like Zn) by absorption is a suitable way to form compact structures that can be used as potential implants. This process could be one of the ways to enrich zinc in black shale to form sphalerite in reducing environments (anoxic-euxinic conditions).

Clausthalite is the common selenide minerals in the black shales and it occurs naturally as solid solution with galena (PbS). The existence of end-member clausthalite is rare in nature. It tends to precipitate at higher redox potentials than galena due to the stability of  $\text{Se}^{2-}$  extending beyond the stability of reduced sulfur. Many researchers have concluded that clausthalite formation is from hydrothermal solutions with relatively low temperature  $\leq$

200° C (Tischendorf and Ungethum, 1964; Frigstad, 1972; Healy and Petruk, 1992 and Bogdanov et al., 2005). Tischendorf and Ungethum, (1964) deduced that the formation of the clausenthalite and galena are controlled by: the oxidation potential and the pH of the solution; and the  $[Se^{2-}]/[S^{2-}]$  ratio as a function of Eh and pH. The solubility product of clausenthalite is smaller than that of galena, and clausenthalite is always formed at higher Eh than galena.

Babu et al., (2002) reported the occurrence of clausenthalite in the uraniferous Mahadek sandstones of Domiasiant and Wahkyn, Meghalaya plateau, India. They suggested the possibility that selenium-bearing solutions are derived from abundant organic matter by the circulating groundwater. The enrichment of the Se / S ratio in the circulating solutions at later stage seemed to favor the precipitation of seleniferous sulphides grading into selenide phases.

### **Phosphates**

The term phosphorites are used for those sediments in which phosphate minerals are the main constituent. Distinctions are made between those rocks which were initially highly phosphatic and those which have been phosphatized much later. Residual phosphate is a term applied to a surface accumulation of insoluble phosphatic materials. These residual or debris phosphates are accumulated like the accumulation of residual gravels which are a residuum reworked by streams (Pettijhon, 1975 and Selley, 2000). The most common components of phosphatic rocks are the several varieties of apatite:

Carbonate fluorapatite (Francolite) –  $Ca_5(PO_4,CO_3)_3F$ ; fluorapatite –  $Ca_5F(PO_4)_3$ ; chlorapatite –  $Ca_5Cl_2(PO_4)_3$ ; and hydroxylapatite –  $Ca_5(OH)(PO_4)_3$ . The general formula may be written  $Ca_5(PO_4,CO_3)_3(F, Cl, OH)$  and francolite is considered to be the most common phosphate mineral in sedimentary rocks. Its chemical composition is quite variable

due to the large number of sites in which substitution is possible and can incorporate V, Mg, Sr, Pb, Na, U, Ce, and Y in various sites in the structure. The chemical composition of francolite is influenced by a number of variables, such as the chemical composition of sea and interstitial waters, thermodynamics and kinetics of precipitation, modes of precipitation (directly from solution or replacement of pre-existing minerals through dissolution/precipitation processes), and postdepositional alteration (during late diagenesis or weathering)( Follmi, 1995).

The origin of phosphates has been debated since the 19th century because of their strong variability in lithology and depositional environments. The origin of phosphate can be divided into three groups: biogenic, chemogenic and volcanogenic-hydrothermal (Follmi, 1996; Baturin, 1999). Biogenic processes include phosphates removed from the seawater by organisms and released again when they die or defecate, settling on the sea bed amongst miscellaneous organic matter. Enrichment in sediments by microbial breakdown of organic matter, releasing organic phosphate to pore waters represents the most fundamental source of phosphate. Chemogenic processes involve direct chemical precipitation of calcium phosphates from sea water at the sediments-water- interface, or transferred into sediments by diffusion (more efficiently by eddy currents). The volcanogenic-hydrothermal hypothesis, though debatable, suggests that sea water penetrates the basaltic oceanic crust (basement rock), leaching phosphorus from the surrounding rocks as the water is heated and circulates. Upon reaching the seafloor, the temperature and pressure of the solutions decrease and phosphates precipitate or are extracted by bacterial mats.

Detrital phosphates are phosphate rocks formed under any kind of the previous types of phosphate origin and are then weathered, eroded and accumulated in other places forming

phosphatic debris. They may be partially dissolved to become a source of phosphorus in sediments. This debris, in turn, may be compacted, cemented and lithified to become new phosphate rocks (Follmi, 1996; Baturin, 1999).

Li and Schieber (2015) studied the Devonian Chattanooga Shale which contains phosphates nodules disseminated in the uppermost black shale. They reported that the phosphatic fossil debris is the main source of phosphate in the black shale. They suggested the possibility of four sources of dissolved phosphate in sediments: microbial breakdown of unsettled organic matter, phosphate desorption from iron and manganese oxyhydroxides, dissolution of phosphatic fossil debris, and direct precipitation of sea-water phosphate at the sediment–water interface.

Calcium phosphate can precipitate under neutral to weakly alkaline conditions and can dissolve under acidic or near neutral conditions (Dorozhkin, 2012). In their schematic model for the phosphate formation in the black shale unit, Li and Schieber (2015) proposed that under oxidizing conditions, a partial dissolution and degradation of framboidal pyrite will drop the pH, leading to partial dissolution of phosphatic fragments. The release of phosphate to pore waters will increase the concentrations of phosphate to supersaturation levels, and then will give rise to apatite precipitation when pore water acidity is reduced and pH rises again. Both increasing pH and upward shift of redox boundary favor reprecipitation of phosphate, and result in overgrowth cryptocrystalline apatite or secondary calcite around the partially dissolved phosphatic fragments. This cycle of reworking, winnowing, dissolution and reprecipitation can be repeated multiple times.



## Discussion

The studied samples are two black shale units composed of detrital clay minerals, organic matter, quartz, framboidal pyrite as well as euhedral pyrite grains, and phosphates grains disseminated through the detrital materials and organic matter. The phosphate clots appear as nodules, pellets and discrete thin lenticular lamination some of them containing sphalerite, clausthalite and sometimes euhedral pyrite minerals.

Leach and Rowan, (1986) suggested that the MVT lead and zinc mineralization in the Ozark region share a genetic link with the Ouachita uplift during the late Paleozoic. The Ozarks region includes the Viburnum Trend, Old Lead Belt, and Tri-State MVT districts, as well as the smaller Northern Arkansas, Central Missouri, and Southeast Missouri Barite districts. They inferred that the MVT mineralizing fluids originated from the south during the Ouachita Orogeny. They suggest that the ores were produced by warm mineralizing fluids which were focused by local structure.

Keller (1988) also proposed that kaolinite-group minerals (such as dickite) encircling MVT deposits are probable geologic indicators of a regional hydrothermal event.

Ragan (1996) in her study of the genesis of MVT deposits of eastern Kansas and the Tri-State zinc-lead mining district, found that occurrences of MVT-type mineralization in eastern Kansas are genetically related to the ores which occur in the Tri-State mining district of Kansas, Missouri, and Oklahoma by widespread hydrothermal processes. She noticed that samples from the Bethany Falls Limestone of the Pennsylvanian Series, Missourian stage, host vertical tube structures that are mineralized to varying degrees. These mineralized tube structures are 0.1-1 m in length and 1-10 cm in diameter, host vertical tubes which are lined

with calcite and contain twinned sphalerite crystals, ranging in size from microscopic up to 3.5 cm in diameter, in a hard granular material composed mainly of quartz and sphalerite, and are thought to be hydrothermal fluid conduits.

Observations collected from SEM/EDS photomicrographs of the phosphate grains in the Hushpuckney and Stark black shales units may suggest that some of those phosphate grains were transported as detrital grains. This interpretation arose from the features of these phosphate grains as follow: 1- Although some of these grains are bounded, compacted and cemented together, the traces of the external edges for these grains are still clear and can easily be distinguished (Figures 5.1 to 5.4 and 5.8). 2- Element maps of phosphorus and calcium show the rounded shape for these grains which may give impression that these grains are individual detrital grains not clots (Figure 5.5). 3- The phosphate clots sometimes occur isolated and scattered in the detrital material and show displacive texture (Figures 5.2 and 5.6 to 5.8). 4- Most of the phosphate clots are showing corrosive surface and this due to dissolution of phosphate because of decreases of pH solutions (Figures 5.3 and 5.4). 5- Phosphate grains are presence only in the black shale submember rich in organic matter and not found in the gray shale submember which is poor with organic matter. 6- Some of the phosphate grains are embracing sphalerite, clausthalite and pyrite minerals as shown in plates in chapter three Figures 5.1 to 5.5, 5.6-B and 5.8.

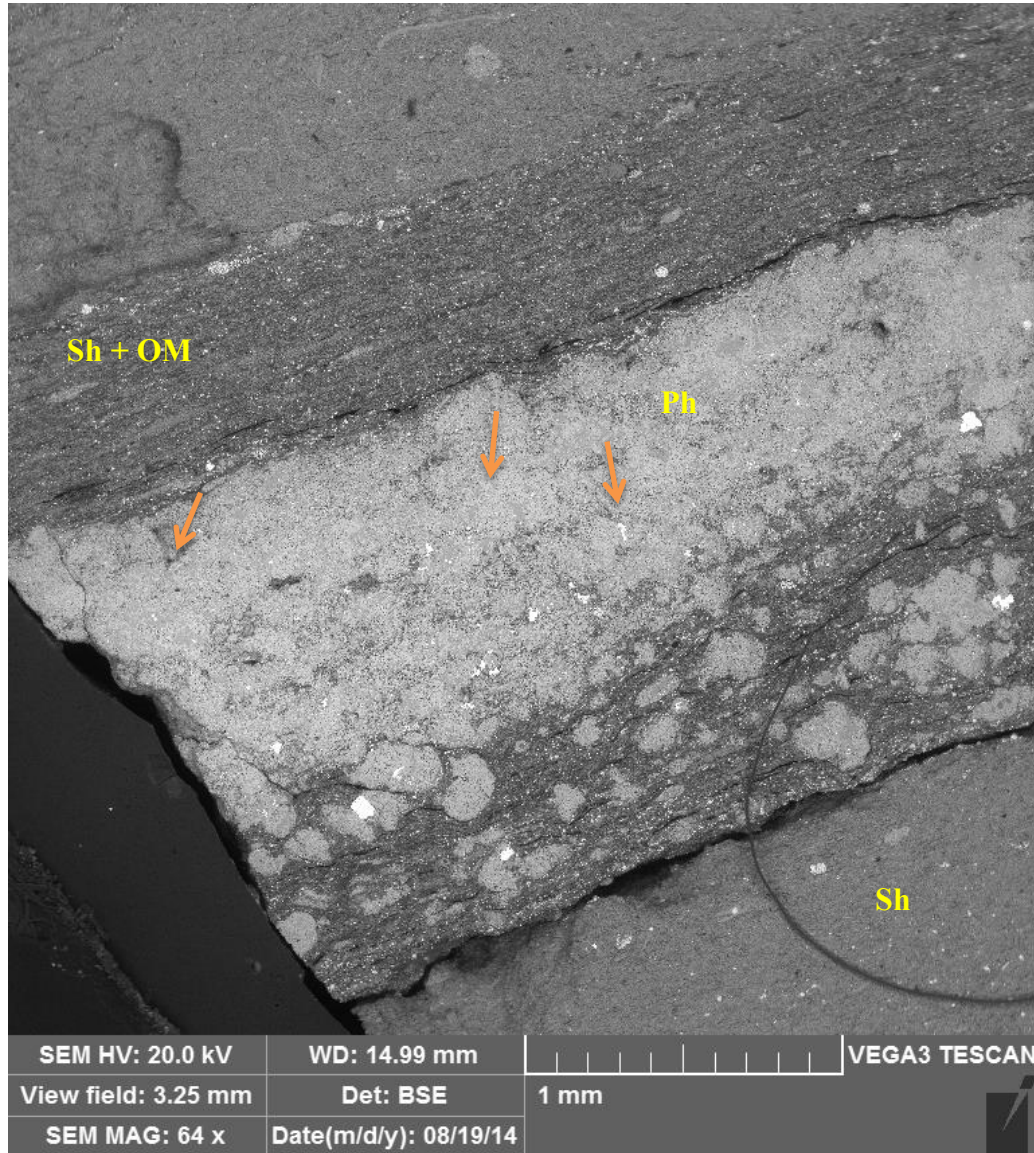


Figure 5.1. Phosphate nodule (Ph) between shale (Sh). The upper part of shale contain organic matter (OM) whereas the lower part poor in organic matter. The phosphate nodule is more compact in its upper part and looser in the lower part. Orange arrows point to traces of phosphate edges (Stark unit, Greenwood, MO).

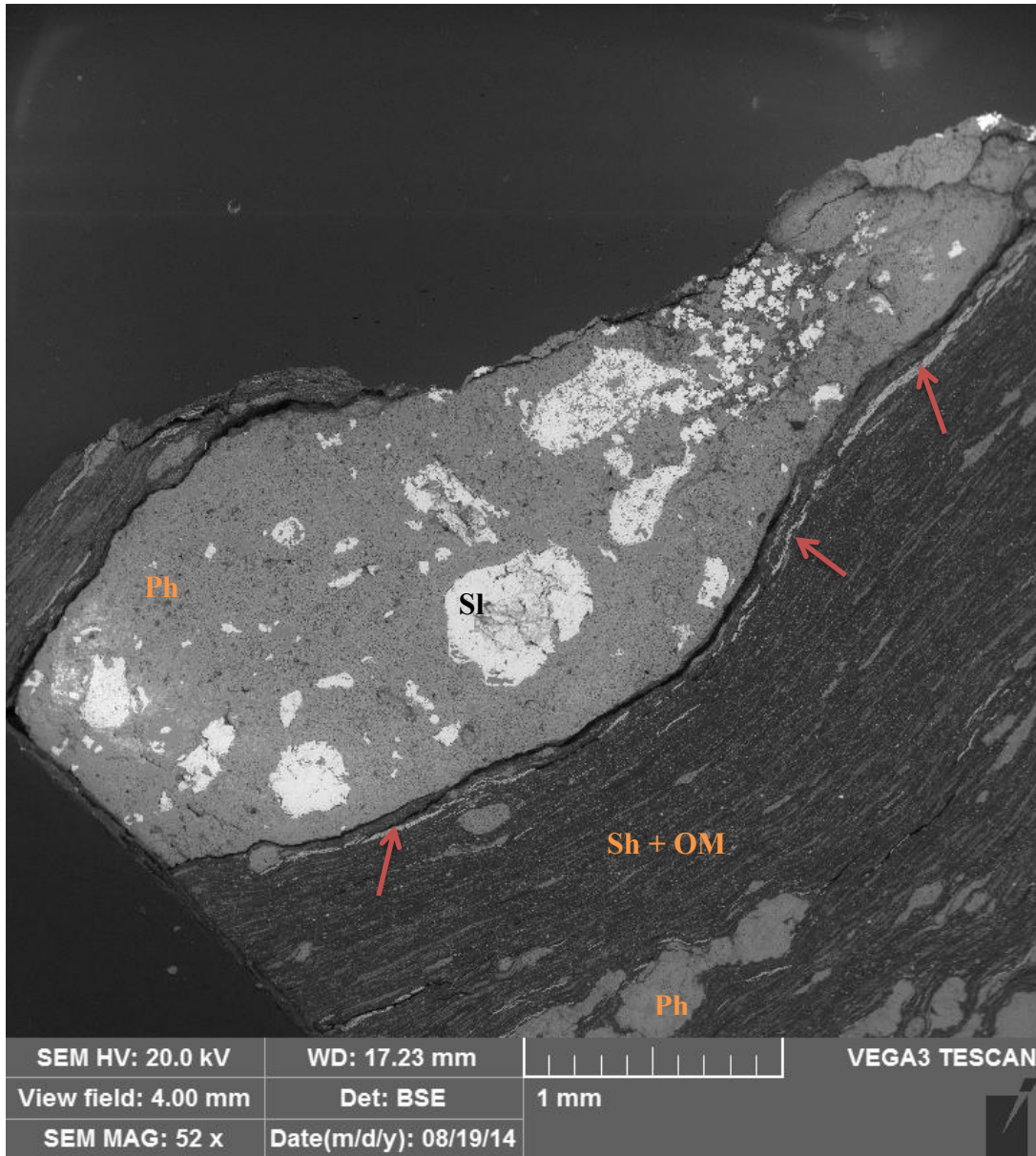


Figure 5.2. Phosphate nodules (Ph) disseminated in shale (Sh) and organic matter (OM). The largest nodule encloses sphalerite (SI), red arrows point to phosphate strips, Stark unit – Greenwood Quarry, Greenwood, MO.

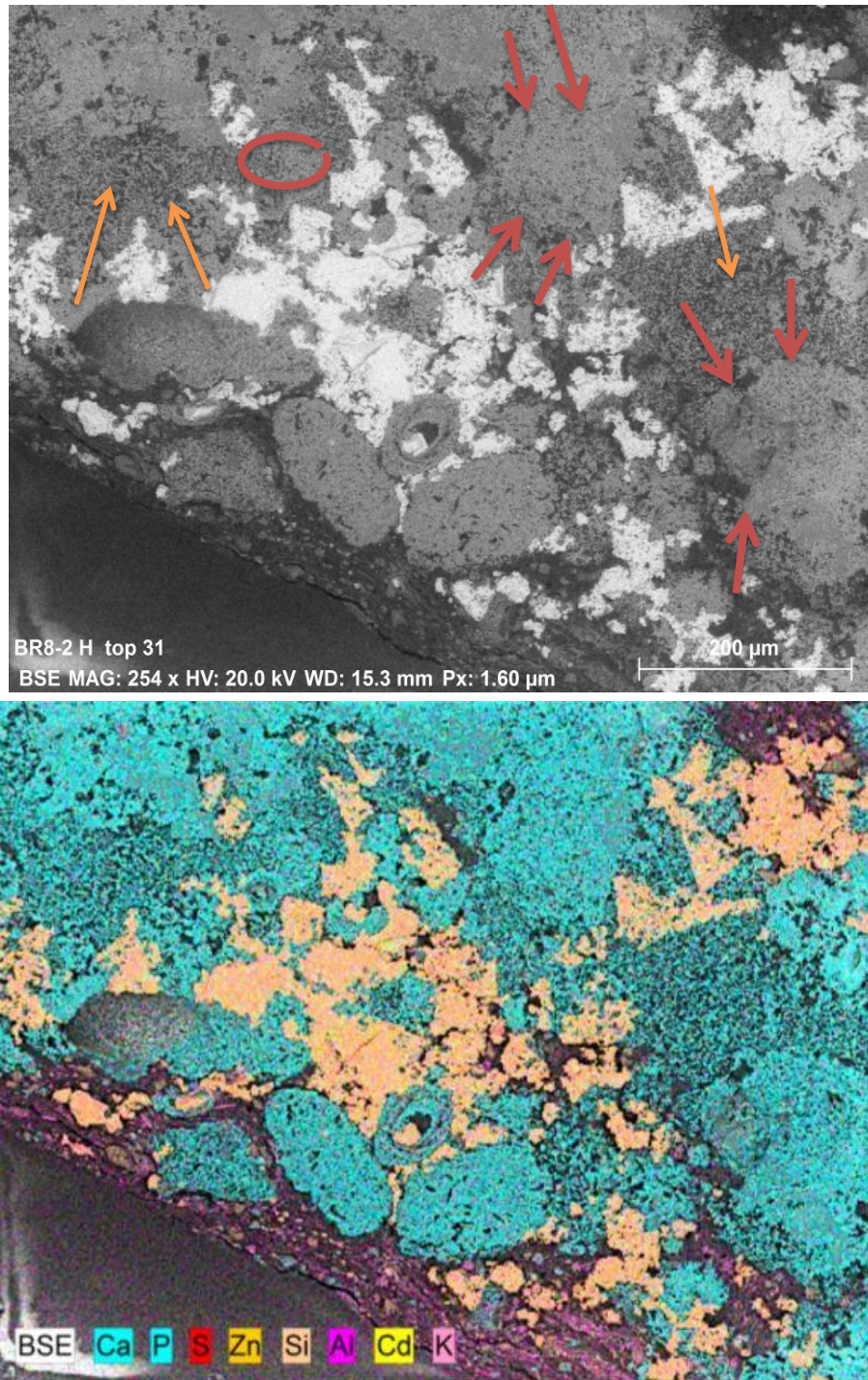


Figure 5.3. EDS images for Hushpuckney. Sphalerite disseminated between the phosphate pellets and grains. The red arrows and line point to the grain edges. Orange arrows point to corroded phosphate grains. Hushpuckney unit (BR8).

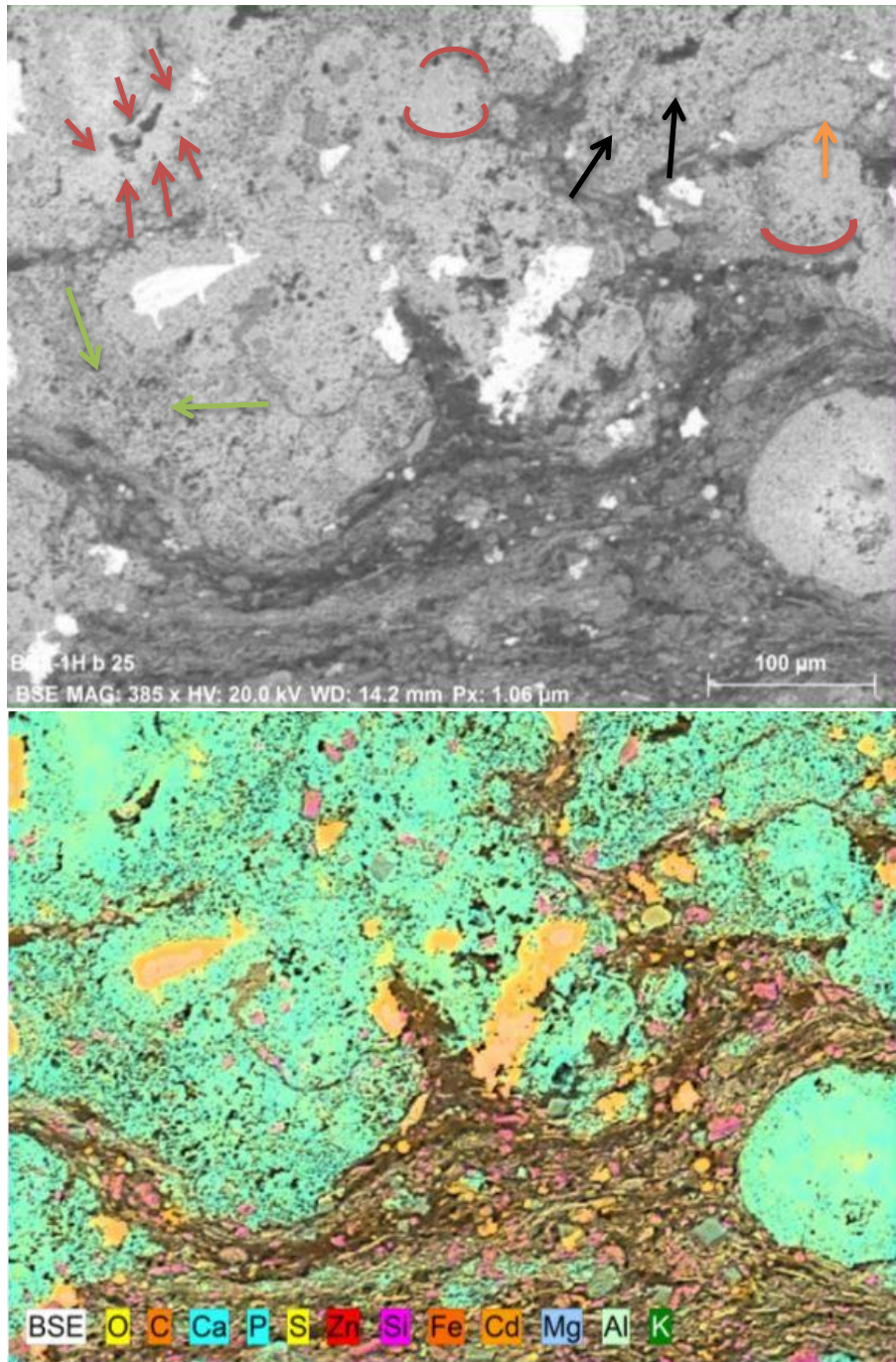


Figure 5.4. EDS images for Hushpuckney. Sphalerite in phosphate grains, red lines and arrows point to phosphate edges, Orange arrow point to concave convex boundary between two grains, Green arrows point to corroded phosphate grain, Black arrows point to growing phosphate strips, Hushpuckney unit (BR8).

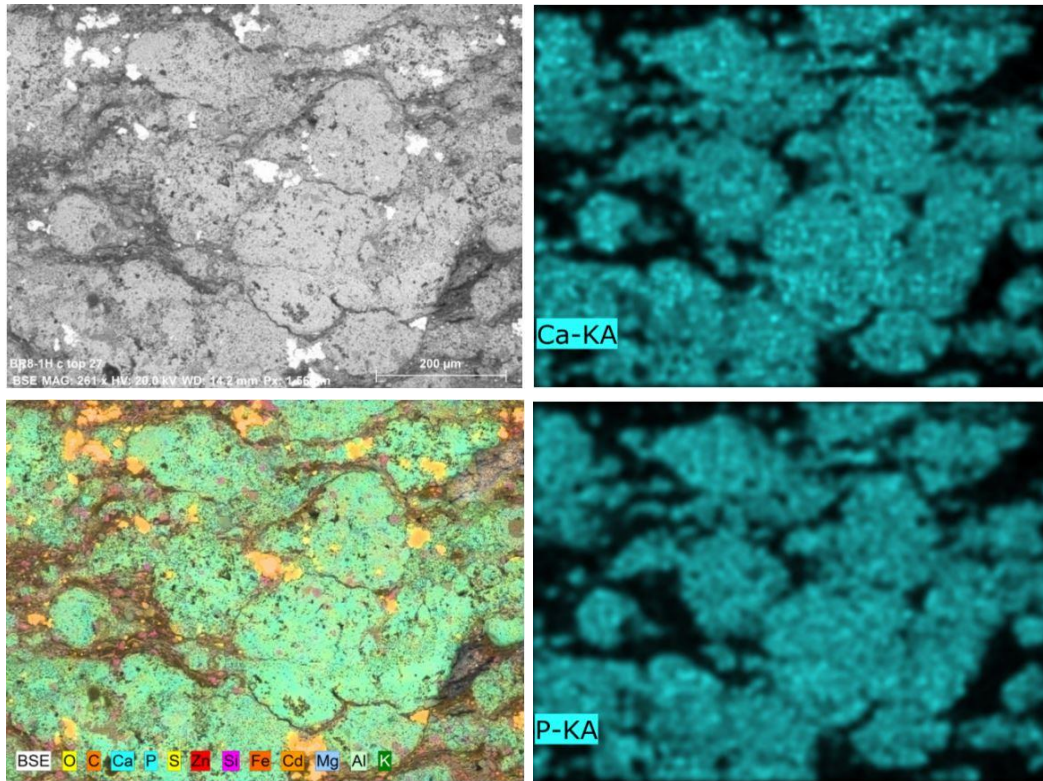


Figure 5.5. EDS images for Hushpuckney. Elemental maps of calcium and phosphorus reveal the rounded shape of phosphate grains containing sphalerite and pyrite in Hushpuckney (BR8).

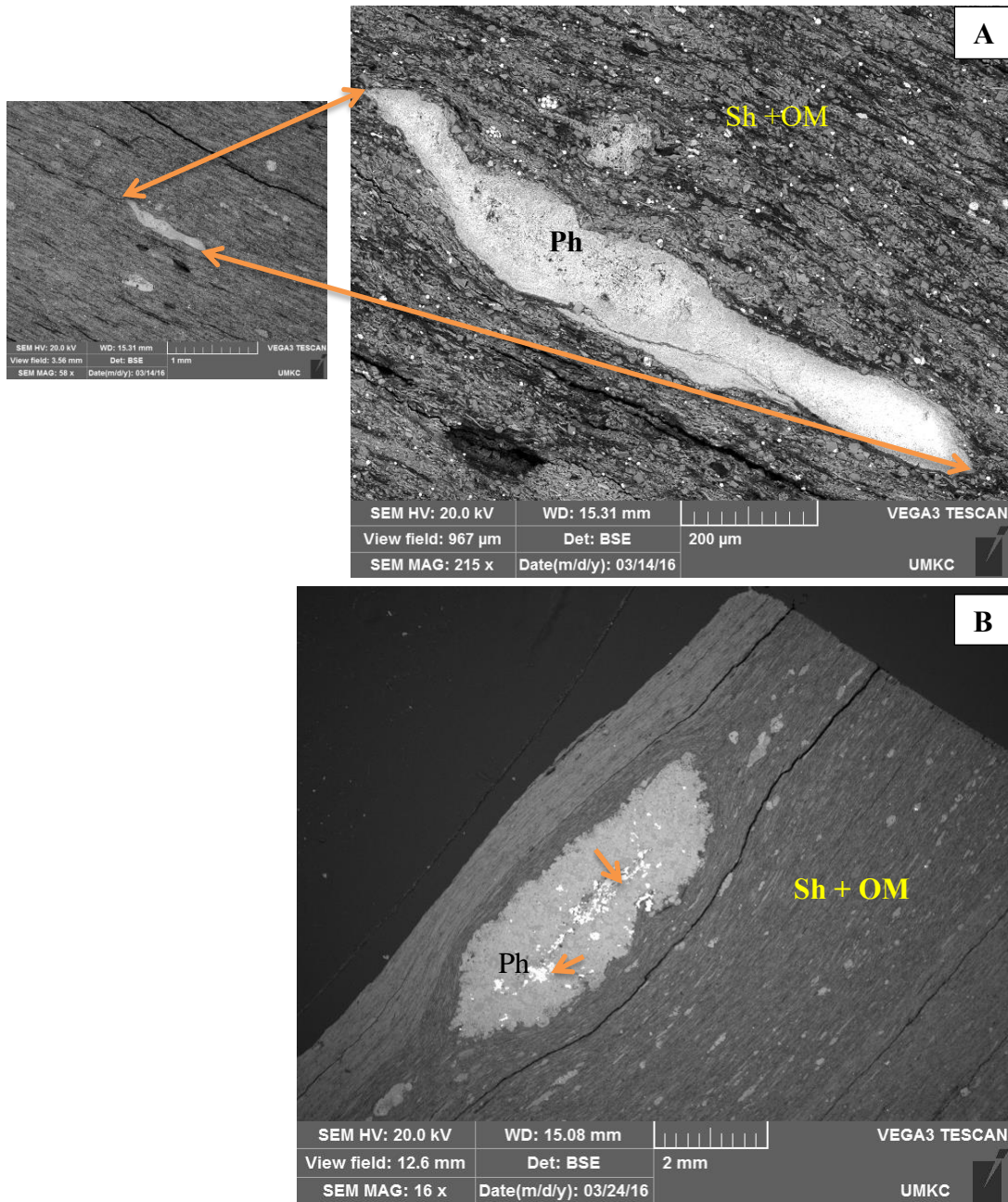


Figure 5.6. A- Phosphate nodule (Ph) in black shale (Sh) and organic matter, framboidal pyrite (very small white spheres), Hushpuckney unit (BR8).

B- Phosphate nodules (Ph) different in size (light gray) disseminated in black shale (Sh) and organic matter (OM), the largest nodule contain sphalerite (orange arrows), Hushpuckney unit (BR8).



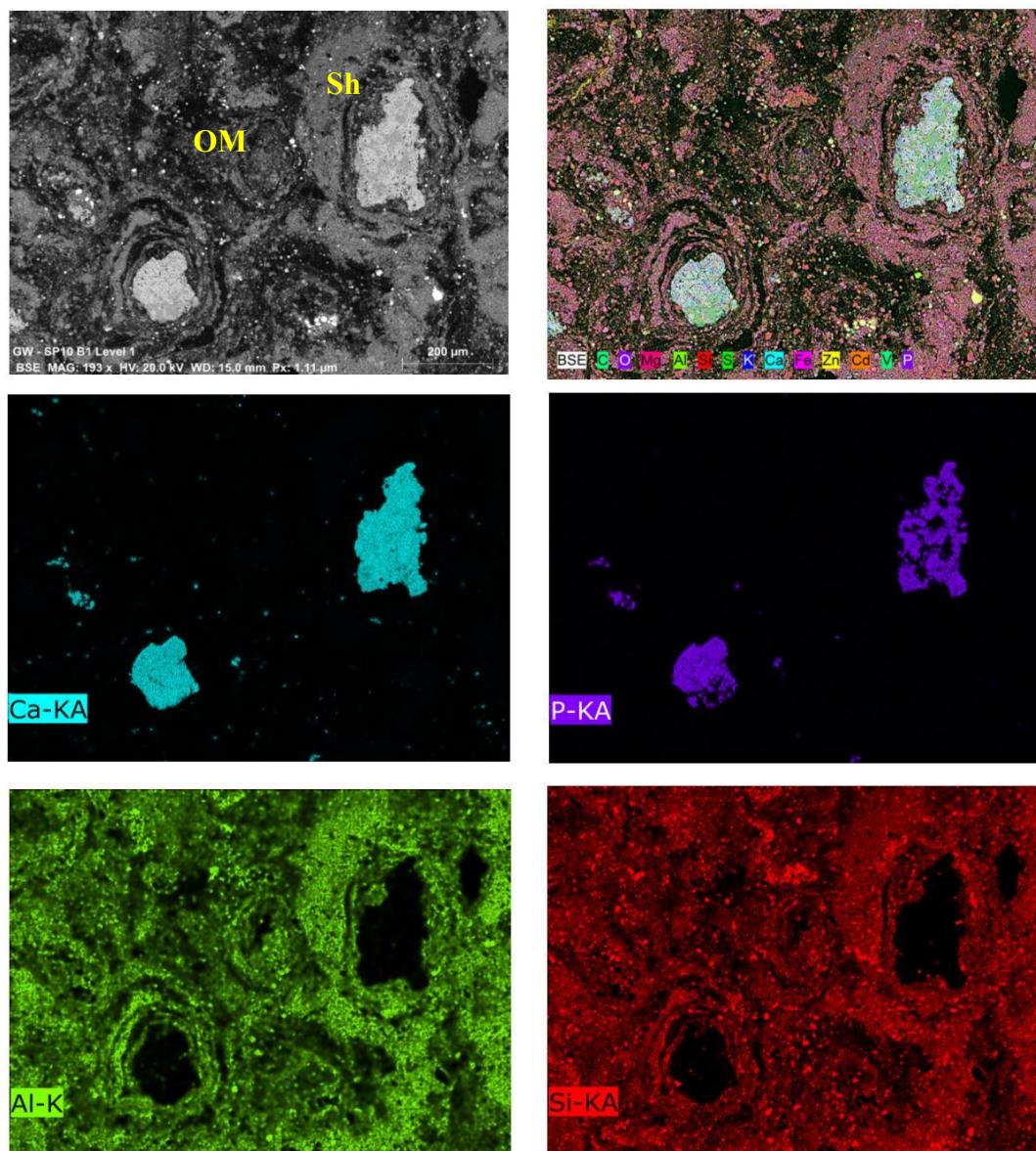


Figure 5.7. EDS images for Stark shale. Elemental maps for Ca, P, Al and Si showing isolated phosphate grains in shale (Sh); the dark area is organic matter (OM), very fine grains of quartz, framboidal pyrite and dolomite disseminated in shale. Note the element map of phosphorus is not filled like the calcium due to dissolution or inclusion of calcite, Stark unit - Greenwood Quarry, Greenwood, MO.

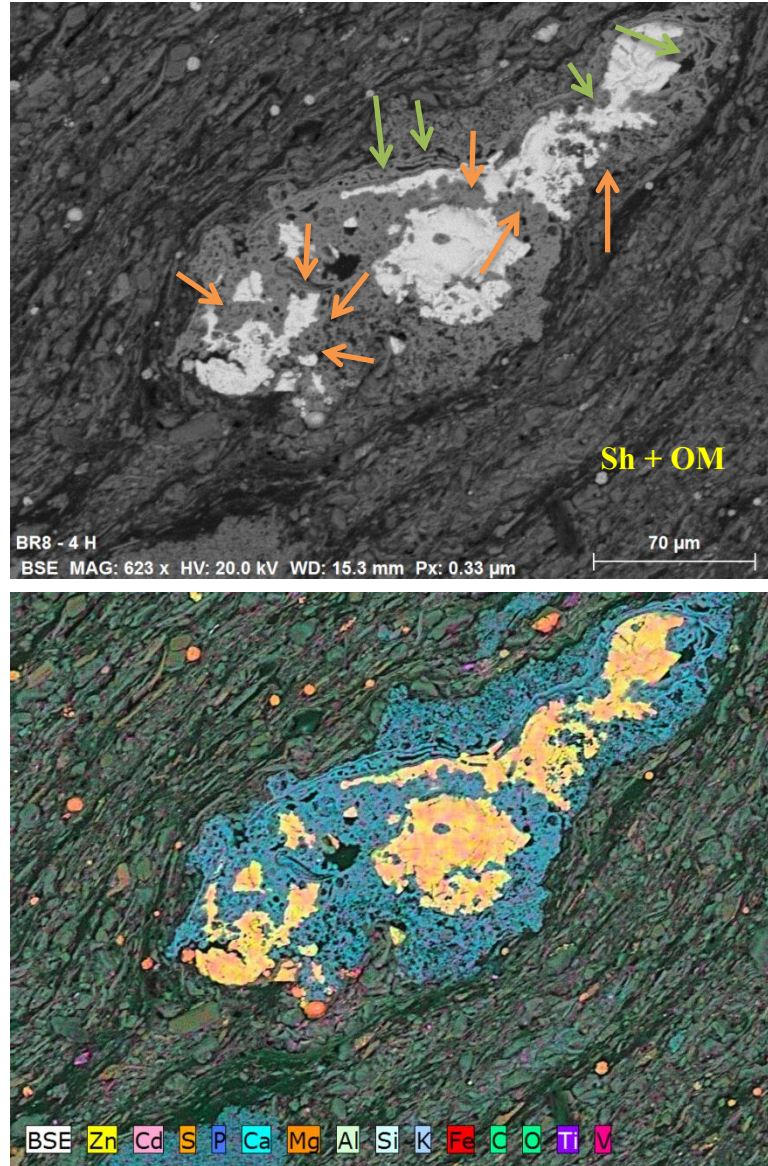


Figure 5.8. EDS images for Hushpuckney shale. Upper image, backscattered electron image. Lower image, composite elemental map with BSE image. Phosphate grains cemented together by new phosphate strips (green arrows), orange arrows pointed to the edges for these grains. These phosphate grains surrounded by shale (Sh) and organic matter hosted sphalerite, note there is no effect on the shale near the sphalerite.

All these observations lead to the conclusion that these phosphate grains have two stages of formation. First, detrital pellets can be transported from other places and accumulate in oxic-suboxic basins. There, they can partially dissolve enriching the pore fluids in phosphorus. Then, if environmental conditions change to suboxic-anoxic with neutral to alkaline pH, phosphates can reprecipitate. The presence of phosphates in laminations and nodules may indicate involvement of bacterial mats. Bacteria, such as sulphur-reducing types, with organic matter in sediments may facilitate phosphogenesis in suboxic-anoxic environments. The presence of framboidal pyrite supports this idea; it can indicate sulphur-reducing environment and microbial precipitation as second stage. Also, this suggestion may be supported by the correlation between phosphorus and calcium and vanadium as reviewed in Chapter 4 where two types of francolite are indicated.

Moore and Reddy (1994) presented a pe-pH diagram showing the stability of apatite as shown in Figure 5.9. This diagram suggests that francolite could form under a range of redox conditions, but is too soluble to persist under acidic conditions below pH 6.4. The presence of abundant marcasite and limestone dissolution in the Tri-State District to the south suggests that the fluids were acidic with pH below 5 (Murowchick and Barnes, 1986).

Some zinc may be hosted in apatites, but not much due to the significant difference in ionic radii between Zn and Ca. The only way that apatite can release Zn is during weathering, which is not relevant in this work. Sphalerite can form in such suboxic environment; being mobilized not from apatite but from organic matter and/or Fe-oxyhydroxides, or introduced in hydrothermal fluids. The correlation coefficient between P and Zn is positive but weak or insignificant. The correlation relationship between P versus Pb and Fe is also insignificant.

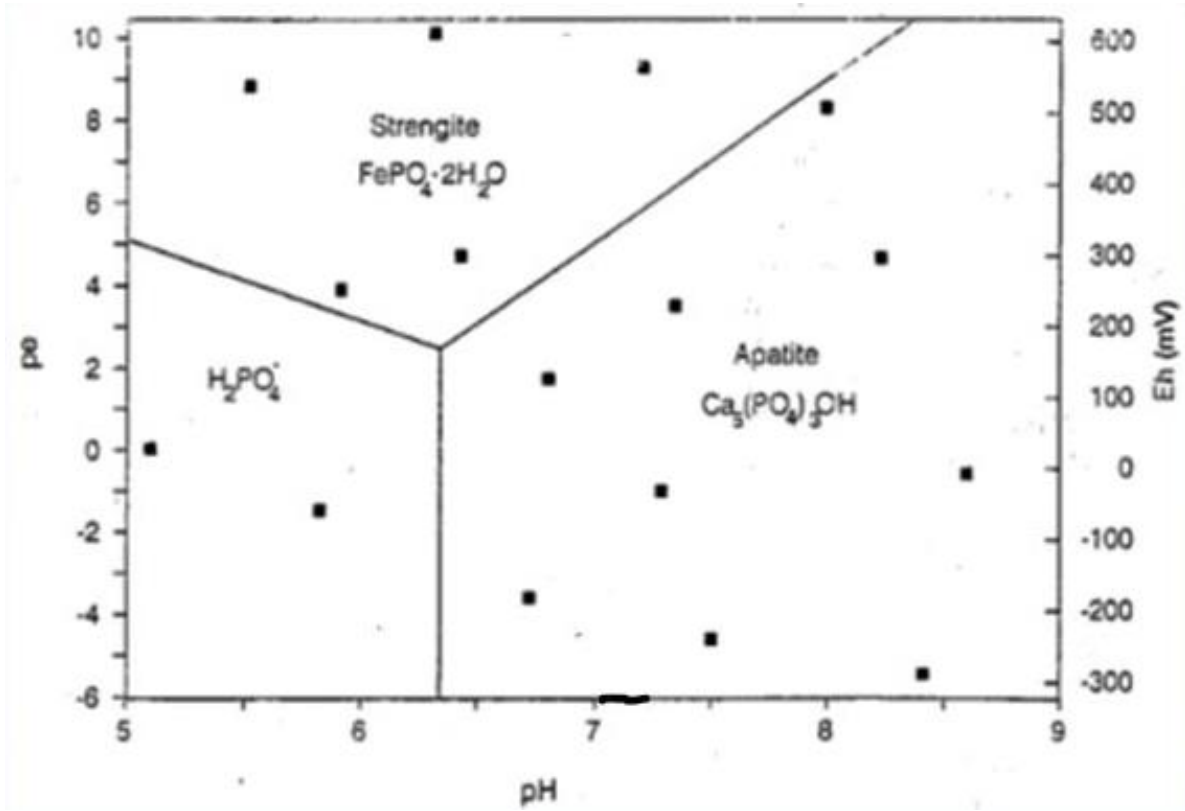


Figure 5.9. Theoretical pe – pH – Eh diagram shows stability fields for strengite and apatite. (After Moore and Reddy, 1994).

The formation conditions for clausthalite, sphalerite and pyrite have been reviewed previously. These conditions suggest the availability of hydrothermal solutions rich in zinc, lead and iron and low to medium temperature (50° - 200° C). These conditions are supposed to be suitable to precipitate sphalerite, clausthalite or pyrite as isolated grains or together. Hydrothermal solutions might be expected to alter the surrounding grains, especially the clay minerals, which were found to be unaltered detrital grains; no authigenic minerals were observed. The formation conditions of clausthalite required moderate (dysoxic) redox potentials and medium temperatures up to 200° C. such conditions might be expected to cause alteration of wallrock, but alteration was not observed in the shale samples. However, the fluid conduits described by Ragan (1996) display clear envelopes of dickite, a hydrothermal polymorph of kaolinite.

In conclusion all these observations encourage the idea that the formation of these minerals from the hydrothermal solutions rich with Zn –Pb coming from the south during the Ouachita uplift, flowing laterally along bedding of the black shale. Upon reaction in the reducing environment, the possibility of precipitating new phosphate is possible.

The other possibility is that the francolite clots were originally fecal pellets. As such, they would concentrate the bacterial sulfide reductive activity, which in turn would localize enrichment of reduced sulfur in the francolite before hydrothermal fluids introduced dissolved metals.

Though the Hushpuckney and Stark black shales are of different ages (though both are Pennsylvanian), they are similar in their cyclic nature, clay minerals, organic matter, and phosphate grains containing sulfide and selenide minerals. Both appear to contain

components derived from seawater during deposition, and both have a later hydrothermal imprint with Zn, Pb, and Cu sulfides and selenides.

## CHAPTER 6

### CONCLUSION

The present study provides insight into the mineralogy and geochemical composition of two black shales units of the Pennsylvanian Kansas City group:

The Hushpuckney shale member of the Swope Formation which consists of two submembers, black shale rich in organic matter in the lower part and gray shale poor with organic matter in the upper part. The black shale contains phosphate nodules which in turn contain sphalerite, clausthalite and pyrite.

The Stark shale member of the Dennis Formation consist of two submembers, black shale rich in organic matter in the lower part and gray shale in the upper part. Unfortunately, almost all the gray shale is highly weathered, while the black shale was unaltered. The black shale contains phosphate nodules which in turn contains sphalerite, clausthalite and pyrite.

Mineralogical study of the Hushpuckney and Stark black shales showed that the two units contain minerals of two origins. Sedimentary minerals comprising the shale include clays, quartz, carbonates and fluorapatite. Calcite ( $\text{CaCO}_3$ ) shows a variety of forms and dolomite ( $\text{CaMg}(\text{CO}_3)_2$ ) is disseminated as rhombohedra in both black shales. Clays (mainly illite, kaolinite  $\text{Al}_2\text{Si}_2\text{O}_5(\text{OH})_4$ , and clinochlore) are detrital in origin. Quartz ( $\text{SiO}_2$ ) grains are very small in size and it is associated with clay particles. Fluorapatite ( $\text{Ca}_5(\text{PO}_4)_3\text{F}$ , “francolite”) occurs as very fine-grained crystalline aggregates in phosphate grains. Trace amounts of detrital rutile ( $\text{TiO}_2$ ) and mica were also found.

Pyrite ( $\text{FeS}_2$ ) exists in two types, framboidal-clusters and euhedral grains disseminated in black shale and phosphate grains respectively. The framboids are diagenetic,

but the coarser euhedral grains could reflect hydrothermal deposition. Other hydrothermal minerals in the shales include sphalerite (ZnS), clausthalite (PbSe) and possibly chalcopyrite (CuFeS<sub>2</sub>) and barite (BaSO<sub>4</sub>). Sphalerite (ZnS) occurs as euhedral to subhedral grains within phosphate grains. Clausthalite (PbSe) exists as massive aggregates near the edges of, or filling the spaces between phosphate grains. In addition, the presence of low-abundance minerals chalcopyrite (CuFeS<sub>2</sub>) and barite (BaSO<sub>4</sub>) might also reflect hydrothermal input.

Geochemical analysis of the Hushpuckney and Stark black shales shows the following (major, minor and trace) elements: Si, Al, Fe, Mg, Ca, K, P, Ba, S, Co, Cu, Ni, Sr, V, Zn, Pb, Sc, La, Ti, Se, Rb and Sb. The geochemical data shows enrichment in Zn and Pb for both black shales submembers. Correlation coefficients set in the two black shale units for P versus other elements, Al versus other elements and element versus element. These linear relationships showed strong positive relationships as in Ca vs. P for fluorapatite, Al vs. Si and K for clay, Pb vs. Se for clausthalite, and Ca vs. Sr for calcite.

The Ni/Co ratio of the Hushpuckney indicates that the shale was deposited in an oxic zone environments whereas the results of the V/ (V + Ni) ratio indicates that deposition occurs within the range of reduced environments from anoxic to euxinic environment. Our interpretation is that the Hushpuckney probably was deposited in a transitional anoxic (dysoxic) environment. The results obtained from the use of the two ratios for the unweathered part of Stark indicate shale deposition under anoxic to euxinic conditions.

SEM/EDS photomicrographs of the phosphate grains in the Hushpuckney and Stark black shales units showed that these phosphate grains were precipitated under reducing environment. These phosphate grains contain sphalerite, clausthalite and pyrite formed from



hydrothermal fluids rich with Zn-Pb coming from the south during the Ouachita uplift, flowing laterally along bedding of the black shale. Under the reducing environment, reaction with, and some remobilization of phosphate occurred along with precipitation of metal sulfides.

## REFERENCE LIST

- Anderson, G. M., Macqueen, R. W., 1982. Ore deposits – 6 Mississippi Valley-type lead-zinc deposits. *Geoscience Canada*. 9 (2), 108-117.
- Algeo, T. J., Maynard, J. B., 2004. Trace-element behavior and redox facies in core shales of Upper Pennsylvanian Kansas-type cyclothems. *Chemical Geology* 206, 289-318.
- Babu, E. V. S. S. K., Nayak, S., Rai, A. K., Krishnamurthy, P., Kok, S. N., 2002. Discrete Selenide phases from the Uraniferous Mahadek Sandstone of Domiasiat and Wahkyan South, West Khasi Hills District, Meghalaya. *Journal of Geological Society of India*, 59, 571-574.
- Bailey, S. E., 1995. The Pennsylvanian Stark shale member as a source of heavy metals in ground water, midwestern USA. Unpublished M.Sc. thesis, University of Missouri – Kansas City 72p.
- Baturin, G. N., 1999. Hypotheses of Phosphogenesis and Oceanic Environment Lithology and Mineral Resources. 34 (5), 411-430.
- Berner, R. A., 1982. Burial of organic carbon and pyrite sulfur in modern ocean: its geochemical and environmental significance. *American Journal of Science*, 268, 1-23.
- Blatt, H., Middleton, G. V., Murray, R. C., 1972. *Origin of Sedimentary Rocks*. Prentice-Hall Inc. Englewood Cliffs, New Jersey.

- Bogdanov, K., Filipov, A., Kehayov, R., 2005. Au-Ag-Te-Se minerals in the Elat site Porphyry-Copper deposit, Bulgaria. *Geochemistry, Mineralogy and Petrology*, 43, 13-19.
- Bolze, C. E., Malone, P.G. Smith, M.J., 1974. Microbial mobilization of barite. *Chemical Geology*, 13, 141-143.
- Breheret, J. G., Brumsack, H. J., 2000. Barite concretions evidence of pauses in sedimentation in the Marnes Bleues Formation of Vocontain Basin (SE France). *Sedimentary Geology*, 130, 205-228.
- Brindley, G. W., Brown, G., 1984. Crystal structures of clay minerals and their X-Ray identification. Mineral Society, No. 5. Spottiswoode Ballantyne Ltd. London.
- Brumsack, H. J., 2006. The trace metal content of recent organic carbon-rich sediments: Implications for Cretaceous black shale formation. *Palaeogeography, Palaeoclimatology, Palaeoecology*, 232, 344-361.
- Camp, W. K., Diaz, E., Wawak, B., 2013. Electron Microscopy of Shale Hydrocarbon Reservoirs. AAPG Memoir 102.
- Carroll, D., 1970. Clay minerals: A guide to their x-ray identification. Geological Society of America, special paper, No. 126, Colorado.
- Carver, R. E., 1971. Procedures in Sedimentary Petrology. John Wiley & Sons. Inc. New York.
- Coleman, R. G., 1959. The natural occurrence of galena-clausthalite solid solution series. *American Mineralogist*, 44, 166-175.

- Coveney, R. M., 1979. Sphalerite concentrations in mid-continent Pennsylvanian Black Shales of Missouri and Kansas. *Economic Geology*, 74, 131-140.
- Coveney, R. M., Martin, S. P., 1983. Molybdenum and other heavy metals of the Mecca Quarry and Logan Quarry shales. *Economic Geology*, 78 (1), 132-149.
- Coveney, R. M., Leventhal, J. S., Glascock, M. D., Hatch, J. R., 1987. Origins of metals and organic matter in Mecca quarry shale and stratigraphically equivalent beds across the Midwest. *Economic Geology*, 82, 915-933.
- Coveney, R. M., Glascock, M. D., 1989. A review of the origins of metal-rich Pennsylvanian black shales, central U.S.A., with an inferred role for basinal brines. *Applied Geochemistry*, 4, 342-367.
- Coveney, R. M., Jr., Watney, W. L., Maples, C. G., 1989. Rates and durations for accumulation of Pennsylvanian black shales in the Midwestern United States. In Franseen, E. K., Watney, W. L. (Eds.) *Sedimentary Modeling: Computer Simulation of Depositional Sequences*. Subsurface Geology Series 12, Kansas Geology Survey.
- Cubitt, J. M., Merriam, D. F., 1979. Geochemical distribution in Pennsylvanian cyclic sediments of the midcontinent (USA). In Belt, E. S., Macqueen, R. W. (Eds.) *International Congress on Carboniferous Stratigraphy and Geology, Part 3: Sedimentology and Geochemistry*, Southern Illinois University Press.
- Davis, J. C., 1973. *Statistics and Data Analysis in Geology*. John Wiley & Sons. Inc., New York.

- Demaison, G. J., Moore, G. T., 1980. Anoxic environments and oil source bed genesis. American Association of Petroleum Geologists Bulletin (AAPG), 64 (8), 1179-1209.
- Drever, J. I., 1971. Magnesium-iron replacement in clay minerals in anoxic marine sediments, Science, 172, 1334-1336.
- Dorozhkin, S. V., 2012. Dissolution mechanism of calcium apatites in acids: a review of literature. World Journal of Methodology, 2 (1), 1-17.
- Evans, A. M., 1993. Ore Geology and Industrial Minerals. An Introduction. 3<sup>rd</sup> edition. Blackwell Science, 389p.
- Folk, R. L., 2005. Nannobacteria and the formation of framboidal pyrite: Textural evidence. Journal of Earth system Science, 114 (3), 369-374.
- Follmi, K. B., 1995. The phosphorus cycle, phosphogenesis and marine phosphate-rich deposits. Earth-Science Reviews, 40, 55-124.
- Forsch, J. M., 1997. The Contributions of Heavy Metals to Surface Water from The Hushpuckney and Stark Shale Members Kansas City Group, Pennsylvanian System in the Kansas City Area. . Unpublished M.Sc. thesis, University of Missouri-Kansas City.
- Frigstad, O. F., 1972. Naumannite from Kongsberg silver deposit, south Norway. Contribution to the mineralogy of Norway, 52 (50), 273-285.
- Frost, J. K., Zierath, D. L., Shimp, N. F., 1985. Chemical Composition and Geochemistry of the New Albany Shale Group (Devonian-Mississippian) in Illinois. Final report prepared to the US. Department of Energy. Report 1985-4.

- Gehring, A. U., Fry, I. V., Luster, J., Sposito, G., 1993. The chemical Form of Vanadium (IV) in Kaolinite. *Clays and clay Minerals*, 41 (6), 662-667.
- Gertsch, B., Keller, G., Adatte, T., Bartels, D., 2011. Trace-element geochemistry of Brazos sections, Texas, U.S.A. (Society for Sedimentary Geology) SEPM special publication No. 100.
- Gibbs, R. L., 1974. Error due to segregation in quantitative clay minerals x-ray diffraction mounting techniques. *American Mineralogist*, 50, 741-751.
- Grim, R. G., 1968. *Clay Mineralogy*. McGraw-Hill, New York.
- Guilbert, J. M., Park, C. F. Jr., 1986. *The Geology of Ore Deposits*. Freeman .
- Hamilton, R. V., 1989. A Geochemical and Environmental Study of the Upper Pennsylvanian Muncie Creek Shale Member. Unpublished M.Sc. thesis, University of Missouri-Kansas City.
- Hardy, R., Tucker, M., 1988. X-ray powder diffraction of sediments. In Tucker, M. (Ed.) *Techniques in Sedimentology* (191-228). Oxford : Blackwell Scientific Publications.
- Hatch, J. R., Leventhal, J. S., 1992. Relationship between inferred redox potential of the depositional environment and geochemistry of Upper Pennsylvanian (Missourian) Stark shale member of the Dennis limestone, Wabaunsee County, Kansas, USA. *Chemical Geology*, 99, 65-82.
- Healy, R. E., Petruk, W., 1992. Graphic galena-clausthalite solid solution in low Fe sphalerite from the Trout Lake Massive Sulfide Ores, Flin Flon, Manitoba. *Economic Geology*, 87, 1906-1910.

- Herzig, P. M., Hannington, M. D., 2006. Input from the Deep: Hot Vents and Cold Seeps. In Schulz, D., Zabel, M. (Eds.). *Marine Geochemistry (457-479)*. Bremen: Springer.
- Hibbard, M. J., 2002. *Mineralogy (A Geologist's point of view)*. 1<sup>st</sup> edition. McGraw-Hill.
- Howe, W. B., Koenig, J.W., eds., 1961. *The Stratigraphic Succession in Missouri*. Missouri Geological Survey and Water Resources. XL, second series.
- Hutchison, C. S., 1974. *Laboratory Handbook of Petrographic Techniques*. John Wiley & Sons. New York.
- Jensen, M. L., Bateman, A. M., 1982. *Economic Mineral Deposits*. 3<sup>rd</sup> edition. John Wiley & Sons.
- Jones, B., Manning, D. A. C., 1994. Comparison of geological indices used for the interpretation of palaeoredox conditions in ancient mudstones. *Chemical Geology*, 111, 111-129.
- Keller, W. D., 1963. Diagenesis in clay minerals. In Ingerson, E. (Ed.) *Proceedings of the 11<sup>th</sup> Conference on Clays and Clay Minerals*, (136-157). 13, Pergamon Press.
- Keller, W. D., 1970. Environmental aspects of clay minerals. *Journal of Sedimentary Petrology*, 40, 788-813.
- Keller, W. D., 1988. Authigenic kaolinite and dickite associated with metal sulfides-probable indicators of a regional thermal event. *Clay and Clay Minerals*, 36, (2), 153-158.
- Kidder, D. L., 1982. *Distribution and origin of Mid-Continent Pennsylvanian phosphorites*. Unpublished M.Sc. thesis, University of Iowa.

- Krauskopf, K. B., 1956. Factors controlling the concentrations of thirteen rare metals in sea water. *Geochimica et Cosmochimica Acta*, 55, 1799-1806.
- Krauskopf, K. B., 1982. *Introduction to Geochemistry*. International Student Edition. McGraw-Hill Book Inc.
- Kronberg, B. I., and Nesbitt, H. W., 1981. Quantification of weathering, soil geochemistry and soil fertility. *Journal of Soil Science*, 32, 453-459.
- Li, Y., Schieber, J., 2015. On the origin of a phosphate enriched interval in the Chattanooga Shale (Upper Devonian) of Tennessee – A combined sedimentologic, petrographic, and geochemical study. *Sedimentary Geology*, 329, 40-61.
- Lott, D. A., Coveney, R. M., Murowchick, J. B., Grauch, R. I., 1999. Sedimentary Exhalative Nickel-Molybdenum Ores in South China. *Economic Geology*, 94, (7), 1051-1066.
- Martin, S. P., 1982. Trace Elements in the Pennsylvanian Age Hushpuckney and Mecca Quarry Shales, Midcontinent, USA. Unpublished M.Sc. thesis, University of Missouri-Kansas City.
- McClellan, G. H., 1980. Mineralogy of carbonate fluorapatites. *Journal of Geology Society*, 137, 675-681.
- Meunier, J. D., 1994. The Composition and Origin of Vanadium-Rich Clay Minerals in Colorado Plateau Jurassic Sandstones. *Clays and Clay Minerals*, 42 (4), 391-401.
- Millot, G., 1970. *Geology of Clays*. Springer-Verlag. New York.



- Moore, P. A., Jr, Reddy K. R., 1994. Role of Eh and pH on Phosphorus Geochemistry in Sediments of Lake Okeechobee, Florida. *The Journal of Environmental Quality*, 23 (5), 955-964.
- Murowchick, J. B., Barnes, H. L. 1986. Marcasite precipitation from hydrothermal solutions. *Geochimica et Cosmochimica Acta*, 50, 2615-2629.
- Nesse, W. D., 2000. *Introduction to Mineralogy*. New York, Oxford. Oxford University Press.
- Ostrom, M. E., 1961. Separation of clay minerals from carbonate rocks by using acid. *Journal of Sedimentary Petrology*, 31, 123-129.
- Parizek, E. J., Gentile, R. J., 1965. *Geology of the Kansas City Group at Kansas City*. Report of investigation. no. 3. State of Missouri.
- Peacor, D. R., Coveney, R. Jr., Zhao, G., 2000. Authigenic Illite and Organic Matter: The Principal Hosts of Vanadium in the Mecca Quarry Shale at Velpen, Indiana. *Clays and clay Minerals*, 48 (3), 311-316.
- Pettijohn, F. J., 1975. *Sedimentary Rocks*. 3<sup>rd</sup> edition. Harper & Row Publishers.
- Potter, P. E., Barry, J., Pryor, A., 1980. *Sedimentology of shale*. Springer-Verlag Inc, New York.
- Pracejus, H. (Editor), 2008. *The ore Minerals under the Microscope. An Optical Guide*. Elsevier.

- Prevot, L., ElFaleh, E. M., Lucas, J., 1989. Details on synthetic apatites formed through bacterial mediation: Mineralogy and chemistry of the products. In Lucas, J., Cook, P. J., Prevot, L. (Eds.) *Apatite and Phosphorites (237-254)*. *Science of Geology Bulletin*, 42.
- Ragan, V. M., 1996. Evidence for extensive hydrothermal events in the genesis of the Mississippi Valley-Type (MVT) deposits of eastern Kansas and the Tri-State zinc-lead mining district of Kansas, Missouri, and Oklahoma. Unpublished. PhD thesis, University of Missouri-Kansas City.
- Rimmer, S. M., 2004. Geochemical paleoredox indicators in Devonian-Mississippian black shales, Central Appalachian Basin (USA). *Chemical Geology*, 206, 373-391.
- Rothwell, R. G., 2006. *New techniques in sediment core analysis*. Geological Society, London, special publications 267.
- Rudy, R. J., 1982. Structural Damage from Shale Expansion at Kansas City, Missouri. Unpublished M.Sc. thesis, University of Missouri-Kansas City.
- Sari, A., Koca, D., 2012. An approach to provenance, tectonic and redox conditions of Jurassic-Cretaceous Akkuyu Formation Central Taurids, Turkey. *Mineral Resources Exploration Bulletin*, 144, 51-74.
- Schultz, R. B., 1989. Geochemical characteristic and inferred depositional environment of Upper Pennsylvanian (Virgilian) black shales in eastern Kansas. In Merriam, D. F. (Ed.) *The Compass, Sigma Gamma Epsilon*, (67, 47-54). University of Kansas.
- Selley, R. C., 2000. *Applied Sedimentology*. Academic Press.

- Soua, M., 2011. Productivity and bottom water redox conditions at the Cenomanian - Turonian Oceanic Anoxic Event in the southern Tethyan margin, Tunisia. *Revue Mediterraneenne de l'Environment*, 4, 653-664.
- Steiner, E., 2008. *The Chemistry Maths Book*. 2<sup>nd</sup> edition, Oxford University Press.
- Suits, N. S., Wilkin, R. T., 1998. Pyrite formation in the water column and sediments of a meromictic lake. *Geology (Boulder)*, 26, 1099-1102.
- Swindale, L. D., Fan, P. F., 1967. Transformation of gibbsite to chlorite in ocean bottom sediments. *Science*, 157, 799-800.
- Tischendorf, G., Ungethum, H., 1964. On the conditions of formation of clausthalite-galena and some observations on the distribution of selenium in galena as a function of oxidation potential and pH. *Geochemistry International (translated)*, 1, 1205-1225.
- Thorez, J., 1976. *Practical Identification of Clay Minerals. A hand book for teachers and students in clay mineralogy*, Belgium.
- Tourtelot, H. A., 1979. Black Shale - Its Deposition and Diagenesis. *Clays and Clay Minerals*, 27, (5), 313-321.
- Trewin, N., 1988. Use of the Scanning Electron Microscope in Sedimentology. In Tucker, M. (Ed.) *Techniques in Sedimentology (229-273)*. Oxford Blackwell Scientific Publications.
- Tribovillard, N., Algeo, T. J., Lyons, T., Riboulleau, A., 2006. Trace metals as paleoredox and paleoproductivity proxies: An update. *Chemical Geology*, 232, 12-32.

- Vine, J. D., and Tourtelot, E. B., 1970. Geochemistry of Black Shale Deposits – A Summary Report. *Econ. Geol.*, v. 65. pp. 253-272.
- Walczyk, D., Malina, D., Krol, M., Pluta, K., Sobczak-Kupiec, A., 2016. Physicochemical characterization of zinc-substituted calcium phosphate. *Bulletin of Materials Science*, 39 (2), 525-535.
- Weaver, C. E., 1958. Geological interpretation of argillaceous sediments. Part 1: Origin and significance of clay minerals in sedimentary rocks. *American Association of Petroleum Geologists Bulletin (AAPG)*, 42 (2), 254-271.
- Weaver, C. E., 1959. The clay petrology of sediments. *Clays and Clay Minerals*, 6, 154-187.
- Weaver, C. E., 1960. Possible uses of clay minerals in the search for oil. *Clays and Clay Minerals*, 8, 214-227.
- Weaver, C. E., 1967. The significance of clay minerals in sediments. In Nagy, B., Colombo, V. (Eds.) *Fundamental Aspects of Petroleum Geochemistry (37-75)*. Elsevier, New York.
- Weaver, C. E., Pollard, L.D., 1975. *The Chemistry of Clay Minerals*. Elsevier, New York.
- Wenger, L. M., Baker, D. R., 1986. Variations in organic geochemistry of anoxic-oxic black shale-carbonate sequences in the Pennsylvanian of the midcontinent, USA. *Organic Geochemistry*, 10, 85-92.
- Wilkin, R. T., Barnes, H. L., Brantley, S. L., 1996. The size distribution of framboidal pyrite in modern sediments: an indication of redox conditions. *Geochimica et Cosmochimica Acta*, 60, 3897-3912.

Ziegler, A. C., 1989. Experimental Leaching of Pennsylvanian Sedimentary rocks to Determine Sources of Metals in Coal Mine Water near Montrose, Missouri. Unpublished M.Sc. thesis, University of Missouri-Kansas City.

## VITA

Safaa Abdulfattah Abdulrazzaq Al-Janabi was born on September 30, 1960 in Baghdad, Iraq. He graduated in 1978 from Al Kindi High School in Baghdad, Iraq. He joined Baghdad University in 1978 and graduated in 1983 with Bachelor of Science degree in Geology, and a Master of Science degree in Geology in 1986. He is currently a doctoral candidate in the Interdisciplinary Ph.D. program at the University of Missouri–Kansas City.

Mr. Al-Janabi began his professional career in 1989 at the natural history museum – Baghdad University then he moved to the geology department – at Baghdad University in 1993 as assistant lecturer in optical mineralogy, sedimentology, crystallography and general geology.

Mr. Al-Janabi joined the University of Missouri–Kansas City in February, 2010. In his first year he completed courses in English to qualify for graduate study. He then pursued the Interdisciplinary Ph.D. degree in Economic Geology at the University of Missouri – Kansas City, Department of Geosciences which he plans to complete in December, 2017.

Mr. Al-Janabi has received a full scholarship from the Iraqi Ministry of Higher Education and Scientific Research to pursue his Economic Geology doctoral degree in the United States.

Mr. Al-Janabi is a member of the Geological Society of Iraq and student member of Geological Society of America.

## Publications

Tamar-Agha, M. Y., and Al-Janabi, S. A. 1997. Palygoskite in the Tayarat Formation (Upper Cretaceous), Well KH-6 at Al-Ansab, Southern desert of Iraq. In (Al-Bassam, K.) (editor). The Iraqi Palygorskite Geology, Mineralogy, Geochemistry, Genesis and Industrial Uses. Proceedings of a symposium (11-34). The State Company of Geological Survey and Mining, Iraq.

Tamar-Agha, M. Y., Al-Zubaidi, A. A., and Al-Janabi, S. A. 2016. A comparative study between the depositional environment and provenance of the Hussainiyat (Lower Jurassic) and the Rutbah (Upper Cretaceous) Formations, Western Desert of Iraq. *Arabian Journal of Geosciences*. 9 (6), (1-13).